Physics Reports 808 (2019) 1–74

Contents lists available at ScienceDirect

Physics Reports

journal homepage: www.elsevier.com/locate/physrep

10 years of pioneering X-ray science at the Free-Electron Laser FLASH at DESY

Jörg Rossbach, Jochen R. Schneider *, Wilfried Wurth

Deutsches Elektronen-Synchrotron DESY, Notkestrasse 85, 22607 Hamburg, Germany
Physics Department, Universität Hamburg, Luruper Chaussee 149, 22761 Hamburg, Germany

ARTICLE INFO

Article history:
Received 5 October 2018
Received in revised form 5 February 2019
Accepted 6 February 2019
Available online 22 February 2019
Editors: R. Redmer and F. Parmigiani

ABSTRACT

Free-electron lasers produce extremely brief, coherent, and bright laser-like photon pulses that allow to image matter at atomic resolution and at timescales faster than the characteristic atomic motions. In pulses of about 50 femtoseconds duration they provide as many photons as one gets in 1 s from modern storage ring synchrotron radiation facilities. FLASH, the Free-Electron Laser at DESY in Hamburg was the first FEL in the XUV/soft X-ray spectral range, started operation as a user facility in summer 2005, and was for almost 5 years the only short wavelength FEL facility worldwide. Hence, most of the technological developments as well as the scientific experiments performed by the user community were new and unique as outlined below. FLASH was driving FEL science and technology and paved the way for many new ideas. Because of using a linear accelerator in superconducting RF technology FLASH combines the extreme peak brightness characteristic for FELs with very high average brightness. It also was the prototype for the European XFEL located in the Hamburg metropolitan area, which started user operation in summer 2017.

The present review provides an overview of the progress made with accelerator science and technology at FLASH for the production of stable beams of well characterized electron pulses, reduction of the pulse jitter to the femtosecond level, generation of ultra-short photon pulses, adequate synchronization of the machine parameters with the experiment, and demonstrating advanced FEL schemes using variable gap undulators. Much of this was done in the very exciting early days of FEL science when it was even not clear if the FEL concept could be realized for X-rays. The development and the operation of the FLASH user facility is described, as well as the techniques developed to make use of the new type of X-ray beams including photon beam diagnostics and damage studies of the optical elements. The review emphasizes breakthrough experiments which demonstrated that many of the ideas collected in the world-wide discussion of the scientific case of free-electron lasers could indeed be realized and they often produced unexpected results. The first experiment on Coulomb explosion of Xe clusters performed in 2002 was a clear demonstration of the feasibility of experiments with free-electron laser beams and opened a lively discussion in the atom, molecular and optical physics community (AMO).

Time resolved single-shot single-particle imaging, summarized in the slogan "Take movies instead of pictures", was one of the most popular science drivers for the construction of free-electron X-ray lasers. As a first step in this direction experiments using a highly focused beam of FLASH demonstrated that pictures of 2 dimensional objects could be reconstructed from single-shot single-particle diffraction patterns. Explosion dynamics of nano-size particles hit by an intense FEL pulse were studied. This method, called "diffraction before destruction", is now very successfully applied with hard X-rays and, to a large extent, solves the radiation damage problem in structural

* Corresponding author at: Deutsches Elektronen-Synchrotron DESY, Notkestrasse 85, 22607 Hamburg, Germany.
E-mail address: jochen.schneider@desy.de (J.R. Schneider).

https://doi.org/10.1016/j.physrep.2019.02.002

biology. A long term goal is to determine the 3 dimensional structure of a large molecule from a single-shot diffraction pattern. Along these lines the 3D architecture of free Ag nanoparticles could be determined from one diffraction pattern only using soft X-rays from FLASH.

To understand light–matter interactions in this new parameter space a number of pioneering AMO experiments have been performed including non-linear interactions in atoms, molecules and clusters. Multiphoton photoionization processes in the presence of intense optical fields have been studied, as well as photo-absorption of XUV photon energies on molecular ions important for astrophysics. The nature of formation and breaking of molecular bonds was investigated in VUV pump–VUV probe experiments using a reaction microscope and a specific delay line. As an example the process of ultrafast isomerization of acetylene molecules C_2H_2 triggered by single photon excitation has been studied. The structural changes during the isomerization process were visualized and an isomerization time of 52 +/- 15 fs was found.

Clusters of variable size, which can be produced routinely, allow distinguish between inter- and intra-atomic effects and are considered model systems for the investigation of light–matter interactions in multi-atom objects. As an example such experimental studies provided instructive data for benchmarking theoretical models describing cluster ionization in intense short-wavelength laser pulses. The combination of single-shot single-particle imaging for determination of the cluster size with spectroscopy was crucial for success of these experiments. The investigations could later be extended to very large Xe clusters providing new insights into the nanoplasma formation and explosion dynamics of such large systems

From early on, studies of high energy density plasmas and warm dense matter have been one of the most prominent research fields in building the scientific case for X-ray free-electron lasers. A good understanding of this complex regime between cold solids and hot dilute plasmas is important for high pressure studies, applied materials studies, inertial fusion, and planetary interiors. With the first observation of saturable absorption of an L-shell transition in Aluminum and pioneering studies of warm dense hydrogen FLASH kicked off research of matter in extreme conditions with free-electron lasers.

In condensed matter experiments the emphasis is not so much on the peak power of the FEL beam and extreme focusing, but on beam properties like polarization and pulse duration. The sample has to stay intact in the beam over hours and the number of photons per pulse impinging on the sample has to be limited to avoid space charge effects. After demonstrating the possibility to record single-shot resonant magnetic scattering images with FELs the first time-resolved demagnetization study using a pump–probe approach with an IR-pump pulse and an XUV probe pulse to record a resonant magnetic scattering pattern as a function of pump–probe delay was also performed at FLASH.

Free-electron lasers offer the possibility to extend the well-established X-ray spectroscopic techniques for the investigation of the static electronic structure of matter to probing the evolution of the electronic structure in the time domain after controlled excitation. At FLASH first time resolved core level photoemission (TR-XPS) experiments have been performed which are element specific and provide information on the dynamics of the local charge state around a specific center. Using 198 eV photons in a surface study at Ir single crystals it was possible to separate surface and bulk contributions in the Ir 4f levels with sufficient instrumental resolution. Time and angular resolved photoelectron spectroscopy (TR-ARPES) is a very powerful tool to study non-equilibrium electron dynamics of condensed matter systems, since it offers the possibility to follow the dynamics of the full band structure of a material. In another pioneering experiment the photo-induced dynamics of the Mott insulator 1T-TaS_2 was studied at FLASH by investigating the dynamics of the Ta 4f photoemission. The formation of a commensurate charge density wave (CCDW) leads to a splitting of the Ta 4f level which decreases first on a sub-picosecond time scale due to electronic melting of the CCDW and afterwards on a picosecond lifetime due to electron–phonon coupling. This leads to transfer of energy from the electronic system to the lattice and a partial melting of the periodic lattice distortions accompanying the periodic charge arrangement in the CCDW phase.

In materials science X-ray absorption and emission spectroscopy are among the most powerful spectroscopies to study the electronic structure of matter. The wavelength of the radiation is scanned over certain element specific resonances which at FLASH 1 can only be done by scanning the electron energy. This is time consuming and makes the experiments difficult. Nevertheless, the first time-resolved X-ray emission spectroscopy (XES) experiment was done at FLASH 1 in order to study non-thermal melting of a silicon sample. From a comparison of the observed valence electronic structure at different times after the photoexcitation it became clear that in the melting process in the first few ps a non-equilibrium low density liquid state is reached. The existence of such a

metastable low density liquid state had been postulated for many systems that show tetragonal bonding in the crystalline phase like water for example, but spectroscopically the time-resolved silicon XES data taken at FLASH verified its existence for the first time. FLASH 2 has tunable undulators and it was demonstrated that scanning of the wavelength is very easy there.

Contents

1. Introduction

Free-electron lasers produce extremely brief, coherent, and brilliant laser-like photon pulses that allow to image matter at atomic resolution and at timescales faster than the characteristic atomic motions. FLASH (**F**ree-Electron **Las**er in **H**amburg) was the first free-electron laser in the XUV/soft X-ray spectral range and officially started operation as a user facility in summer 2005. In pulses of about 50 fs duration it provides as many photons as one gets in 1 s from modern storage ring synchrotron radiation facilities. Because of using a linear accelerator (Linac) in superconducting RF technology FLASH combines the extreme peak brightness with very high average brightness (Rossbach, 2016). FLASH opened exciting and fundamentally new opportunities for the investigation of ultrafast processes in atoms, molecules, clusters and nanoparticles, in condensed matter and matter in extreme conditions including non-linear spectroscopy and single-shot single particle imaging. Over the first 10 years of FLASH operation 230 scientific papers have been published in refereed journals.

Soon after the discovery of the principle of a free-electron laser (Madey, 1971) and its first realization with an optical cavity operating in the infrared wavelength range by John Madey and his group at Stanford University (Deacon et al., 1977) the theoretical basis for single-pass X-ray FELs was established (Kondratenko and Saldin, 1980; Bonifacio et al., 1984). These papers stimulated lively discussions in the accelerator community in a series of workshops organized by Brookhaven National Laboratory and SLAC, Stanford. Already in 1992, detailed suggestions were made to use the existing SLAC Linac equipped with low-emittance electron guns to drive FELs in the 4 to 0.1 nm wavelength range (Pellegrini, 1992).

At that time, DESY, as the prime German accelerator and particle physics laboratory, shared the vision of a large part of the particle physics community to build a TeV-scale electron–positron linear collider, and pursued this project vigorously when Bjørn H. Wiik became Director General of the laboratory in 1993. However, early on, there were clear indications from the funding agencies in Germany that such a large research facility should be attractive not just to the particle physics community. Thus DESY developed, within an international collaboration, a conceptual design for a 500 GeV $e^+ e^-$ linear collider with integrated X-ray laser facility (Brinkmann et al., 1997). Based on the good experience with superconducting technology at the large hadron–lepton collider HERA at DESY and the need for high luminosity at the linear collider, the challenge was accepted to realize the accelerator in superconducting RF technology by the TESLA collaboration, which by the end of 2002 included 50 institutions from 12 countries.

In the 1990ies, construction of a single-pass FEL for the VUV regime was very ambitious. The experimental evidence was restricted to the microwave regime, i.e. to wavelengths longer by many orders of magnitude (Orzechowski et al., 1985). There were concerns that the basic principle might not work at VUV and X-ray wavelengths and that the required accelerator technology would not be manageable. Not least, it was clear that there would be quite a difference between a proof-of-principle demonstration and a reliable user facility. Such concerns were even more serious in terms of realization of hard X-ray FELs. Thus there was quite a consensus that a demonstration and operational experience in the VUV regime would be indispensable before realization of an X-ray FEL could be pursued (Pellegrini, 1990). Based on these considerations, DESY decided to build a test facility for the development of the superconducting linear accelerator within the TESLA collaboration, and to combine this with an FEL user facility in the VUV–XUV spectral range. It was easy to formulate a convincing scientific case. The conceptual design report for the FEL was submitted in June 1995 (Åberg et al., 1995), the project was approved in October of the same year and the construction of the so-called TESLA Test Facility Free-Electron Laser (TTF FEL) started.

Already the first stage of the TTF FEL project aimed at wavelengths and power levels, where neither classical lasers nor FEL oscillators could compete. First lasing was observed on Febr. 22nd, 2000, at a wavelength of 109 nm and proved that the FEL gain process was well understood and under control in the VUV wavelength regime. Shortly after, in September 2000, the "Low-Energy Undulator Test Line (LEUTL)" at the APS at the Argonne National Laboratory reached FEL lasing and saturation at 530 nm (Milton et al., 2001), while FEL saturation at 98 nm was demonstrated at TTF FEL on Sept. 10th, 2001.

These achievements gave sufficient confidence to proceed with the project planning for X-ray FELs: The approval process for LCLS at Stanford started mid of 2001 when DOE officially acknowledged that such a device should be built, and in March 2001 the TESLA collaboration presented the Technical Design Report (TESLA collaboration, 2001) at a colloquium on Scientific Perspectives and Technical Realization of TESLA at DESY, which attracted more than 1100 scientists, 40% from abroad. The reaction of the science community at large and the funding agencies was positive. After an evaluation of the TESLA proposal by the German Science Council, the German Government decided in February 2003 that the XFEL part of the proposal should be realized in Hamburg as a European project, with Germany paying half of the cost.

After the 2003 government decision to aim for a European XFEL facility in the Hamburg metropolitan area the focus at the TESLA Test Facility shifted more and more towards the development of the VUV FEL and the facility was named FLASH, Free-Electron Laser in Hamburg, in April 2006. In many respects FLASH is the prototype of the European XFEL. The technical and scientific mile stones achieved by FLASH in due time were instrumental for the decision process for the European XFEL. The Technical Design Report for Eu-XFEL, the European X-ray Free-Electron Laser facility (Altarelli et al., 2006), was presented in July 2006, civil construction started in January 2009, first electron beams were accelerated at the end of 2016, and first lasing was demonstrated on May 4th, 2017.

FLASH was the first free-electron laser facility which managed the difficult transition from an accelerator R&D project to a photon science user facility, including stable operation of the Linac and synchronization of the machine parameters

with the experiment, as well as the development of adequate beamline optics, novel diagnostics and data acquisition concepts. Groundbreaking experiments in a wide range of disciplines attracted the attention of the international science community and paved the way for the revolution in X-ray science observed today leading to the construction of a number of X-ray FEL user facilities covering the wavelength range from UV to hard X-rays. Many of the early FLASH experiments and the techniques pioneered at the facility stimulated important developments at the Linac Coherent Light Source at Stanford Linear Accelerator Laboratory SLAC, the first hard X-ray FEL (Bostedt et al., 2016a).

The goal of the present paper is to provide an overview of the progress made with accelerator science and technology, the development and the operation of the first VUV-FEL user facility, the techniques developed to make use of the new type of X-ray beams, and the results of pioneering experiments which opened new research fields.

2. Accelerator development

Originally, the international TESLA collaboration was exclusively motivated by the challenge of a colliding beams facility for electrons and positrons at center-of-mass collision energies in the TeV-region. As synchrotron radiation losses scale with the fourth power of the relativistic Gamma factor (particle energy in units of its rest energy), power losses of low rest-mass particles into synchrotron radiation would become prohibitively large in the TeV energy range. Thus, it was clear that acceleration of electrons or positrons up to TeV energies cannot be established within the circular ring concept. A "Linear Collider", consisting of two linear accelerators oriented head-on such that two powerful beams of electrons and positrons would collide, would be the only way out. To reach beam energies of (say) 500 GeV per particle species, each linear accelerator would extend over more than 10 kilometers in length, even if ambitious accelerating gradients of 50 MV/m could be realized.

The established and technologically proven technology of achieving many Megavolts of accelerating voltage per meter was (and still is) based on accelerating the particles inside a radiofrequency resonator. In order to give sufficient room to the particle beam, and in view of availability of powerful RF generators, resonator frequencies in the few GHz regime would be adequate, resulting in resonator diameters of a couple of Centimeters, see e.g. Fig. 1. In the early 1990ies, it was a consensus among most of the experts worldwide, that the RF resonators should be made from normal-conducting copper operated at room temperature and at resonator frequencies between 3 GHz and 11 GHz. While operation of such resonators at accelerating gradients of some 50 MV/m seemed feasible, the Ohmic losses in the resonator walls would, even for copper, result in dramatic heat losses, meaning that the resonators have to be operated in a pulsed mode, with duty cycles of typically 10^{-4}. Still, the total electric power consumption of the entire collider laboratory would be at the 200 MW level. For an illustration of a typical linear collider in normal conducting technology, see e.g. Raubenheimer et al. (1996).

In the early 1990ies, as an alternative technology choice for a TeV-scale linear collider, the employment of superconducting RF technology started to be seriously considered. Superconductivity offers indeed several advantages when applied to Linac technology. In the first place, one profits from the dramatically reduced Ohmic losses in the resonator walls. One might think that this offers both higher accelerating electric field and a much larger duty cycle. In fact, however, the maximum electric field E_{acc} is fundamentally limited by the critical magnetic field B_c of the superconductor, which is approx. $B_c \approx$200 mT for niobium at 2 K, corresponding to $E_{acc} \approx$ 45 MeV/m, averaged over the length of the cavity axis. In reality, such a value is seldom reached, and it was indeed among the essential missions of the international TESLA collaboration to establish a cost-effective technology to reliably produce Linac structures providing (at least) $E_{acc} \approx$ 23 MeV/m. While this became the decisive challenge for the TESLA Test Facility (TTF) (TESLA collaboration, 1993; Tigner, 1993; Edwards, 1993, 1995), further objectives included experimental verification of the component's performance in terms of field quality, electron beam dynamics, diagnostic tools and control procedures. Fig. 1 illustrates the key component of the accelerator, the superconducting radiofrequency resonator, consisting of nine coupled cavity cells. Due to its success it represents the core accelerator component of both FLASH and the European X-ray FEL until now.

While first plans for a Linac-driven free-electron laser (FEL) for wavelengths far below the visible were discussed at Stanford, USA (Cornacchia and Winick, 1992), it was realized very soon, that a superconducting accelerator like TTF would be perfectly suited to drive such device, mainly for the following reasons:

1. Due to the large iris diameter of the accelerator cavities, wake field effects, originating from the electro-magnetic interaction between the bunch charge and the surrounding walls, are very small compared to standard normal conducting cavities. It is thus possible to operate the Linac at a large range of electron bunch parameters without taking into account the potential impact on electron beam quality by such wake fields. This is particularly relevant in view of the kA-level peak current required by the FEL gain process and in view of the variety of ultra-short pulse lengths in the fs-regime requested by users.
2. Due to its excellent power efficiency, a superconducting Linac can be operated at very high duty cycle, up to continuous wave operation, a fact that allows for very high average brightness and for large flexibility in terms of timing structure.

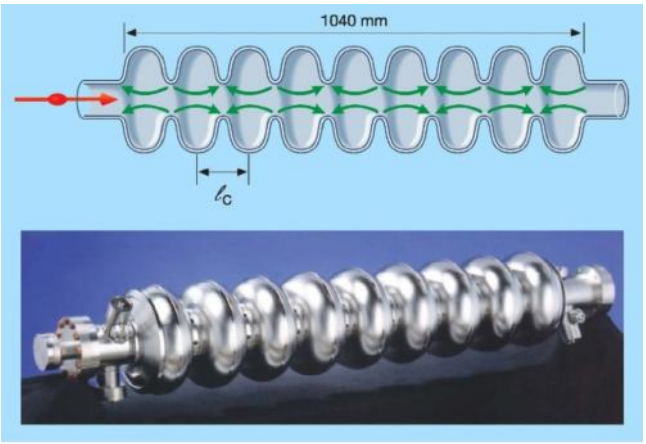

Fig. 1. Longitudinal cut (top) and photo (bottom) of the nine-cell RF resonators developed by the TESLA collaboration and used for FLASH. The resonators consist of pure niobium, cooled by superfluid helium of 2 K. They run at a resonance frequency of $f_0 = 1.3$ GHz and are operated in the standing-wave π-mode, where the direction of the accelerating electric field alternates from cell to cell when observed at a certain moment, as illustrated in the top sketch. The cell length $l_c = c/(2f_0)$ is chosen such that the field direction has inverted when the electrons, moving (almost) at speed of light c, pass from one cell to the next, thus providing continuous acceleration (Schmüser et al., 2014).

2.1. TESLA test facility, phases 1 and 2

Because of its superior properties, it was the visionary spirit of B.H. Wiik to develop superconducting FEL technology from the very beginning in a way applicable within a large range of wavelengths, down to the X-ray regime (Brinkmann et al., 1997; Altarelli et al., 2006). As there were no normal incidence mirrors at very short wavelengths, and no suitable coherent sources to seed the FEL process, the Self-Amplified Spontaneous Emission (SASE) principle (Kondratenko and Saldin, 1980; Bonifacio et al., 1984) was the most promising concept to adopt. It relies on amplification of spontaneous undulator radiation by many orders of magnitude within a single passage of a long undulator.

Based on the understanding that on the way to Ångstrøm wavelengths intermediate steps would be indispensable, it was more or less clear that, in terms of science applications, the most important step would be to jump from the microwave regime (Orzechowski et al., 1985; Kirkpatrick et al., 1989) across the wavelengths accessible by classical lasers down to wavelengths far below the visible. Thus, a jump by four orders of magnitude was proposed (Rossbach, 1996) to reach 100 nm, a wavelength regime where the SASE FEL principle is superior to other types of lasers. This could be done with the available TTF accelerator by adding a suitable electron source, a longitudinal bunch compressor generating the required kA-level peak current within the electron bunch, and a 14 m long undulator. This installation was called TTF FEL, Phase 1 or, in short, TTF1 FEL. Coordinated work on its realization started in 1994 at DESY, Hamburg, Germany.

Besides proving the principle, it was even more important to make broad scientific use of this new type of radiation source as soon as possible. Thus, in a second phase, the scientifically attractive vacuum ultraviolet (XUV) wavelength range between 6 nm and 40 nm was to be achieved. To this end, the TTF Linac had to be upgraded to maximum beam energy of 1 GeV, an additional bunch compressor and a 30 m long undulator had to be installed, and a hall for user experiments had to be built. A proposal (Åberg et al., 1995) of a two-stage realization of a SASE FEL user facility based on the TTF, as outlined above, was endorsed by an international advisory committee. This device was the TTF2 FEL, also called VUV-FEL. In April 2006, when regular user operation was established, it was renamed as Free-Electron LASer in Hamburg (FLASH) (Rossbach, 2016).

2.2. Free-Electron Laser studies at TTF

In the configuration operational during the first phase of the TTF project (TTF1), the average performance of the installed 16 cavities offered an operational electron energy somewhat beyond 200 MeV, corresponding to a mean accelerating gradient of approx. 13 MeV. This allowed, according to the FEL resonance condition Eq. (1)

$$\lambda_l = \frac{\lambda_u}{2\gamma^2}\left(1 + \frac{K^2}{2}\right), \tag{1}$$

for an FEL wavelength λ_l of some 100 nm when using a state-of-the-art undulator design. In Eq. (1), λ_u is the undulator period, γ is electron energy in units of the electron's rest mass, and K the undulator parameter. Indeed, FEL lasing was demonstrated on Febr. 22, 2000, at 109 nm wavelength, using two "TESLA modules" consisting of a cryostat with eight

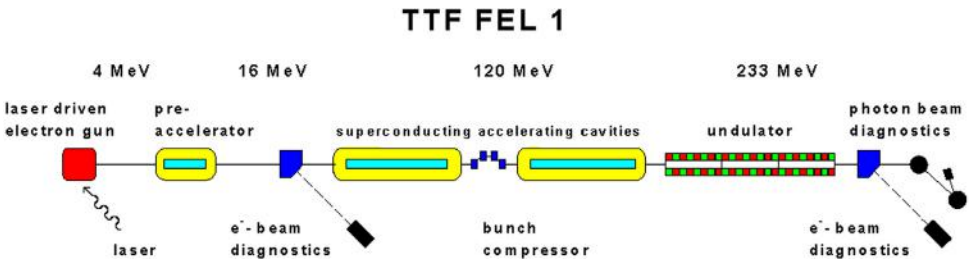

Fig. 2. Configuration of the TESLA Test Facility (TTF1) for the first observation of Self-Amplified Spontaneous Emission (SASE) in a free-electron laser (FEL) in the Vacuum Ultraviolet regime at 109 nm wavelength (11 eV) (Andruszkow et al., 2000). The observed free-electron laser gain (approx. 3000) and the radiation characteristics, such as dependency on bunch charge, angular distribution, spectral width and intensity fluctuations all corroborated the existing models for SASE FELs.

nine-cell cavities each, and a 14 m long undulator, see Fig. 2 (Andruszkow et al., 2000). A further important step was achieved in 2001 with the demonstration of FEL gain saturation at the predicted saturation power level and free tunability in the wavelength range between 80 and 120 nm (Ayvazyan et al., 2002a,b).

At shorter and shorter wavelengths, the impact of details in the particle distribution within the electron bunches and of disturbing external fields increases. Thus, an indispensable tool for the development of future high-gain FELs was a fully 3D time-dependent numerical simulation code capable of taking into account aspects like beam halos, wake fields and non-periodic focusing, to name a few. The code GENESIS 1.3 developed at that time at DESY is meanwhile a worldwide used reference tool (Reiche, 1999). For a recent review on the physics of free-electron lasers see (Pellegrini et al., 2016).

A complication that came up in these early years of high gain, single-pass FELs and that has to be mastered until now is related to the kA-level peak current needed to achieve a reasonably short FEL gain length. If such high electron densities would be generated at low, nonrelativistic particle energies, Coulomb space charge forces would increase the transverse electron bunch emittance very rapidly. The way out was (and still is) first accelerating the electron bunches to ultra-relativistic energies of, say, 100 MeV, where Coulomb forces are efficiently suppressed, because they are scaling according to $1/(\sigma_s\gamma^2)$, with σ_s the bunch length. Unfortunately, at ultra-relativistic energies any velocity differences are fading away, so the longitudinal compression is accomplished by a magnetic chicane. Here the path length difference of particles with different momenta is used. By introducing a correlated momentum chirp along the bunch, the compression results in the required kA-level peak current, combined with bunch lengths well below 100 fs. For an illustration, see Schmüser et al. (2014).

While such short bunch lengths are of utmost importance for users, they will make the synchrotron radiation emitted during magnetic deflection to be radiated coherently for all wavelengths larger than the bunch length. Coherent radiation means an increase of radiation power by many orders of magnitude as compared to the incoherent radiation regularly experienced. This effect was well known in principle but efficiently suppressed at previous electron accelerators where the bunch length was of comparable size as the metallic vacuum beam pipe. The new powerful coherent synchrotron radiation (CSR) generates very large electro-magnetic fields that are capable to seriously impair the electron bunch quality in terms of momentum and transverse phase space distribution. It was thus indispensable to understand this effect theoretically (Derbenev et al., 1995, 1996) and model it numerically (Limberg et al., 2002; Zagorodnov and Dohlus, 2011), see Fig. 3.

The upgrade of TTF in terms of beam energy went on by fabrication, installation and commissioning of three further accelerating TESLA modules. They were installed into a new tunnel, including a 30 m long fixed-gap, permanent magnet undulator (Pflüger, 2000), a collimator system protecting the undulator from accidental losses of electrons, and a second bunch compressor (Limberg et al., 2002) which made it possible to increase the peak current to approximately 1–2 kA as required for FEL operation, see Fig. 4.

At a beam energy of 445 MeV, FEL gain and saturation was demonstrated at 32 nm wavelength (Ayvazyan et al., 2006). Again, experimental evidence, including GW-power radiation, agreed well with the theoretical expectations, and was registered with relief by everybody worldwide working on FELs at even shorter wavelengths.

While measuring the total energy of photon pulses was quickly realized (though by far not trivial, e.g. due to the huge dynamical range to be covered), detailed experimental information about its length was very difficult to achieve. From the accelerator point of view, its basis is, in the first place, the longitudinal charge distribution inside the electron bunch. A number of approaches were launched to determine this important parameter:

- The electro-optical sampling (EOS) technique uses the transition radiation pulses, emitted by the ultrashort electron bunches, to induce a birefringence in an optically active crystal, and this birefringence is sampled with polarized ultrashort laser pulses. The main challenge was to establish the time overlap between the laser pulses and the electron bunches (Brunken et al., 2003). Probing the electric field of the electron bunches at resolution better that 100 fs could be demonstrated already in 2005 (Steffen et al., 2005).
- A more direct measurement of charge distribution in the time domain could be established by a rapid transverse deflection system (TDS). It acts on the electron beam by an RF resonator operating on a transverse deflecting mode

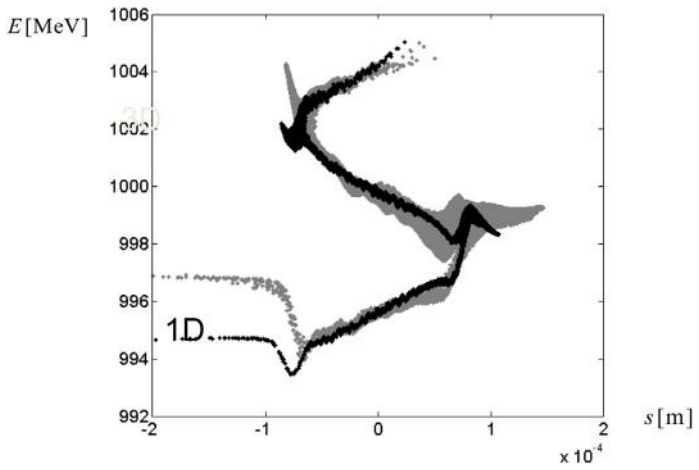

Fig. 3. Illustration of the longitudinal phase space distribution of an electron bunch at FLASH when numerically simulated (Zagorodnov and Dohlus, 2011). Vertical axis: electron energy horizontal axis: longitudinal coordinate inside the electron bunch. Coulomb space charge forces are taken into account as well as cavity wake fields and coherent radiation effects in 1D (black) and in 3D (gray), respectively. Note the short bunch length below 100 μm rms achieved by longitudinal bunch compression in two magnetic chicanes.

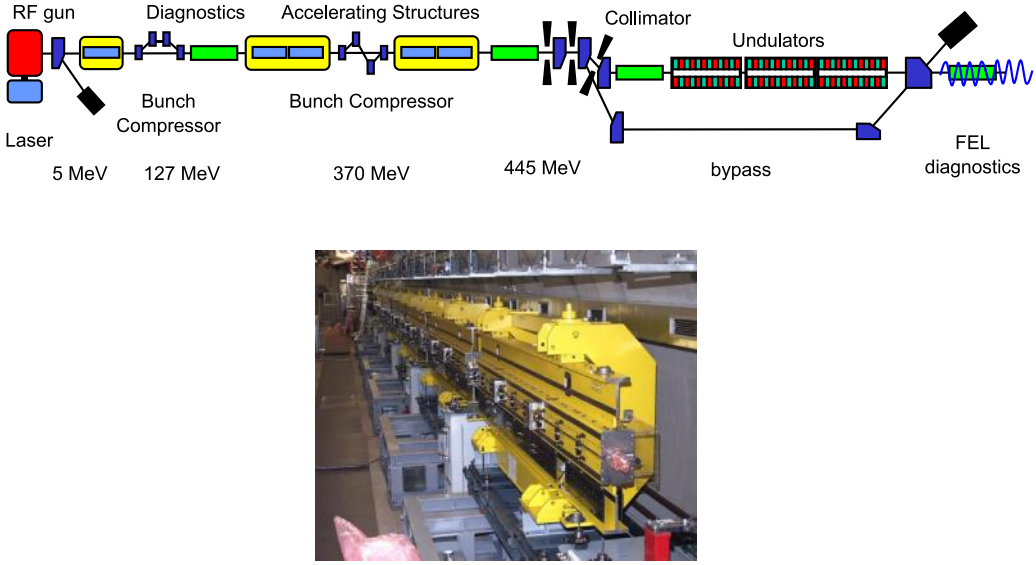

Fig. 4. Top: Configuration of the TESLA Test Facility (TTF2) as of Jan. 14, 2005, for demonstration of 32 nm FEL wavelength. The accelerator tunnel was extended to 250 m to give room for more accelerator modules, a collimator system and a 30 m long undulator. Also an experimental hall was added (not shown here), which made the total lengths of the facility 330 m. **Bottom:** Photo of the 30 m long FLASH undulator after installation into the FLASH accelerator tunnel. At this time, it was by far the longest undulator constructed and installed for FEL purposes (Pflüger, 2000).

synchronized with the frequency of the regular Linac. The transversely streaked bunch is observed on a screen where the longitudinal profile is translated in a transverse one — in some sense like an oscilloscope using an ultra-relativistic electron beam. This comes at much higher costs than EOS and requires several meters space of valuable accelerator beam line, but it results in much better resolution. If a static magnetic dipole deflection is applied in the orthogonal direction, the momentum distribution can be observed simultaneously, see Fig. 5. TTF2 FEL was the first FEL using such device, demonstrating a temporal resolution of approx. 15 fs rms (Hüning et al., 2005).

- In a quite different approach, radiation carrying the time information of the bunch is observed in the frequency domain. This radiation can be the optical transition radiation (OTR) emitted when electrons cross the interface of two media of different dielectric constants. Often, a metallic foil is used. For wavelengths larger than the bunch lengths, the OTR is emitted coherently, so the intensity is dramatically increased. It is thus the infrared and THz wavelength regime which contains the relevant information on the longitudinal charge distribution on a scale down to a few Micrometers. An infrared spectrometer was invented (Delsim-Hashemi et al., 2005) to measure the relevant spectral

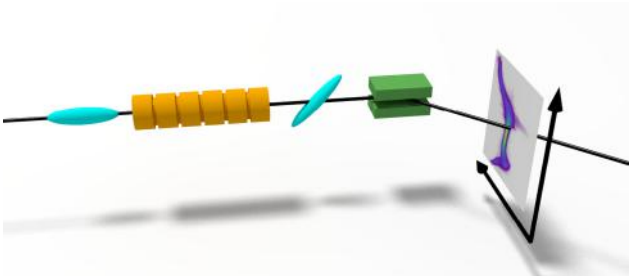

Fig. 5. Schematic of the transverse deflection system installed at FLASH. The electron bunch (blue) travels from left to right and receives a time-dependent vertical deflection when passing the rf resonator (yellow). A magnetic dipole deflection (green) in the orthogonal (horizontal) direction provides momentum dispersion. The image on the observation screen (right) provides information on the longitudinal charge distribution and momentum distribution within the electron bunch simultaneously.
Source: Courtesy C. Lechner and T. Plath.

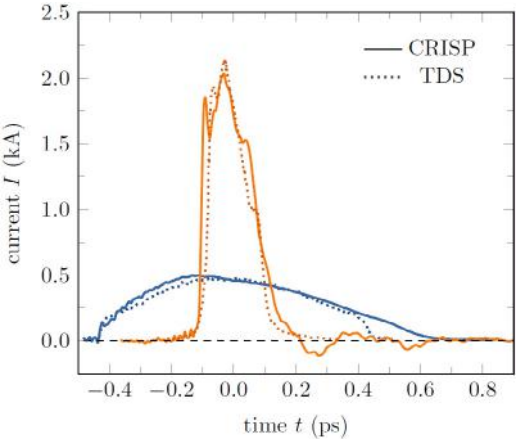

Fig. 6. Two different longitudinal electron bunch current profiles measured at FLASH with a TDS (dotted curves) and reconstructed from the OTR power spectrum (solid curves), measured with the CRISP4 single-shot infrared spectrometer (Wesch et al., 2011). The measurement in frequency domain is particularly powerful in making bunch structures in the Micrometer range visible.

range within a single shot, which is important, since the charge distribution might fluctuate from bunch to bunch. In spite of the loss of phase information when measuring the power spectrum, the most likely compact profile can be reconstructed by phase retrieval methods (Lai and Sievers, 1997). As the method works in the frequency domain, it is particularly attractive when it comes to bunch structures in the few Micrometer range, where the TDS method is limited, see Fig. 6 for a comparison.

2.3. Ten years of progress on FEL technology at FLASH

2.3.1. Steps towards 4 nm wavelength

After regular user operation of FLASH started in 2006, most of the running time was dedicated to a large and ever growing community of scientific users. They were asked and authorized to define the parameters of the facility, which was generally operated on a 24/7 basis. The range of accessible parameters was of course limited by the technical constraints. To expand the scope of experimental possibilities, and to consolidate machine performance, quite some fraction of the beam time was regularly devoted to studying accelerator issues and FEL techniques.

The most significant progress was certainly achieving even shorter FEL wavelengths. In August 2006, 700 MeV beam energy was reliably obtained from the installed five TESLA modules (see Fig. 4), and FEL gain saturation was achieved at 13.7 nm wavelength with radiation pulse energies of 70 μJ, corresponding to 10 GW radiation power (Ackermann et al., 2007).

When an FEL operates in the saturation regime, the microbunching of the electrons starts to develop higher harmonic content which leads to appearance of odd harmonics in the FEL spectrum, see e.g. (Schmüser et al., 2014). In fact, 0.25 μJ energy content was observed at the 3rd harmonics (4.6 nm) and 10 nJ at the 5th harmonics (2.75 nm), respectively. These pulses were intense enough that they could be used scientifically, see e.g. (Gutt et al., 2009, 2010). This achievement

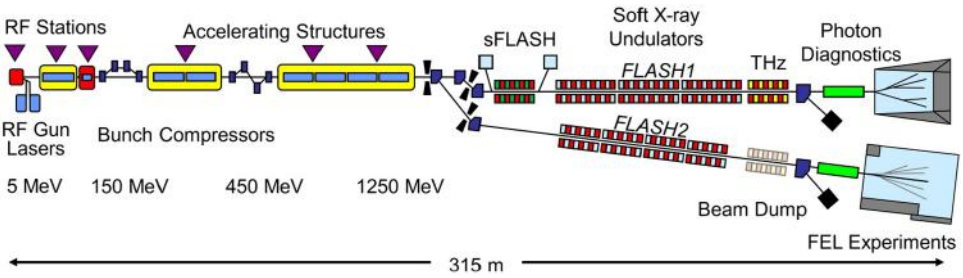

Fig. 7. Schematic layout of FLASH with seven TESLA accelerator modules installed. The second FEL beamline (FLASH2) is also shown, see text. The accelerating section operating at 3.9 GHz (3rd harmonic of the fundamental accelerating frequency) is located downstream of the first regular TESLA module and colored red. "sFLASH" indicates a variable-gap undulator section to study seeding options, see text.

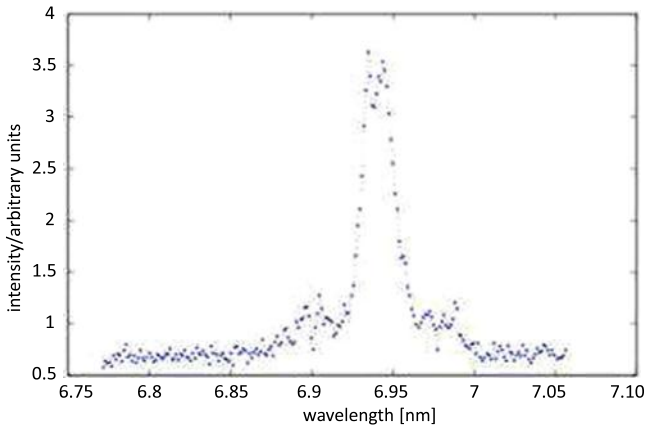

Fig. 8. Single-shot spectrum of FEL radiation below 7 nm (fundamental harmonics) at FLASH, DESY as of Oct. 2007. *Source:* From Rossbach (2008).

was not only the proof that higher FEL harmonics can be attractive to users, but it was also the first time that the so-called water window became accessible to FELs, a wavelength range transparent for aqueous systems and thus crucially important for the investigation of biological samples.

For achieving the FLASH design wavelength of 6 nm, the full design energy of 1 GeV was needed, which could be realized by installation of two more TESLA modules. This happened in 2007 and was (and still is) the maximum number of Linac modules fitting into the existing accelerator tunnel, see Fig. 7. FEL operation at 6.5 nm was then achieved on Oct. 5, 2007 (Rossbach, 2008). Fig. 8 shows an early single-shot wavelength spectrum.

With the TESLA modules exceeding the design accelerating fields, even 1.25 GeV beam energy could be realized, thus reaching 4.1 nm wavelength in Sept. 2012. Fig. 9 summarizes the wavelength steps from 109 nm down to 4 nm at TTF/FLASH over nine years. None of these steps came for free, because most of them stood for a challenge in entering a parameter range where no prior experience was available. Some of these achievements will be illustrated in the following. Most of them are characteristic for high-gain FELs in general, some of them for a superconducting one like FLASH. More details can be found in (Schreiber and Faatz, 2015).

2.3.2. Third-harmonic, 3.9 GHz rf linearizer

Compression towards ultra-short bunches needs, in the first place, full control of longitudinal phase space dynamics. This is compromised by the sinusoidal time dependence of the accelerating field which is imprinted to the longitudinal momentum profile within the bunch. This effect was removed at FLASH by installation of a 3rd harmonic rf system in 2009, see Fig. 10.

The 3rd harmonic RF system allows to linearize the accelerating field's sinusoidal time dependence at least in the time range where the bunch is present, and it adds a degree of freedom when imprinting the needed linear momentum chirp to the bunch. Fig. 11 illustrates the effect of this linearization during an early test at FLASH in 2010 (Harms et al., 2010). This system was an important asset towards more controlled compression of the electron bunch.

2.3.3. Generation of small emittance beams

Providing a small electron beam emittance was an issue for high-gain FELs from the very beginning. But the challenge became the harder the shorter the FEL wavelength was. The reason is, essentially, that electrons passing the undulator at

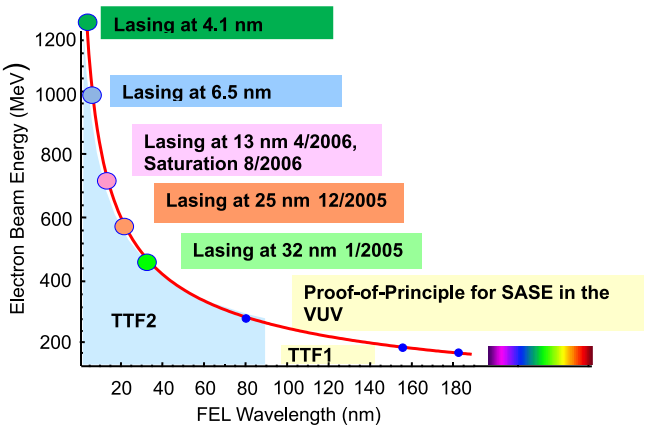

Fig. 9. History of world record demonstrations of FEL gain at shorter and shorter wavelengths at FLASH. In all cases, FEL saturation was achieved and agreement with FEL theory could be proven.

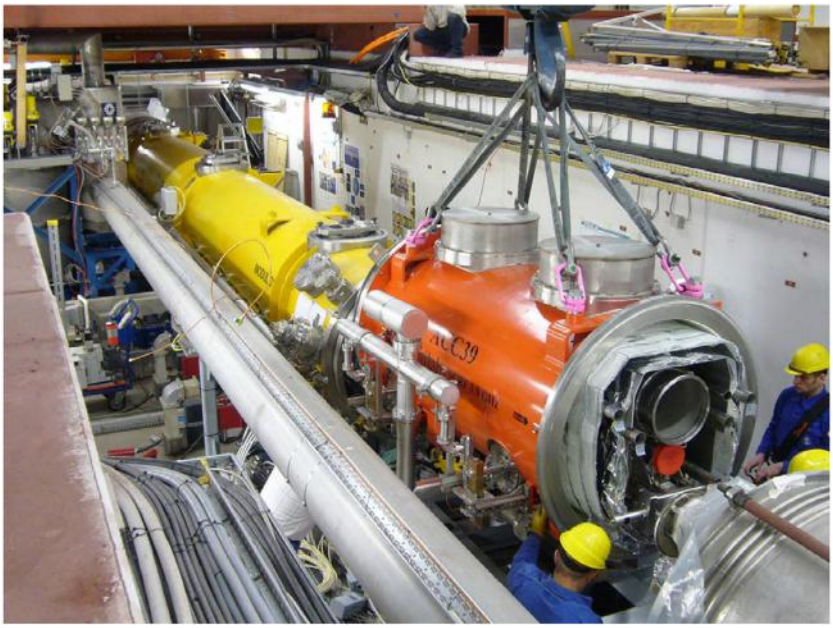

Fig. 10. Installation of the cryo-module (red) containing four 3.9 GHz superconducting cavities. A neighboring regular TESLA accelerating module containing eight 1.3 GHz nine-cell cavities is also seen (yellow).
Source: Courtesy: Kai Jensch, DESY (Schreiber and Faatz, 2015).

an angle experience a reduction in longitudinal velocity compared to the on-axis particles. This results in smearing the microbunching process which becomes more critical the shorter the FEL wavelength is. The magnitude of the longitudinal velocity spread can in principle be reduced by arranging the electron optics for a large beam size (i.e. a large beta function). But this would result in a lower electron density and longer gain lengths, so there is an optimum in between. The beam emittance ε is, loosely speaking, the product of transverse beam size and beam divergence, and a rough estimate calls for an emittance

$$\varepsilon < \frac{\lambda_l}{4\pi} \tag{2}$$

for FEL operation at the wavelength λ_l (Schmüser et al., 2014). Fortunately there is a mechanism in most accelerators, called adiabatic damping, by which the emittance is decreased almost automatically in inverse proportion to the beam energy. It is thus the "normalized" emittance $\varepsilon_n = \varepsilon/\gamma$ that is conserved during acceleration along a Linac. But still, due to the $1/\gamma^2$ scaling in Eq. (1), there remains a factor of $1/\gamma$ to be gained when reducing the FEL wavelength. It is easy to calculate from these equations a normalized emittance of $\varepsilon_n < 10^{-6}$ m to be required for FLASH operation at 6 nm.

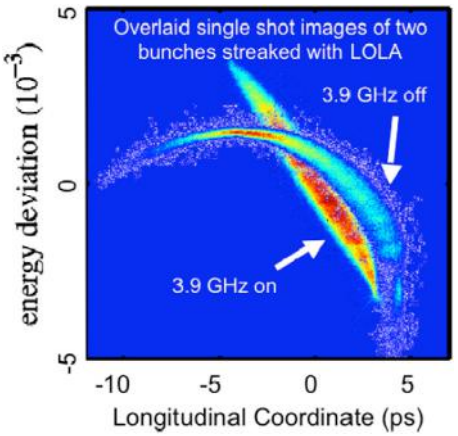

Fig. 11. Comparison of longitudinal bunch distribution in FLASH with/without the 3rd harmonics RF system in operation (from (Harms et al., 2010)). The transverse deflecting RF system mentioned before (called LOLA) was used for this measurement.

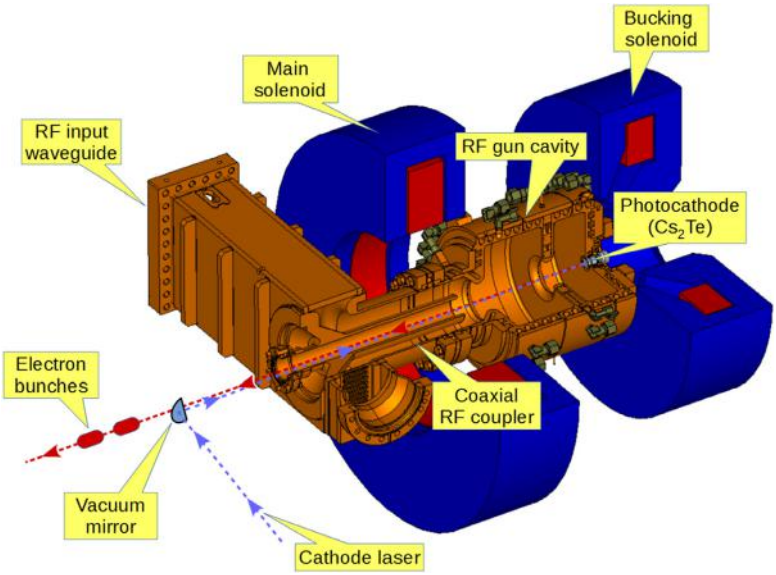

Fig. 12. Cut through the electron source of FLASH. The Cs_2Te photocathode is mounted at the backplane of a 1.3 GHz copper cavity. It is excited in a TM_{010} like mode such that the electron field assumes its maximum value at the cathode. The RF power is guided to the cavity through a waveguide and a coaxial coupler in a symmetric way thus generating as little field asymmetry as possible. The UV cathode laser beam is reflected onto the cathode by a small mirror outside the electron beam axis. A solenoid coil provides transverse focusing, while a second solenoid called "bucking coil" compensates the magnetic field in the cathode region, where the electrons have very low momentum.
Source: Courtesy I. Isaev, DESY.

In consequence, DESY initiated an ambitious program towards an electron injector providing the required small beam emittance. The concept is based on a laser-driven photo-cathode mounted inside a 1½-cell radio-frequency cavity (Fraser et al., 1986). The challenge was to combine a peak accelerating field on the cathode of some 50 MeV/m with an RF pulse length as long as 800 μs needed for the long bunch trains at FLASH. While the large electric field, needed to keep Coulomb forces under control, made it impossible for superconductivity to be applied, its combination with the long RF pulses required massive water cooling to remove the Ohmic losses in the normal conducting resonator. Fig. 12 shows the FLASH electron injector, developed at the DESY site in Zeuthen near Berlin.

To conduct the R&D program, the Photo-Injector Test facility Zeuthen (PITZ) was established, located in the DESY branch in Zeuthen. A normalized emittance of $\varepsilon_n \approx 1.3 \cdot 10^{-6}$ m (rms) was already demonstrated in 2007 (Asova et al., 2007) for the bunch charge of 1 nC, which was the design charge at that time. In fact, this rather large charge was the result of a conservative approach giving room to tolerances in the bunch compression process, accepting that only a fraction of the bunch charge would contribute to lasing. Based on this assumption, determining the emittance of the entire (so-called

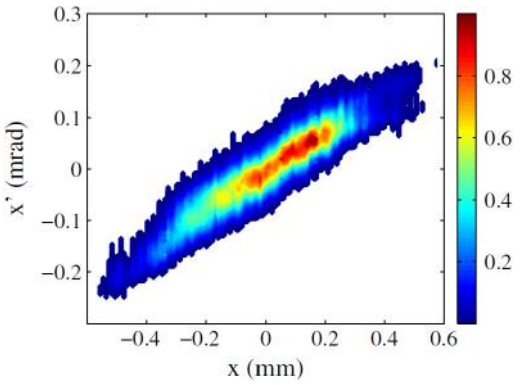

Fig. 13. Measurement of world-record small emittance at PITZ for 0.1 nC bunch charge. The result for the vertical phase space distribution is similar to the horizontal one shown here.
Source: From Krasilnikov et al. (2012).

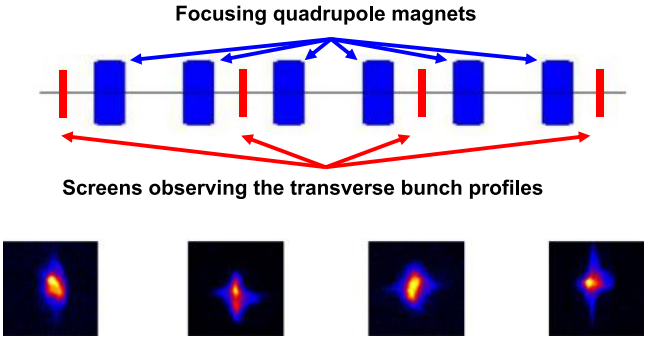

Fig. 14. Schematic illustration of emittance measurement established at FLASH using the four-screen method.
Source: Courtesy L. Staykov, DESY.

projected) emittance was conservative anyhow, since the smaller slice of the bunch actually lasing would certainly have a smaller emittance.

Further experimental optimization yielded unprecedented low emittance beams in the whole charge range between 0.02 nC and 2 nC (Krasilnikov et al., 2012). As an example, a projected, normalized emittance of $\varepsilon_n \approx (0.212 \pm 0.006) \cdot 10^{-6}$ m (rms) was demonstrated for 0.1 nC bunches, see Fig. 13. The ability to control the phase space distribution at such small bunch charges is particularly attractive since it provides very small emittance values and permits generation of very short bunches (see below).

2.3.4. Tomographic reconstruction of emittance

As mentioned before, the bunch formation process, in particular the bunch compression, comes along with powerful collective effects. They do not only disturb the longitudinal phase space distribution (see Fig. 3) but may also prevent conservation of the normalized emittance. It is thus mandatory for controlled FEL operation to measure the transverse phase space distribution after the bunch formation is completed.

Since the transverse phase space distribution of the electrons cannot be assumed to be a Gaussian one, a simple observation of the spot size on a single observation screen cannot reveal the particle distribution in phase space. The standard procedure is thus to observe the image changes on a screen while the electron optics is varied in a controlled way upstream of the screen. Each optics setting corresponds to a projection of the phase space distribution under a different angle. A very precise and reliable method to do so uses several screens with fixed, well-known linear optics properties in between (Löhl, 2005; Löhl et al., 2006), see Fig. 14. This measurement can be performed very rapidly since no change of magnetic components is required. This also guarantees that no space charge effects will disturb the results, which is always an issue when varying the focusing of a small-emittance, kA-level electron bunch.

Recovery of the phase space distribution from the screen images is, in principle, ambiguous, since information is lost as a result of the projections. Thus, a tomographic reconstruction technique was implemented using the maximum entropy algorithm (MENT) (Scheins, 2004). It is based on the idea to find the most likely phase space distribution which could explain the observed screen images. FLASH was the first FEL where such a system was implemented.

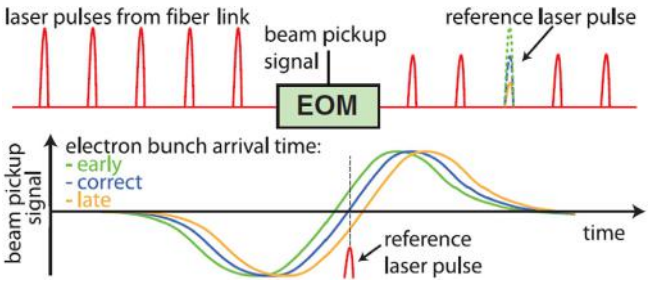

Fig. 15. Operation principle of the electron bunch arrival-time measurement based on an electro-optical modulator (EOM). *Source:* From Löhl et al. (2010).

2.3.5. Femtosecond-level control of electron bunch timing

While femtosecond-scale photon pulses are an invaluable asset of high-gain FELs, both their generation and their scientific use rely on the ability to control the timing of electron bunches with fs precision.

The main contribution to potential timing jitter of electron bunches is due to dispersive effects in the magnetic bunch compressor chicanes. As described before, the compression is accomplished by intentionally introducing a correlated momentum chirp along the bunch and then using the energy-dependent path length in such chicanes. Unavoidably, at the same time such a chicane also converts any beam energy jitter into an arrival-time jitter at the FEL undulator. Beam energy jitter at the chicane can be caused by amplitude fluctuations of the accelerating fields upstream of the chicane or by variations of the rf phase.

In the first place, timing requires a reference clock, which was realized at FLASH by a mode-locked fiber laser. Next, one needs a tool comparing the arrival time of the electron bunches at a certain location to the time stamp derived from the clock laser pulses. To this end, a novel electro-optical detection scheme was developed (Löhl et al., 2010). The beam-induced bipolar signal from a pickup electrode with more than 10 GHz bandwidth is utilized to modulate the amplitude of the laser pulse train by means of a commercial Mach–Zehnder type electro-optical modulator (EOM), see Fig. 15. The relative timing between a reference laser pulse and the zero-crossing of the pickup signal translates into a modulation voltage of the laser pulse. By comparing the laser pulse energy of the sampling pulse to that of the adjacent pulse it was possible to deduce the electron arrival time in respect to the clock laser pulses at as low as 6 fs resolution (rms) (Löhl et al., 2010).

One backbone of this system is a stable distribution of the laser clock pulses along the entire distance from the fiber laser to the various locations of beam pickup stations, i.e. over several hundred meters. This was accomplished by active stabilization of an optical fiber based timing link, where 10 fs long-term stability was achieved over more than 300 m distance (Kim et al., 2007).

With the help of the described bunch arrival detection and two beam-based feedback systems acting on the RF field amplitudes, it was possible to stabilize the arrival time jitter to some 12 fs (Pfeiffer, 2014). It should be noted that this possibility is unique to superconducting accelerators due to the long duration of the RF pulse. Almost simultaneously, also the electron bunch compression was stabilized, yielding a significant reduction of the FEL pulse energy jitter.

Finally, further improving and combining such kind of tools with THz-streaking diagnostics of photon pulses (Ivanov et al., 2018) into a facility-wide system, a timing stability of 30 fs (rms) was demonstrated for 90 fs long photon pulses at FLASH (Schulz et al., 2015). This performance is expected to be improved for shorter photon pulses.

2.3.6. Generation of ultra-short photon pulses

Electron bunch lengths of a few 100 fs are an almost automatic result of longitudinal bunch compression when generating the kA-level peak currents needed for high FEL gain. Some users, however, desire photon pulses as short as possible. The shortest FEL pulse length supported by the basic FEL process is determined by the number of microbunches interacting with the radiation field within one FEL power gain length, the so-called cooperation length (Bonifacio et al., 1984). This translates into the coherence length τ_{coh} of SASE pulses which depends primarily on FEL gain and wavelength (Saldin et al., 2000; Schmüser et al., 2014). A typical value experimentally determined at FLASH is approx. 3 fs at 8 nm wavelength (Singer et al., 2012). A photon pulse of such duration generated in an FEL can be considered fully coherent, due to the excellent degree of transverse coherence of FEL radiation (Ischebeck et al., 2003). The spectrum of such a pulse will consist of a single, smooth spike in frequency domain, rather than the spiky spectrum of longer SASE pulses.

The most direct way of generating such short FEL pulses would be based on electron bunches as short as the cooperation length (Rosenzweig et al., 2008). This cannot be accomplished by simply more aggressive longitudinal compression because of the coherent space charge forces. The alternative approach followed at FLASH was to install a new photo-injector laser system providing shorter electron bunches already at the cathode, and running at small bunch charges between 20 pC and 100 pC (Rönsch-Schulenburg et al., 2014). The latter approach has the advantage that the compression factor can be reduced thus improving the stability, because bunch length and timing become less

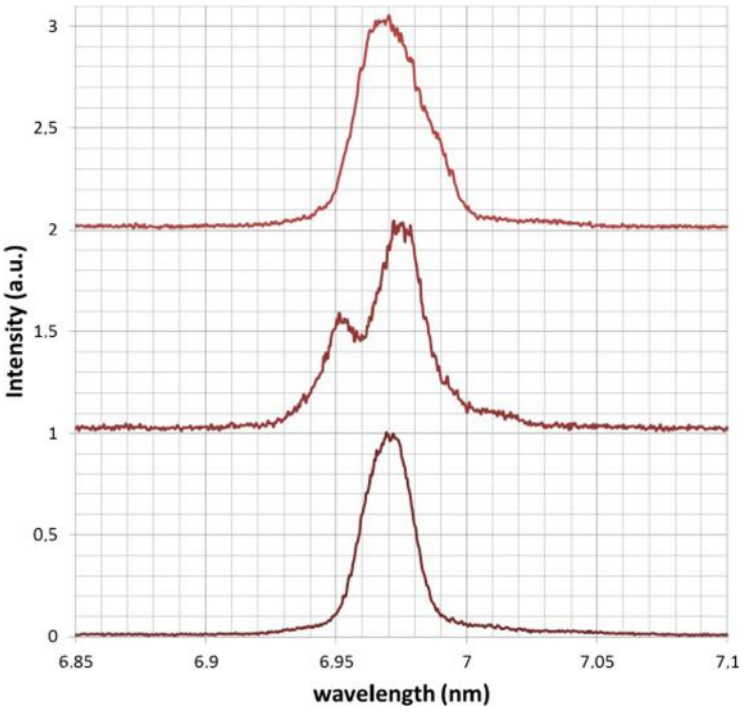

Fig. 16. Three typical examples of SASE FEL-spectra measured at FLASH, when the short-pulse laser was applied at a bunch charge of 55 pC, from Rönsch-Schulenburg et al. (2014). It is important to note that these are single-shot spectra generated by a single electron bunch not yet reaching FEL saturation. Due to the start-up from noise in the SASE-mode of FEL operation, one expects a number of spikes in frequency domain randomly distributed within the FEL's bandwidth, if the radiation pulse length exceeds the coherence time (Saldin et al., 2000). This behavior is smeared out if averaged spectra would be observed, and also in FEL saturation regime. From the appearance of (almost) single spikes in the single-pulse spectra one can therefore conclude that the pulse length is close to its minimum value determined by the coherence time.

susceptible to RF fluctuations, and because collective effects are decreased. Indeed, almost-single-spike FEL pulses could be demonstrated at FLASH, see Fig. 16 (Rönsch-Schulenburg et al., 2014). From the appearance of such type of spectra one can conclude that the pulse duration is close to its minimum value determined by the coherence time.

2.3.7. Seeding

An alternative way towards better longitudinal coherence is initiating the FEL process by overlapping the electron beam with a suitable photon pulse at the entrance of the FEL undulator. If the photon pulse is longitudinally coherent, and if its intensity exceeds the spontaneous undulator radiation level, its coherence properties will be transferred to the FEL gain process such that the FEL output pulse replicates the coherence properties of the input (Huang and Kim, 2001).

The most direct method would certainly be to inject an externally generated photon pulse of desired parameters (wavelength, intensity, pulse length, coherence, polarization) (DiMauro et al., 2003). For short wavelengths in the XUV regime, generation of sufficiently intense photon pulses is extremely challenging (Hergott et al., 2002), even more so if a high pulse repetition rate is required to match the high bunch rate at FLASH (Willner, 2012). To attain EUV wavelengths with classical lasers, up-conversion of photon frequencies by means of nonlinear high-harmonic generation (HHG) in gases is utilized (Ferray et al., 1988).

To study HHG-seeding at FLASH, a HHG source at 38 nm was realized (Maltezopoulos et al., 2014), and a 10 m long dedicated variable-gap undulator section was installed, named sFLASH (schematically indicated in Fig. 7). Direct HHG-seeding was demonstrated in 2012 (Ackermann et al., 2013). With the sFLASH-undulator accordingly tuned, not only the fundamental FEL-wavelength at 38 nm was seeded, the smallest directly seeded FEL wavelength to date, but also its 2nd harmonic at 19 nm. With the observed energy contrast of the seeded FEL photon pulses of only a factor of five above the competing SASE pulse energies, and in view of the known difficulties in reaching even shorter wavelength than 38 nm (in particular at high repetition rates) (Hergott et al., 2002; Willner, 2012), the HHG technique was considered not attractive for seeded user operation at FLASH.

An alternative to HHG seeding consists of modulating the energy profile of the bunch by a laser pulse at larger wavelength λ_{las} (e.g. 267 nm), where plenty of laser power can be delivered, and then generating a density modulation in the electron bunch by passing a weak magnetic chicane. If the introduced energy modulation exceeds the original energy spread in the bunch, the density modulation will contain many high harmonics n/λ_{las} which may seed the FEL gain in a subsequent, appropriately tuned undulator. This method has been named High-Gain Harmonic Generation (HGHG) (Yu,

1991). It is successfully employed for user operation at the FERMI FEL (Allaria et al., 2012), and it was also demonstrated at FLASH at 38 nm wavelength, corresponding to the n=7th harmonic of the modulating seed laser (Hacker et al., 2015). To reach lasing at shorter wavelength down to a few nm in seeded operation driven by an external laser either cascaded HGHG (Allaria et al., 2013) implemented at the FERMI FEL or Echo Enabled Harmonic Generation (EEHG) are possible solutions. First lasing in an EEHG setup was demonstrated at the SDUV-FEL test facility in Shanghai (Zhao et al., 2012). Later generation of very high harmonics was shown at Stanford (Hemsing et al., 2016) and recently also tested at FERMI for lasing down to 5 nm (Allaria et al., 2019).

Both the HHG, the HGHG, and the EEHG seeding methods require the availability of an external seeding source. A quite different approach was invented at FLASH, later coined self-seeding (Feldhaus et al., 1997). It starts with the conventional SASE process and, at a sufficient intensity level, a narrow spectral range is cut out which is then used for seeding in a second FEL stage. Depending on the wavelength regime, the spectral filtering is accomplished either by gratings or Bragg crystals. As the latter one can be arranged within a rather compact unit, it was successfully implemented at LCLS/SLAC (Amann et al., 2012).

2.3.8. Controls for a superconducting FEL

At the time when FLASH was constructed, controlling a superconducting FEL like FLASH represented a bunch of challenges that could not be mastered by just using commercially available solutions. This fact is mainly related to the extraordinary requirements on timing on the femtosecond scale and to the large number of electron bunches a superconducting Linac is capable to accelerate which can, if misdirected, easily destroy accelerator components.

Operation of two or more beam lines by one accelerator (see section k) requires a reliable synchronization of subsystems, a machine protection system (MPS) that acts according to the source of a technical failure, and a control system with separated parameters for each beam line. At FLASH, the control system provides a clear separation of these different tasks. It is called DOOCS (Distributed Object Oriented Control System) and makes use of hardware based synchronization and protection. All critical signals are distributed via separate timing and machine protection fiber optical networks. Software controlled parameters are transferred via Ethernet.

10 Hz is the typical rate of RF pulses and trigger frequency of FLASH. It is derived from the 50 Hz mains frequency to be synchronous with the dominating noise source. Within each RF pulse of 800 μs duration, trains of electron bunches can be accelerated. In terms of controls, there is large flexibility on the internal timing pattern within each bunch train. It is the task of the timing system to inform subsystems about the characteristics of all individual bunches before a bunch train arrival. For high flexibility in defining the structure of the bunch trains, the timing of bunches can be defined based on a 9 MHz raster. This 9 MHz raster allows 4.5, 3.3 or 1 MHz (or lower) bunch repetition rates which can be supported by the current photo injector laser system.

The operator defines for every electron bunch a source, the destination, the maximum allowed charge and an optional special usage. The "source" in FLASH is one of the three photo injector lasers. Beam lines or electron dumps can be defined as destinations. The charge information is used by a toroid protection system and can be used by diagnostics and for beam loading compensation by the low level RF control system (LLRF). Special diagnostics, like the Transverse Deflecting Structure to measure the bunch length (see Fig. 5), can pick out a single bunch, and all other subsystems are informed.

The timing system distributes a table with 7200 entries (800 μs * 9 MHz) prior to the release of a bunch train. From this table the bunch related clocks and triggers are extracted for the local devices. A module of the machine protection system (MPS) is located in the crate of the main timing module and provides information about restrictions in the accelerator via a hardware connection. If e.g. the operator wants 100 bunches in a beam line, but a screen is inserted, the MPS tells the timing to allow one bunch only. In addition, the MPS can inhibit the photo injector laser for a certain beam line within a microsecond after an interlock event occurred. Restrictions in one beam line do not hinder the operation of the other lines.

With one central timing module the topology is a multi star. All long links are drift compensated to a level of 10 ps rms between the sender and the receivers. The central node sends triggers and data encoded on a stable 1.3 GHz clock derived from the master oscillator. At the respective receiver up to 23 individual channels can be configured to deliver clocks, extracted data and delayed triggers. Channels can also be combined to provide complex outputs.

Most of the front-end crates are equipped with a timing receiver. With the information encoded in the timing it is defined to which beam line all bunches in a subsystem belong to. This allows the server processes to identify for every beam line e.g. the first bunch and to store the bunch information in separate archives. The LLRF system is using this timing information to define the required RF pulse profile.

Data taken from fast ADCs by the front-end processors are marked with an RF pulse number and sent to central data acquisition servers (DAQ). The DAQ collects the data from more than 100 crates. Middle layer servers attached to the DAQ are receiving these synchronized streams to process them. The results can be used as feedbacks or in operator displays. Selected results and raw data are stored on disk with tens of TB capacity for about two weeks or permanently on tape. In case of a critical event, the cause can be analyzed later on with full bunch resolution from all diagnostics and RF controls. Some FEL user experiments are using this DAQ system as well to archive their measurements together with data from the accelerator.

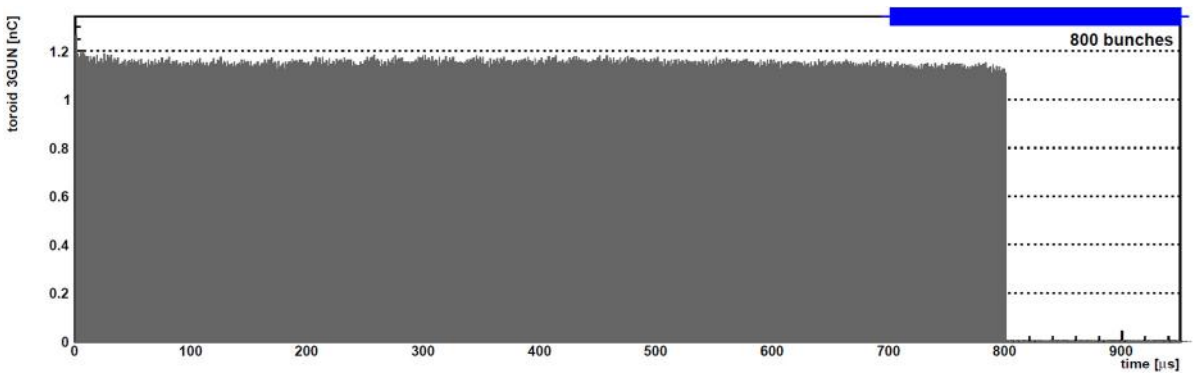

Fig. 17. Train of 800 electron bunches accelerated within a 800 μs long RF pulse in the FLASH superconducting Linac.

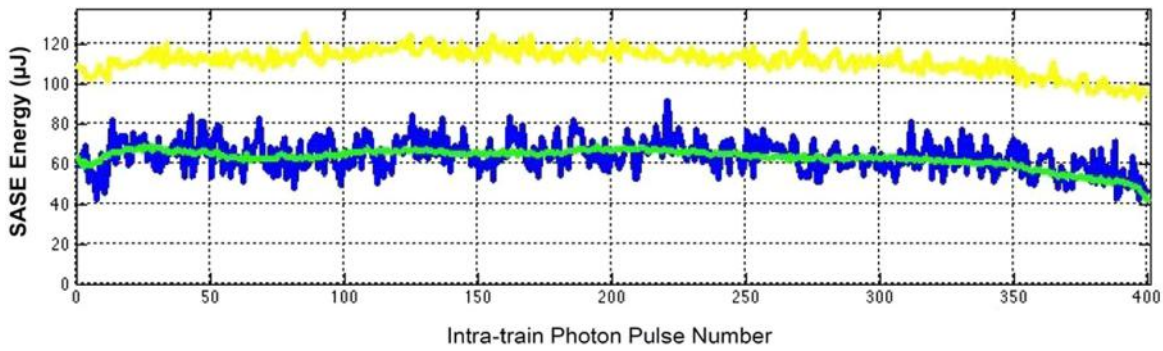

Fig. 18. Pulse energy of 400 photon pulses in one train, pulse spacing 1 μs, photon wavelength 9.9 nm. Blue: Actual value, Green: Average, Yellow: Maximum pulse energy achieved during a twelve-hour user run.
Source: Courtesy S. Schreiber, DESY, reproduced from Honkavaara et al. (2015).

2.3.9. Long bunch trains

As pointed out above, it is among the key benefits of a superconducting Linac that it can be operated at a large duty cycle. In principle, even cw operation is an option, but this would require either operation at a moderate accelerating gradient resulting in a longer accelerator, or a very powerful (and energy-hungry) liquid helium refrigeration plant would be needed, see e.g. (Rossbach, 2016). Also a low-emittance electron gun operating in cw mode is a major challenge.

The compromise found for FLASH is operating the Linac at 10 Hz repetition rate with 800 μs long flat-top RF pulses suitable for acceleration, thus running at a duty cycle of approx. 1%. For FEL user operation, the entire accelerator system, from the electron gun through the FEL photon diagnostics was prepared for 1 MHz bunch repetition rate within the RF pulses, resulting in up to 800 electron bunches accelerated at 10 Hz repetition rate, see Fig. 17. The challenges included stability of RF parameters over the entire bunch train, controls of electron bunch diagnostics at full repetition rate, and beam loss protection shielding the undulator system from radiation damage (Fröhlich, 2009).

For user operation the stability of FEL photon pulses is what matters rather than the apparent stability of electron bunches, which may contain some intrinsic variations not showing up in the measurable electron bunch properties but having impact on the FEL gain. Fig. 18 illustrates the stability of FEL photon pulse energies within long bunch trains at FLASH operating in SASE mode. Note that the fluctuations seen in the record of a single pulse train (blue) reflect the statistics of the SASE process and not the variations of electron bunch parameters within the bunch train.

2.3.10. Combined operation of an FEL and a THz-undulator

The quality of the electron bunch after having passed the FEL undulator is still excellent. It can be used to drive a further radiation source which is particularly attractive since both radiation sources, driven by the same electron bunch, are naturally synchronized. The first attempt ever to equip an FEL in this way was made at FLASH in 2007 by installation of an electro-magnetic undulator consisting of nine periods, each 400 mm long, see Fig. 19 (Grimm et al., 2010). The device supports wavelengths in the range from 1 μm to 200 μm (Grimm et al., 2007). As the electron bunch length is in just this range, the infrared radiation emitted is coherent and very powerful. It contains information about the longitudinal bunch profile but it is also used as a THz radiation source synchronized to the VUV and soft X-ray pulses of the FEL. As an early example, the THz field has been used to realize a few-femtosecond X-ray streak camera (Frühling et al., 2009).

Fig. 19. Photo of the electro-magnetic infrared undulator prior to installation at FLASH. It supports wavelengths in the range between 1 μm and 200 μm.

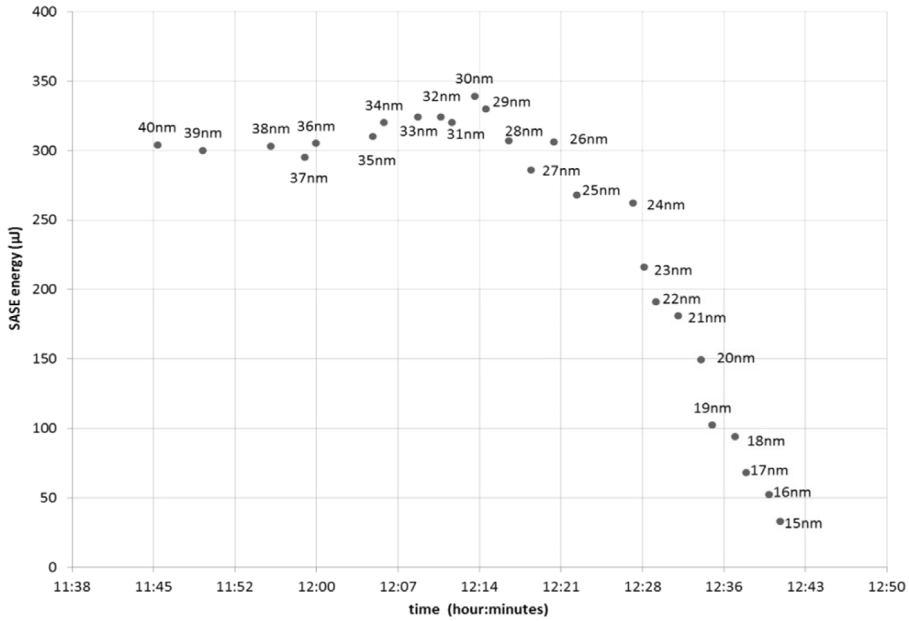

Fig. 20. Wavelength change in FLASH 2 by variation of the undulator gap. 26 different wavelengths, between 40 nm and 15 nm, are reached within 55 min of operation time. During this procedure, FLASH 1 produced simultaneously SASE radiation at some 200 μJ pulse energy at constant wavelength of 13.5 nm.
Source: Courtesy B. Faatz and J. Rönsch-Schulenburg, DESY.

It uses a pump–probe scheme that samples the transient response of a gas target to ionization by soft X-ray radiation in the presence of the intense synchronized terahertz field.

Borrowing the concept from attosecond metrology, the femtosecond X-ray streak camera fills the gap between conventional streak cameras with typical resolutions of hundreds of femtoseconds and streaking techniques operating in the sub-femtosecond regime. Its single-shot capability permits determination of the duration and time structure of individual X-ray pulses.

2.3.11. Simultaneous operation of several FELs

In view of the large request on FEL beam time, a second FEL undulator called FLASH 2 has been installed and put into operation in 2014. The long bunch train from the superconducting Linac is split into two bunch trains by a kicker/septum arrangement such that two long bunch trains are delivered to the two FEL at 10 Hz repetition rate (Faatz et al., 2016). While the electron beam energy cannot be changed within the bunch train due to the long RF filling time, the wavelength of FLASH 2 can nevertheless be tuned independently of the FLASH 1 wavelength because the FLASH 2 undulator has a variable gap, see Fig. 20 for illustration.

The variable-gap undulator of sFLASH installed for seeding tests (see section g) is also capable of running in SASE mode. If this is done at moderate wavelength of about 40 nm, FEL gain close to saturation can be achieved within the

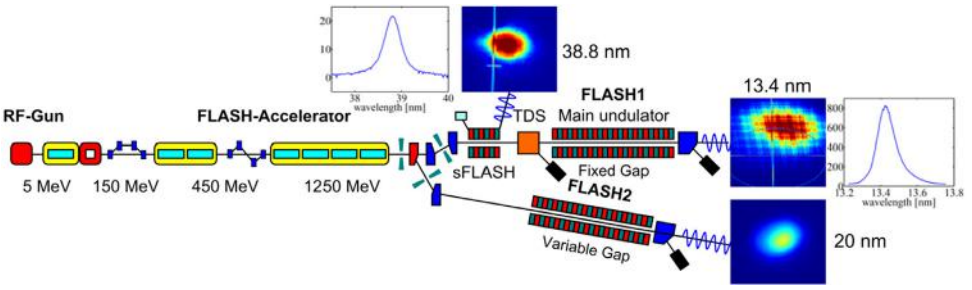

Fig. 21. Schematic view of the FLASH facility equipped with three FEL undulators, from Plath et al. (2016). Images of the FEL radiation produced by each of the three beamlines are shown, as well as an averaged wavelength spectrum of FLASH1 and sFLASH, measured during the simultaneous operation. The image shown for FLASH1 is somewhat blurred due an intensity diagnostics device placed in front of the CCD screen.

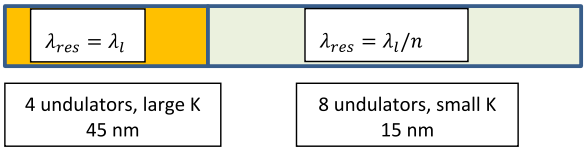

Fig. 22. Schematic view of the Harmonic Lasing Self-Seeding (HLSS) realized at FLASH2. The K-parameter of the first 4 undulator segments was tuned for 45 nm wavelength, the remaining 8 segments were tuned to 15 nm. The FEL gain reached saturation at 15 nm (Schneidmiller and Yurkov, 2012).

10 m undulator length while the electron beam remains qualified for SASE at FLASH1 at 13.4 nm. In this way, three FELs can be operated at FLASH, with two FELs running in series at the same beam line (Plath et al., 2016). A schematic view of the FLASH facility equipped with three FEL undulators is shown in Fig. 21.

2.3.12. Advanced FEL schemes using variable gap undulators at FLASH 2

The availability of a variable-gap undulator opens up a multitude of advanced FEL options at FLASH, a number of which have already been realized and others being under preparation (Faatz et al., 2017).

A rather straightforward application is opening the undulator gap in the downstream undulator region where the FEL gain process reaches saturation. At FEL saturation, the electron beam has lost so much of energy to the radiation that it drops out of the resonance bandwidth. This can be compensated by slightly opening the undulator gap, leading to considerably larger photon pulse energies. Even gradually closing the undulator ("inverse tapering") can be useful since it permits microbunching of the electron beam while suppressing first-harmonic radiation (Schneidmiller and Yurkov, 2013). These techniques, could now, with the advent of FLASH2, also be realized at FLASH.

An even more tricky scenario makes use of the fact that the FEL process not only supports gain at the fundamental resonance wavelength λ_l given by Eq. (1) but also at odd higher harmonics λ_l/n , with $n = 3, 5, \ldots$. This is called "harmonic lasing" (McNeil et al., 2006; Schneidmiller and Yurkov, 2012). It should be noted here that this effect is not to be mixed up with the appearance of higher, nonlinear harmonics in the microbunching process when the gain of the fundamental wavelength reaches saturation and which gives rise to rather weak higher harmonics in the FEL spectrum at saturation.

As the high-power level of the higher harmonics is normally smaller for harmonic lasing than for the fundamental, the short wavelength is regularly not visible in the FEL radiation output. If, however, the undulator is abruptly tuned from a large wavelength λ_l to a shorter one λ_l/n, well before the large wavelength section runs into saturation, the microbunching generated at the nth higher harmonics of the first section will seed the FEL gain at λ_l/n in the second undulator section. In this second undulator section, λ_l/n acts now as the fundamental FEL wavelength and runs into saturation at high power, eventually at higher power and smaller bandwidth than regular SASE would do at this same wavelength. This "Harmonic Lasing Self-Seeding (HLSS)" has been successfully realized at FLASH for the first time (Schneidmiller et al. (2017)), see Figs. 22 and 23 and Section 3.1

The nonlinear harmonics mentioned before can be used at FLASH2 to produce both a fundamental and a higher harmonic wavelength at the same intensity. To this end, a first section of the FLASH2 undulator was tuned to 9 nm wavelength and the K-parameter was changed abruptly to 4.5 nm resonance in the second section. This was done at a longitudinal position where the nonlinear (in this case: second) harmonics content generated in the first section was big enough to drive the second harmonics in the second undulator to the same intensity level, see Fig. 24 (Faatz et al., 2017).

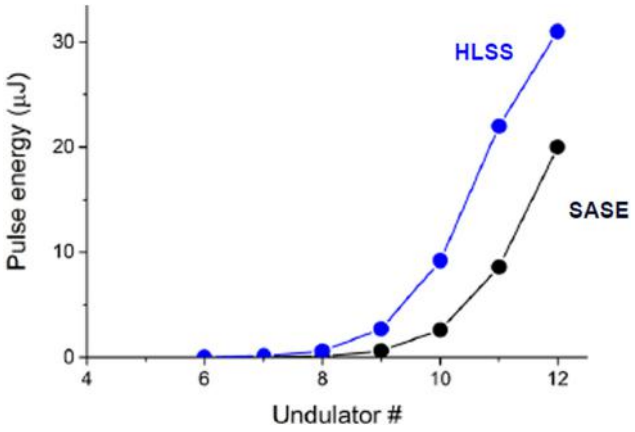

Fig. 23. Pulse energy achieved for 15 nm wavelength at FLASH2 in the Harmonic Lasing Self-Seeding (HLSS) configuration, as compared to regular SASE mode (Schneidmiller and Yurkov, 2012).

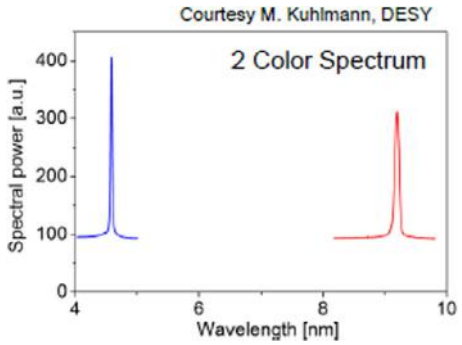

Fig. 24. Two-color mode realized at FLASH2 by tuning the second part of the undulator to the second harmonics of the first one. *Source:* Courtesy M. Kuhlmann.

3. Photon beams

3.1. Beamlines

User operation started in 2005 in the FLASH1 experimental hall which after a naming ceremony in 2015 is now the "Albert Einstein Hall". The experimental hall is 30m behind the dipole magnet that separates the electron and the photon beam in the accelerator tunnel. Fig. 25 shows the layout of the FLASH1 experimental hall (Tiedtke et al., 2009). The FEL, the THz beamline and a synchrotron radiation beamline (originating from the last bending magnet deflecting the electrons into the beam dump) enter into the hall from the bottom of the schematic. Before the separation of beamlines, the FEL radiation passes through a set of photon diagnostics and beam manipulation tools. The first two diagnostic units (not shown in the figure) that are located 20 and 25 m behind the last undulator segment, respectively, are equipped with apertures ranging between 0.5 and 15 mm that allow to align and center the FEL beam. They also include single-shot pulse energy monitors based on MCPs (multi-channel plates) (Bittner et al., 2007) and a VUV spectrometer (see below) (Nicolosi et al., 2005) that can be used by the operators to set the required photon energy for an experiment. These sections are followed by an arrangement of two gas-monitor detectors (GMD) for pulse energy and beam position determination (see below) (Richter et al., 2003; Tiedtke et al., 2008), in front of an attenuation system based on gas absorption (Hahn and Tiedtke, 2007) and two more GMDs behind the gas attenuator. The gas attenuator and different sets of solid thin films mounted in filter wheels in the beamlines can be used to vary or adjust the pulse energy according to the needs of specific experiments.

The photon beam is transported into the experimental hall across a first mirror unit that offsets the photon beam with respect to the line-of-sight of the electron beam and the potentially harmful radiation created by beam losses in the undulator section and steers the beam to either the three "pink" beamlines (BL1–BL3) which transport the full SASE bandwidth to the experiment or to the plane grating monochromator and its branchlines (PG0–PG2). All mirrors in the photon beamlines are operated under grazing incidence angles of less than 4° to provide high degrees of reflectivity over the entire wavelength range and avoid the risk of damage due to the high peak powers. In addition, the first generation

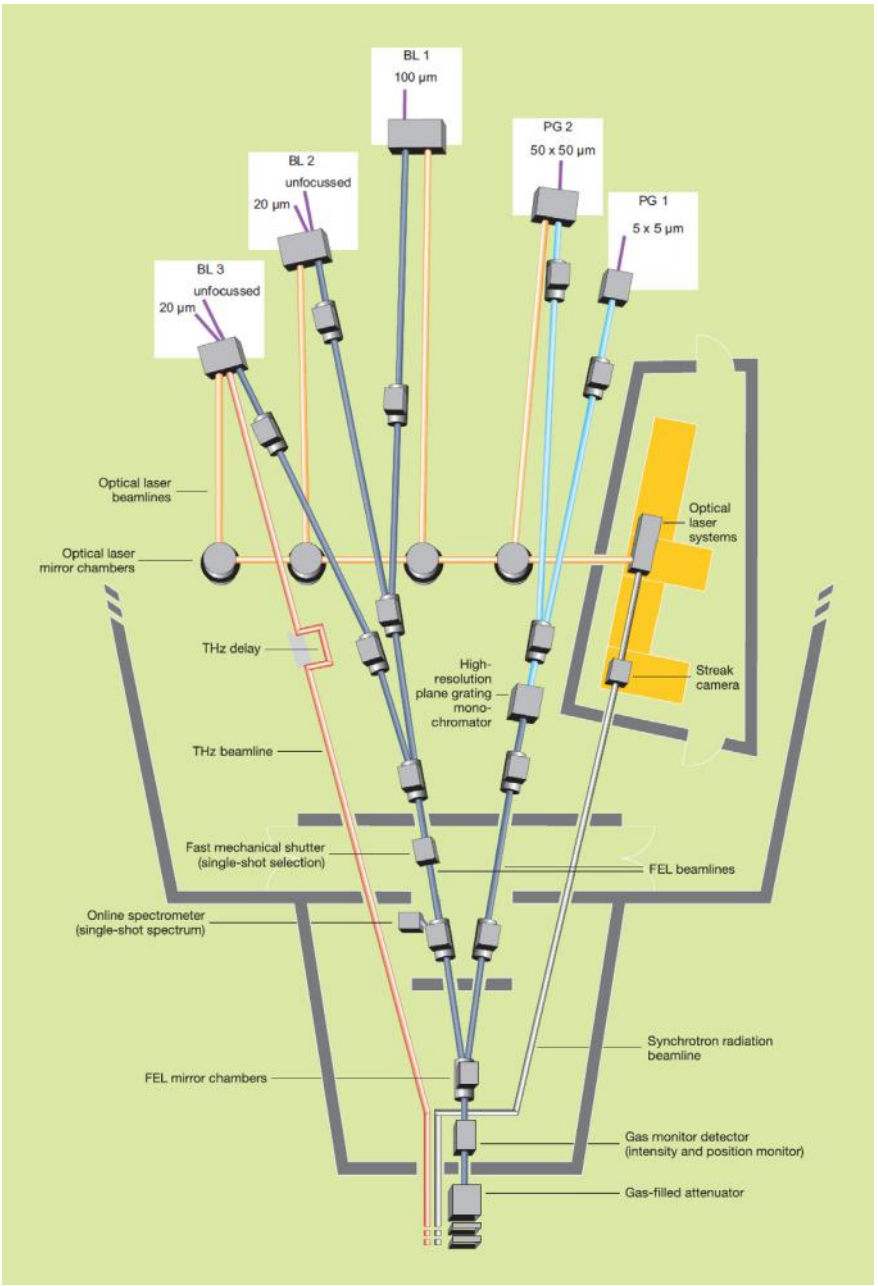

Fig. 25. Schematic view of the FLASH 1 experimental hall. Beamlines are highlighted by a color code: 'direct' FEL beam in dark blue, monochromatized FEL beam in light blue, optical laser in orange and THz radiation in red. Different experimental stations are named 'BL' in case of direct FEL beam or 'PG' for the monochromatized FEL beam. Approximate focal sizes are given next to the station name.

of mirrors at FLASH1 has a coating of amorphous carbon (Steeg et al., 2004) since operation beyond the carbon K-edge was not anticipated. Recently, for the BL beamlines Ni-coated mirrors were added so that also experiments using photon energies beyond the carbon K-edge are possible with reasonable intensities.

BL3 is mainly dedicated to THz pump — X-ray probe experiments thereby making use of the THz pulses generated in a special undulator section from the same electron bunch as the X-ray pulse (see Fig. 25) (Gensch et al., 2008). This ensures not only tunable THz radiation with high pulse energies but also stability of the phase of the THz field with respect to the arrival time of the X-ray pulse (Frühling et al., 2009). A difficulty in these experiments is the nanosecond pathlength delay between the THz and FEL beamline due to the large divergence of the THz beam which requires a dedicated longer THz beamline accommodating the THz focusing components. Presently, the technical solution to enable

temporal overlap in the experiment is to extend the pathlength of the soft X-ray FEL beam employing normal-incidence multilayer mirrors which unfortunately restricts the usable wavelength range. In order to increase the flexibility for these pump–probe experiments, a double bunch pattern with a leading electron bunch generating the THz pulse and a following one (nanoseconds later) to produce the X-ray pulse was tested in early 2017 (Zapolnova et al., 2018). BL2 with its X-ray split-and-delay unit (Wöstmann et al., 2013) (see below) is mainly used for XUV pump–XUV probe experiments.

The original concept of user operation at FLASH was based on open beamline ports for instruments provided by the users for their individual experimental needs. With FLASH being the first short wavelength FEL this ensured maximum flexibility and was very helpful in discovering which science areas would benefit most from the new radiation source with its unique properties. After the experience gained in the first ten years of user operation regarding user needs, the facility now offers a mix of facility operated endstations and open beamline ports. At BL1 the CAMP multi-purpose endstation (Strüder et al., 2010), formerly successfully used at LCLS, has been installed as a permanent endstation. The instrument can host several spectrometers and features high sensitivity pnCCD imaging detectors. In combination with a dedicated Kirkpatrick–Baez (KB) focusing optics and a multilayer-based split-and-delay optics for delay ranges up to nanoseconds in front of the endstation, this setup, is heavily used for time-resolved experiments on photoinduced molecular reactions as well as single-shot imaging experiments of individual nano-objects.

The two beamlines with an integrated plane-grating monochromator PG1 and PG2 (Martins et al., 2006; Gerasimova et al., 2011) complement the FLASH1 beamline portfolio. The plane-grating monochromator can either be operated in high-resolution mode or as a very efficient filter if higher harmonics of the FEL radiation are used. PG1 hosts a dedicated high-resolution RAMAN spectrometer (Dziarzhytski et al., 2016, 2018). In addition, there is the option to operate PG2 in spectrometer mode when an image screen is inserted at the exit slit position. In this way, by introducing a sample in the beamline, single shot transient absorption spectroscopy becomes feasible. In certain photon energy ranges the reflected (zero order) beam from the grating can be transported to a special branchline called PG0 in parallel to the first order beam in PG2. Currently PG0 is used for temporal diagnostics of the radiation pulses with a dedicated THz streaking setup (see below). PG2 has also an integrated split-and-delay unit for XUV pump—XUV probe experiments (Sorgenfrei et al., 2010) and is designed as an open port beamline. However, since 2016 a newly developed instrument for time- and angle-resolved photoelectron spectroscopy (tr-ARPES) on solids and surfaces is installed semi-permanently at PG2. The combination of the high repetition rate of FLASH and the highly efficient single-shot detection of photoelectrons makes this a rather unique instrument for soft X-ray tr-ARPES and time-resolved X-ray photoelectron spectroscopy (tr-XPS), serving an increasing user demand.

Since 2014 FLASH has a second FEL line, FLASH2 (Faatz et al., 2016; Plönjes et al., 2016) (see Fig. 21). After commissioning, FLASH1 and FLASH2 are run simultaneously in user operation since the beginning of 2016. The superconducting accelerator of FLASH runs in so-called burst mode and can deliver up to 800 electron bunches in a train with a bunch-to-bunch separation of 1 μs and a 10 Hz repetition rate of the bunchtrains. Using two independent photocathode lasers for FLASH1 and FLASH2 the number of bunches from a bunchtrain as well as the intra-train bunch separation going to either of the two FEL lines can be chosen freely, taking into account that 20 to 50 μs are needed to switch bunches between FLASH1 and FLASH2. The independent photocathode lasers also ensure that the bunch charge can be adjusted individually for the two FEL lines. In combination with fast RF changes in the time window needed for switching, this enables different compression schemes and hence different pulse durations for user experiments in FLASH1 and FLASH2.

While the original FLASH1 FEL line is equipped with fixed gap undulators, i.e. requires changing the electron beam energy to change the photon energy, the new FLASH2 FEL line has variable gap undulators which allow to scan the photon energy (see Fig. 20). The scanning range of the photon energies in FLASH2 spans from one third of the FLASH1 photon energy up to the FLASH1 photon energy for a given electron energy in the accelerator.

The variable gap undulators also enable novel operation modes, such as advanced tapering schemes, frequency doubling and harmonic lasing self seeding. With undulator tapering photon pulse energies up to 1 mJ have been demonstrated at FLASH2 (Faatz et al., 2017). A particularly interesting option in this respect is reverse tapering which in combination with a harmonic afterburner for circular polarization may allow experiments with variable polarization at photon energies beyond the water window at FLASH2 (Faatz et al., 2017). Tuning the FLASH2 undulators individually, it is also possible to push the photon energy range of FLASH beyond the current limit of 300 eV in the fundamental. Setting the first part of the undulator section to twice the final wavelength in a frequency doubling scheme it has been shown that the photon energy range of FLASH2 can be extended up to 400 eV with stable pulse energies of a few μJ which is significantly higher than what has been achieved if the full undulator section is set to the final wavelength at the same electron energy (Faatz et al., 2017). An even more interesting option is harmonic lasing self seeding (HLSS) which had been proposed as a method to reach higher photon energies with increased brightness. At FLASH2 HLSS was recently demonstrated for the first time experimentally and the theoretical predictions were confirmed (Schneidmiller et al., 2017). FLASH2 can accommodate up to six beamlines and experimental stations. Since spring 2016, the beamlines FL24 and FL26 are open for users. FL24 provides an open port for user supplied experiments and has been equipped with a KB focusing optics with bendable mirrors in order to adapt focus size and focal length to the user demands. At FL26, the permanent end station REMI, a reaction microscope from the Max-Planck Institute for Nuclear Physics in Heidelberg, is installed for advanced AMO and molecular femtochemistry experiments.

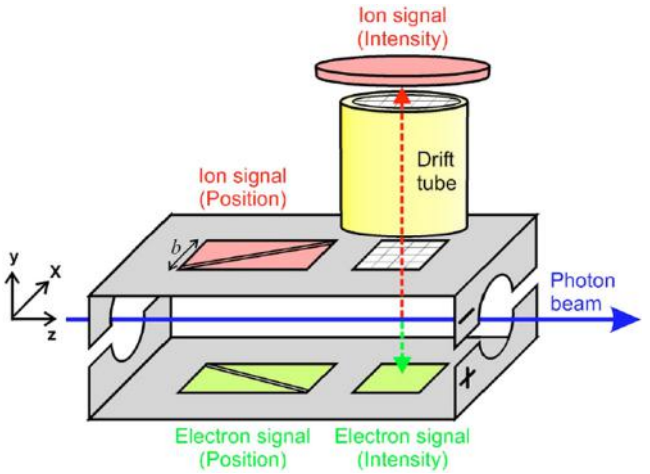

Fig. 26. Schematic of a FLASH dual GMD for the online measurement of the photon intensity and the beam position (Tiedtke et al., 2008).

3.2. Beam diagnostics, beam properties

With FLASH being operated in SASE mode and hence showing shot-to-shot fluctuations in all relevant photon beam parameters it is very important for experiments to have information on as many parameters of the photon pulses on a single-shot basis as possible. Many of the necessary diagnostic tools to characterize photon pulse properties such as pulse energy monitors, on-line spectral distribution monitoring, wavefront sensors, pulse duration measurement tools and cross-correlation tools to determine the relative timing between external optical lasers and FEL have been developed at FLASH and are now in operation at many FEL facilities world-wide. A particular challenge for online single-shot monitoring of the photon beam properties is of course the high repetition rate in burst mode operation with the pulse spacing of 1 μs. While detection schemes based on point detectors can easily cope with repetition rates in the MHz regime, this is extremely challenging for higher dimensional detectors such as 1D line detectors or 2D imaging detectors.

3.2.1. Pulse energies

Already before FLASH started operation as a user facility diagnostics tools to monitor the pulse energy of the radiation were needed in order to characterize the performance of the FEL and to check whether saturation is reached in the amplification process. Furthermore the fluctuations in pulse energies provide information about the number of radiation modes being present in the pulses. A simple but very efficient tool to measure relative pulse energies is a detector which amplifies the photons scattered from a mesh in the beam with MCPs (Bittner et al., 2007). Such devices have been used from the very beginning in the facility.

However, for experiments a reliably calibrated tool is needed to supply an absolute measurement of the pulse energies. Since this tool should be transparent and be able to operate over the full wavelength range a team with members from the Physikalisch-Technische Bundesanstalt (PTB), the Ioffe Institute, Sankt Petersburg, and DESY developed the so called gas monitor detectors (GMDs) which are based on photoionization of gases and measuring the generated electron and ion signals after separation in a homogeneous electric field (Tiedtke et al., 2008) (see Fig, 26). Both signals can be recorded in pulsed mode for every electron bunch. Detecting the ion-current in a slow averaging mode with a time constant of a few seconds allows calibration with a radiation standard as for example a synchrotron source and a calibrated photodiode as a secondary standard. The measured ion currents for a given gas density in combination with the known photoionization cross sections can then reliably be converted to average absolute pulse energies with an accuracy of better than 10%. The electron signal can be used as a relative measure of the pulse energy of the individual radiation pulses on a single-shot basis (see Fig. 26).

The ion detection part includes a drift tube which can be used for a given gas target to distinguish between different charge states. In the second version of the GMDs a set of split electrodes was added for ions and electrons, respectively, that allows to determine also the position of the FEL beam.

Meanwhile, based on the development at FLASH, standard GMDs or X-GMDs (specifically developed for hard X-ray FELs) are used at all major FEL facilities as absolute pulse energy monitors.

3.2.2. Spectral diagnostics

For a SASE FEL the spectral distribution within a radiation pulse depends on the distribution of longitudinal modes that are amplified. Averaging over many pulses the spectral distribution is in most cases given by a single Gaussian distribution with a typical relative bandwidth of the order of a percent. The bandwidth of the individual radiation modes is related

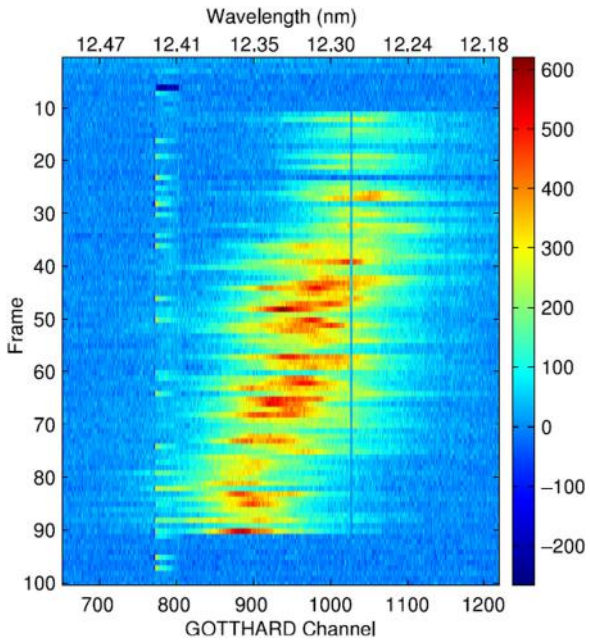

Fig. 27. Image of 100 frames taken with a readout frequency of 200 kHz. After some frames without a signal, one can clearly see the wavelength distribution of all pulses of the pulse train (starting at frame 10 and ending at frame 90) and a shift to higher mean wavelengths towards the end of the pulse train. FLASH ran with 200 kHz and 80 bunches (the 13th (frame23) has been kicked out) (Palutke et al., 2015).

to the full temporal width of the FEL pulse while the total spectral width for the average spectrum is determined by the Fourier transform of the coherence time (see below). At FLASH several options have been realized to determine the spectral profile of single shots as well as the average distribution over many shots. A set of grating spectrometers is available for characterization of spectral properties of the radiation pulses. In the photon diagnostic section in front of the FLASH1 experimental hall, already at the start of user operation, a grazing-incidence spectrometer with a VLS grating was installed which can be used by the FEL operators to set the desired wavelength for user experiments (Nicolosi et al., 2005). A higher resolution option is given by the PG2 beamline which, as described above, can also be operated in spectrometer mode. This has already been used early on to characterize the FEL operation by looking at the number of longitudinal modes being present in single shot spectra (Wellhöfer et al., 2007). Since neither of the two options can be run simultaneously with user experiments to provide the experiment with online spectral diagnostics, two additional grating spectrometers are now in operation at FLASH. For transparent experiments with dilute targets a facility operated compact spectrometer can be installed behind the experiment (Frassetto et al., 2011). This compact spectrometer which is also a grazing-incidence spectrometer with two spherical variable line spacing gratings covers the full spectral range of FLASH including higher harmonics down to below 2 nm. Since it has been carefully calibrated at different synchrotron sources it was also used in studies of the higher harmonic content of the SASE radiation (Düsterer et al., 2006; Frassetto et al., 2010). In order to provide similar information also to non-transparent experiments, two different approaches have been pursued at FLASH. The first approach is again based on a grazing-incidence spectrometer with VLS grating which is permanently installed in front of the BL beamlines (Brenner et al., 2011). The grating is optimized to send 90+% of the beam in zero-order to the experiments while the remaining 1%–10% can be used for online single-shot spectral characterization. All of these grating spectrometers are based on imaging the spectral distribution in the focal plane of the grating using CCD cameras. Since none of the currently available CCD cameras can read out images at a MHz rate single shot spectral diagnostics is either limited to single bunch operation at FLASH or to diagnosis of a single bunch in multi-bunch operation by triggering the camera to a specific bunch. However, there has been considerable progress in the availability of fast 1D detectors recently.

Since the characterization of the spectral distribution can also be achieved with a line detector in the focal plane of a grating spectrometer it has been demonstrated at FLASH experimentally that the spectral distribution of single pulses can be monitored for a sequence of the pulses in multi-bunch operation (Palutke et al., 2015) (see Fig. 27). The Gotthard detector used in this experiment will soon be upgraded so that a full bunch train at MHz repetition rate can be spectrally monitored. After the first demonstration of the capabilities of this approach the online VLS spectrometer in front of the BL beamlines has now been upgraded with the new detector.

A completely different approach towards online spectral characterization of FEL pulses is based on photoionization of gas targets and measuring the spectral distribution of known photoemission lines with time-of-flight spectrometers. Here the online diagnosis tool is basically transparent to the FEL radiation due to the low gas density used. Early attempts using this approach had shown that this should even be able to provide single-shot spectral distributions (Wellhöfer et al.,

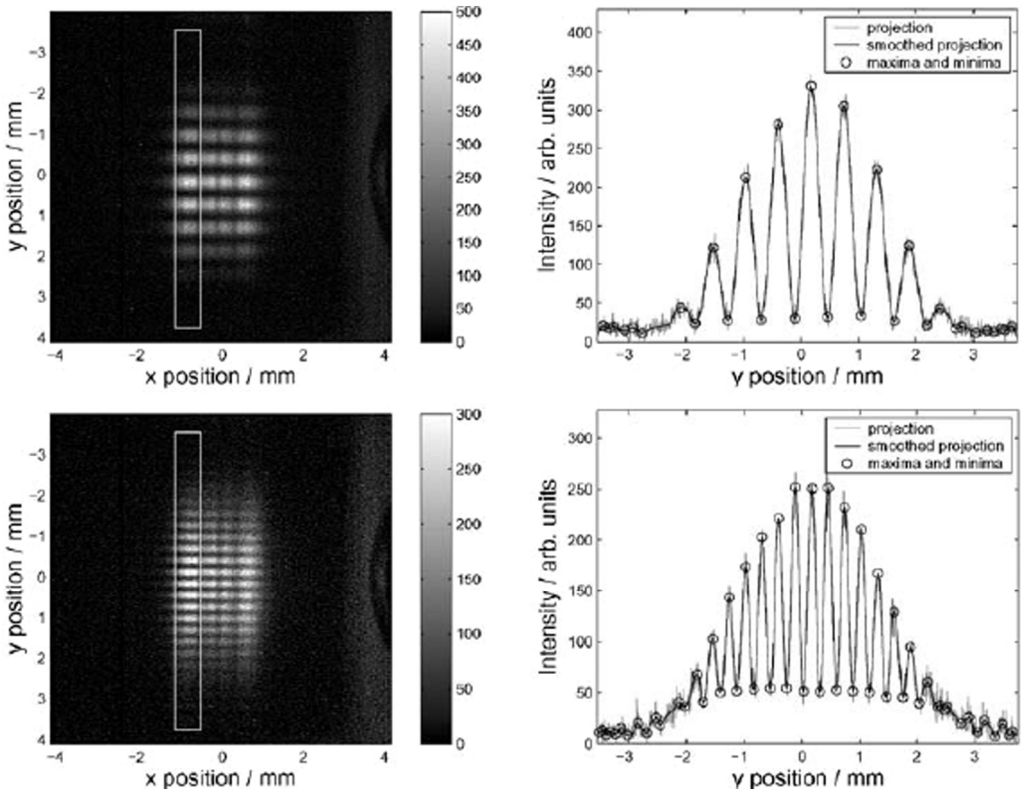

Fig. 28. Diffraction pattern for horizontal double slits with 0.5 mm (upper row) and 1 mm separation. Left: camera images, right: projection of the selected region (Ischebeck et al., 2003).

2008). After successful tests at FLASH1 the online photoionization spectrometer (OPIS) is now available for users as part of the FLASH2 photon diagnostic section (Braune et al., 2016).

3.2.3. Wavefront characterization and coherence properties

An important property of FELs is the high coherence of the radiation. While the temporal or longitudinal coherence of SASE FELs is limited due to the existence of several longitudinal modes within a radiation pulse, the emitted radiation is almost fully transversely coherent, i.e. the source is close to diffraction limited. This is due to the fact that the fundamental Gaussian mode TEM_{00} has its highest intensity on the beam axis while the higher TEM_{mn} modes extend to larger radial distances. Therefore, the fundamental mode will grow faster than the other modes, owing to its superior overlap with the electron beam. When the saturation regime is approached, the fundamental mode will usually dominate and the FEL radiation will possess a high degree of transverse coherence. This is in contrast to classical undulator radiation, where the degree of transverse coherence critically depends on the electron beam size (as long as the electron beam emittance does not fall below the diffraction limit value as it is aimed at modern storage ring designs). Already in the early phase of TTF the transverse coherence has been measured using a Young's double slit experiment and compared to wavefront propagation simulations (Ischebeck et al., 2003).

In this experiment it was shown that the FEL radiation at 100 nm is close to fully transversely coherent and that the degree of coherence is getting smaller beyond saturation when more transverse modes contribute to the overall intensity (see Fig. 28). The degree of transverse coherence is of course key for all experiments which aim at single-shot imaging (see below). Several experimental campaigns have been devoted to extend the original double slit experiment to shorter wavelength leading to similar results (Singer et al., 2008). An alternative approach to a full characterization of the radiation field is to reconstruct the Wigner distribution function from two-dimensional intensity profiles of the beam via tomography. Such a reconstruction based on caustic measurements at FLASH beam line BL2 allowed to determine the global degree of coherence, wavefront and modal composition of the FEL beam and compare this to theoretical expectations (Schäfer et al., 2011).

Characterization of the wavefront at the end of a beamline after the FEL radiation passed quite a few optical elements is an important aspect of photon diagnostics. For this propose at FLASH a versatile Hartmann-type wavefront sensor for the full spectral range of FLASH was developed in collaboration with LaserLab Göttingen, which is routinely used to precisely

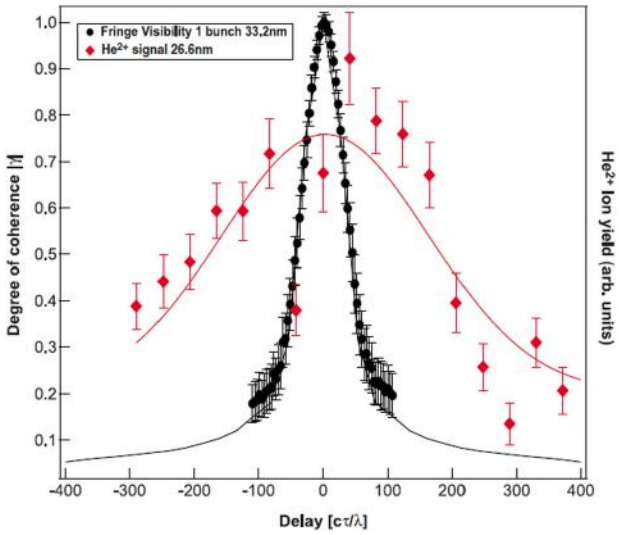

Fig. 29. The typical longitudinal coherence time, as observed in the fringe visibility (left axis), is much shorter than the corresponding pulse length which can be deduced from the nonlinear autocorrelation visible in the yield of the generated He^{2+} (right axis). The black solid line is calculated by applying the Wiener–Khinchin theorem to single shot spectra. The wavelength of the radiation is 33 nm and the calculated coherence time is close to 6 fs (Sorgenfrei et al., 2010).

characterize the optimum focusing conditions (Flöter et al., 2010) . With the same technique it is also possible to fully reconstruct the wavefront of the radiation at the end of the different beamlines (Keitel et al., 2016).

While the degree of transverse coherence of the FEL radiation is very high the longitudinal coherence is significantly lower and depends on the number of longitudinal modes being present in the SASE pulses. Similar to the double-slit experiments it is also possible to measure the longitudinal coherence in an interferometric way using a Michelson or a Mach–Zehnder type interferometer (see Fig. 29). At FLASH such devices exist in the form of two split-and-delay units which have been developed for XUV pump–XUV probe experiments (Wöstmann et al., 2013; Sorgenfrei et al., 2010). In these devices the incoming beam is split in two by wavefront division at the edge of a mirror. After passing a mirror unit where one of the beams can be delayed with respect to the other, the beams are recombined. Measuring the visibility of interference fringes which can be detected on a screen where the two beams impinge under a slight relative angle the coherence time can be deduced (Roling et al., 2011; Schlotter et al., 2010).

Combining this type of experiment with a double-slit experiment the full coherence volume of the beam can be determined (Singer et al., 2013).

As pointed out above the degree of longitudinal coherence of a pulse, i.e. the ratio of coherence time to pulse duration, depends on the number of longitudinal (spectral) modes, i.e, the monochromaticity of the radiation pulses. In the limit of single spike SASE operation coherence time and pulse duration are equal. The spectral bandwidth of the SASE FEL radiation which is typically of the order of a percent, can be reduced by going to seeded operation (see above) or by using the PG beamline as a spectral filter, the latter at the expense of average pulse energy. With the latter approach it has recently been demonstrated at FLASH that even attosecond interferometry is possible at a SASE FEL (Usenko et al., 2017).

A particularly elegant way to measure the full coherence properties is to perform Hanbury-Brown and Twiss interferometry experiments to determine the second order correlation function of the photon pulses based on intensity measurements. Such an experiment has been successfully performed at FLASH, for the first time at an FEL (Singer et al., 2013). The analysis of the second order correlation function clearly shows that SASE FELs can be fully described as chaotic light sources following Gaussian statistics. The same experiment has recently also been conducted at FERMI which is a fully externally seeded FEL (Gorobtsov et al., 2018). In this case analysis of the second order correlation function shows that a seeded FEL fulfills in terms of photon statistics the criteria of a laser-like source according to definition given by Glauber.

3.2.4. Cross-correlation techniques and pulse duration characterization

After more than 10 years of user operation today some 70%–80% of the experiments use the short FEL pulses for time-resolved experiments. These experiments are performed in some kind of pump–probe configuration where a first pump pulse triggers a certain dynamics which is then probed with a second pulse which arrives after variable delay. Approximately half of the experiments use the FLASH1 optical fs lasers: either a burst mode system with 400 pulses/burst, ∼50 μJ/pulse, and pulse durations <90 fs (fwhm) or a multi-mJ single pulse (10 Hz) system that provides ultra-short pulses below 50 fs (Redlin et al., 2011). From 2018 on, a newly developed OPCPA (optical parametric chirped pulse amplifier) based high repetition rate, high power laser, which delivers shorter pulses (∼20 fs), is available for FLASH2.

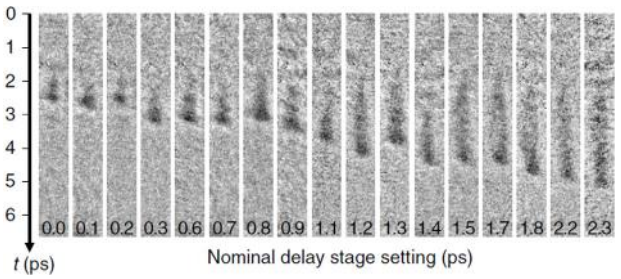

Fig. 30. Selection of 17 single-shot measurements during a delay scan of the visible laser, which covers the entire time window of the experiment (2.3 ps). The nominal delay stage setting is indicated at the bottom of each image. The time axis t is shown on the left; the time-zero is arbitrarily set to the top of the image. The steady downward movement of the boundary of reflectivity change is superimposed by random EUV/visible delay fluctuations (Maltezopoulos et al., 2008).

For pump–probe experiments in combination of an optical laser with the FEL the jitter between the two in principle independent laser sources has to be minimized to achieve the highest possible time resolution. Early sideband experiments (see below) have shown that the jitter can be quite significant, on the order of several 100 fs in the early days of FLASH operation (Radcliffe et al., 2007). Reducing the jitter contribution can either be done by measuring the relative arrival time for each individual pulse pair or by improving the overall synchronization scheme of the facility. At FLASH both avenues have been followed. Experiments on X-ray induced transient reflectivity changes in semiconductors (Gahl et al., 2008) showed that this effect can be used to build a single-shot cross correlator (Maltezopoulos et al., 2008) where the time-coordinate of the relative arrival time of the two pulses is mapped onto a spatial coordinate (see Fig. 30).

These so-called time-tools which have been pioneered at FLASH are now in use in different configurations at many FEL facilities. A drawback of the approach for a burst-mode high-repetition rate FEL such as FLASH is again that this type of diagnostics requires fast imaging detectors.

Alternatively the jitter between optical lasers and FEL pulses can be minimized by stabilizing the electron beam arrival time and by synchronization of RF and lasers. At FLASH all lasers are fully synchronized to the fiber laser based optical clock of the facility. Together with RF feedback making use of the electron beam arrival monitors, a timing stability better than 30 fs rms for user experiments has been demonstrated in burst mode operation (Schulz et al., 2015) already in 2013. In the meantime improvements in electronics and beam arrival monitors have led to a timing stability of 14 fs rms. These developments are crucial for time-resolved experiments which integrate over the full bunchtrain in multibunch operation.

Given precise knowledge of the pulse duration of the optical laser the above mentioned cross-correlation techniques can also be used to determine the FEL pulse duration (Riedel et al., 2013).

Roughly 30% of the time-resolved X-ray pump/X-ray probe experiments performed at FLASH require suitable split-and-delay units (SDUs). Three of the FLASH1 beamlines, BL1, BL2 and PG2, are equipped with permanently installed SDUs with time resolution down to 100 as and maximum delay times ranging from several picoseconds (BL2, PG2) to almost a nanosecond (BL1). At FLASH2, beamlines FL26 and FL24 will also have permanent SDUs. All units can be moved into the beam on user demand and are otherwise transparent. In X-ray pump/X-ray probe experiments, the achievable time resolution is governed by the pulse duration of the FEL pulses. A real-time tool to determine the average pulse duration has been implemented using the analysis of statistical properties of measured SASE FEL spectra (Engel et al., 2016). Major efforts have been undertaken to generate shortest possible SASE pulses and develop single shot pulse duration diagnostics. Following a campaign where several options for online pulse diagnostics have been explored (Düsterer et al., 2014), a test setup for THz streaking has recently been implemented successfully at the zero order branchline of the PG monochromator (Ivanov et al., 2018). With this setup, arrival time monitoring and single shot pulse diagnostics down to a few femtoseconds is possible. This has been demonstrated in combination with single spike SASE operation of FLASH. There, a short pulse injector laser has been used to produce electron bunches which sustain only a single SASE radiation mode. Pulses with a pulse duration below 10 fs (fwhm) have been achieved and measured, see Section 2.3.6 and Fig. 16).

3.2.5. Polarization

The undulators used at FLASH1 and FLASH2 produce linear polarized radiation. For a certain class of experiments in particular to study magnetism it is sometimes desirable to use circular polarization. At FLASH this has been recently realized by implementing a four-mirror polarizer for the photon energy range of the 3d transition metal M-edges (von Korff Schmising et al., 2017). The polarizer is positioned upstream of any focusing optics and can be used for any of the three BL beamlines at FLASH1 delivering the direct and "non-monochromatized" FEL beam.

3.3. Damage studies

The extreme peak brightness of FLASH in combination with the high absorption probability of the XUV and soft X-ray radiation raised already early on concerns whether transport across optical elements would lead to significant damage of

the optical elements. Furthermore, there were quite some doubts whether dynamic studies of condensed matter samples would not be affected by significant beam damage. Single-shot beam damage would, in particular, prevent accumulation of signals over many pulses in burst mode since the short time between individual pulses would not allow moving samples. To study the impact of the radiation on typical materials used not only in the beam transport but also in condensed matter experiments, already early on (in the TTF1 phase) a dedicated experimental station was built by a collaboration including researchers from Poland and DESY (Sobierajski et al., 2005) which was later upgraded to increase the flexibility (Sobierajski et al., 2013).

A number of damage studies on different inorganic materials at different wavelength have been performed at FLASH using this chamber (Krzywinski et al., 2007) or a similar endstation (Hau-Riege et al., 2007a,b; Chalupský et al., 2009a,b; Hau-Riege et al., 2009). In these experiments a possible modification of the sample surface is typically studied ex-situ using different microscopy techniques (Nomarski interference contrast, atomic force, or scanning electron microscopy). The common finding of these studies is that the single shot damage threshold is essentially given by the melting threshold. The fluences at which single shot damage occurs are roughly on the order of several tens of mJ/cm^2 and do not dependent significantly on the wavelength. This can be understood as a result of ultrafast non-equilibrium excitation of the electronic system which after rapid electronic thermalization on sub-ps time scales equilibrates with the lattice on time scales of several ps. While the dynamics in the electronic system is wavelength dependent the final temperature reached depends only on the deposited energy independently of the wavelength of the exciting radiation (see e.g. Medvedev et al., 2013).

On amorphous carbon thin films which can be used as mirror coatings for some of the optical elements at FLASH the question was addressed whether the damage threshold of thin films is different from bulk materials (DastjaniFarahani et al., 2011). While no tendency for delamination or fracture of the films due to thermal stress was observed indeed slightly higher damage threshold values were obtained which were attributed to the fact that in the surface region part of the deposited energy is carried away by escaping photoelectrons.

Since imprints of the FEL spot into Poly(methyl methacrylate) (PMMA) were – and are still – used to study the size and the shape of the focused radiation at the beamlines (Chalupský et al., 2007, 2010) also studies of the mechanism behind ablation of PMMA induced by the FEL radiation pulses have been performed (Chalupský et al., 2009a,b). In these studies evidence was found for non-thermal desorption/ablation processes for the organic molecular solid in these studies.

A class of materials which is also heavily used at free-electron lasers sources are inorganic scintillators which serve to convert the short wavelength photons to optical photons in applications like screens for imaging the source size or spectrometers as part of the detector system. Also here knowledge of the damage threshold is important and was investigated at FLASH for several scintillator materials (Burian et al., 2015). Apart from damage the question of the linearity of the response of scintillators to the FEL radiation is very important for their use. This has been investigated for the mostly used Ce:YAG scintillator material (Krzywinski et al., 2017).

A highly interesting regime for damage studies on optical elements is the wavelength regime around 13.5 nm which is the preferred wavelength for lithography with high intensity XUV sources. Free electron lasers such as FLASH are ideal for such studies, which are important for the next generation of lithographic processing in the semiconductor industry. As part of these studies the damage mechanisms of Mo/Si and MoN/MoSi multilayer optics were investigated at FLASH. While for the Mo/Si multilayer silicide formation due to enhanced atomic diffusion in molten silicon was detected as the main cause for damage (Khorsand et al., 2010), for the MoN/MoSi multilayers the main damage mechanism was found to be molecular dissociation followed by N_2 formation which leads to the generation of bubbles in the multilayer structure (Sobierajski et al., 2011).

More recently a study including industry partners was launched to find out whether exposure to multiple pulses, where the individual pulses are below the single shot damage threshold (SSDT), would cause any modification in the surface region of XUV mirrors affecting the reflectivity (Makhotkin et al., 2018). FLASH as a high repetition rate XUV and soft X-ray FEL provides an ideal platform for such investigations. In an earlier study on silicon it was shown that heat accumulation for pulse trains with a pulse distance of 1 μs can lead to melting if the mean fluence is beyond a certain threshold value (Sobierajski et al., 2016). The main finding of this study was that even for irradiation with up to 16 million pulses with fluences below 10% of the single shot damage threshold no changes of the internal structure of the optical coatings were observed. Reflectivity changes on the percent level (see Fig. 31) have been attributed to XUV supported surface oxide formation which was corroborated by X-ray photoelectron spectroscopy.

4. Examples of science

On September 18, 2001, about one week after lasing at 98 nm wavelength (12.7 eV) in saturation had been demonstrated by the free-electron laser at the Tesla Test Facility (TTF) the first gas phase experiment on Xe atoms and clusters had been performed successfully by Thomas Möller and his group (Wabnitz et al., 2002). The goal was to gain deeper insights into understanding the interaction of high intensity, short-wavelength, short-pulse radiation with matter. Xe atoms were chosen because they can be ionized even by single 12.7-eV photons (the ionization potential of Xe atoms is 12.1 eV). Fig. 32 shows the schematics of a typical gas phase experiment. In the experiment by Wabnitz et al. the FEL beam was focused to a spot of 20 μm diameter. FEL and target beam cross at the focal point where the maximum power density of the photon beam was estimated at 7 x 10^{13} W cm^{-2} assuming pulse duration of 100 fs. The resulting ions were detected with a time-of-flight (TOF) mass spectrometer. TOF mass spectra for different cluster sizes recorded at a

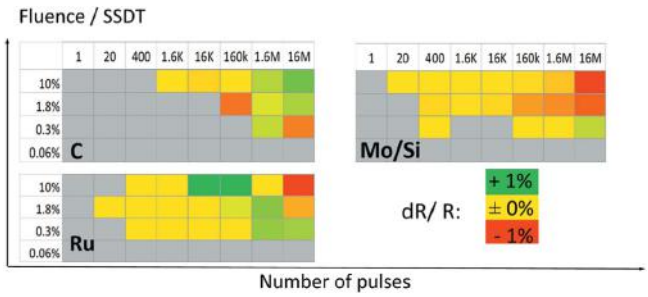

Fig. 31. Overview of reflectivity changes dR/R determined from EUV reflectivity maps for different number of pulses corresponding to different values of fluence, and different single-shot damage threshold (SSDT) values (Makhotkin et al., 2018).

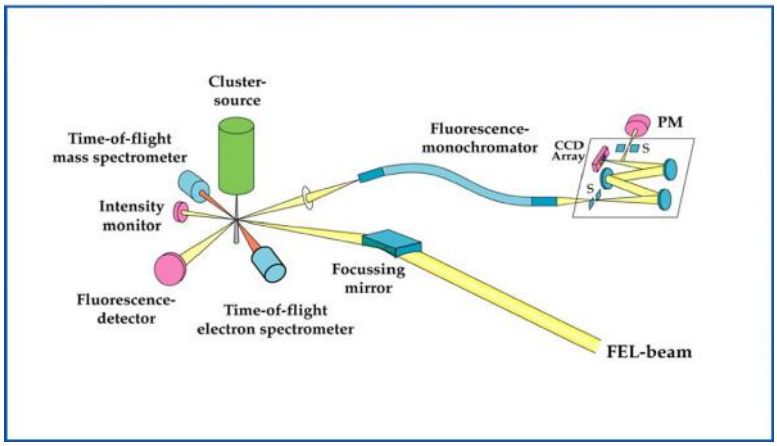

Fig. 32. Schematics of a typical gas-phase experiment at a free-electron laser. A steady stream of target particles crosses the focus of a FEL beam which has a very high power density in the focal spot. As a result most target particles explode. The produced ions, electrons and photons are then detected by a variety of spectroscopies. In cases where the target is smaller than the focal spot it is of great advantage to add an imaging device which allows full characterization of the individual target as well as the determination of the position where it interacts with the FEL beam, i.e. at maximum intensity in the center of the focal spot or more in the halo of the beam.
Source: Courtesy T. Möller, TU Berlin.

power density of 2 x 10^{13} W cm^{-2} are shown in Fig. 33. The most striking result is the surprisingly different ion signal from atom and cluster beams. Whereas only singly charged ions are observed after irradiation of isolated atoms, atomic ions with charges up to 8+ are detected if clusters are irradiated at the same power density. A strong dependence of the observed ion spectrum from the power density was observed and interpreted as a clear indication for optical nonlinear processes to dominate the ionization of the clusters at the power levels used in the experiment. Three questions are discussed by Wabnitz et al.: (1) What is the ionization mechanism that causes the massive electron ejection observed in the experiment? (2) How can the high charge states of the fragments and their high kinetic energy be explained? (3) Which process allows the cluster to absorb the observed large amounts of energy?

Wabnitz et al. conclude that absorption of short-wavelength radiation and subsequent ionization in clusters differs considerably from that in the optical spectral range. Absorption and ionization start by single-photon absorption as described by quantum mechanics. After many unbound electrons are created, plasma is formed. The absorption in such cluster plasma is stronger than predicted by calculations with classical models. Quantum-mechanical modeling is needed at these short wavelengths to explain the efficient energy deposition seen in the experiment. On the other hand, the classical simulation clearly shows that electrons can leave the cluster by a photon-assisted thermionic emission. Field ionization, the dominant ionization process at optical frequencies, does not contribute to cluster ionization.

This first FEL experiment caused a lively discussion in the atom, molecular and optical physics community (AMO). It was a clear demonstration of the feasibility of experiments with free-electron laser beams and stimulated a lot of the activities leading to the results presented in the following.

4.1. Single-shot single-particle coherent diffractive imaging

Compared to the best synchrotron radiation facilities in operation today the gain in peak brightness by free-electron lasers is about 9 orders of magnitude, which leads to X-ray beams of almost full translational coherence. This opens the

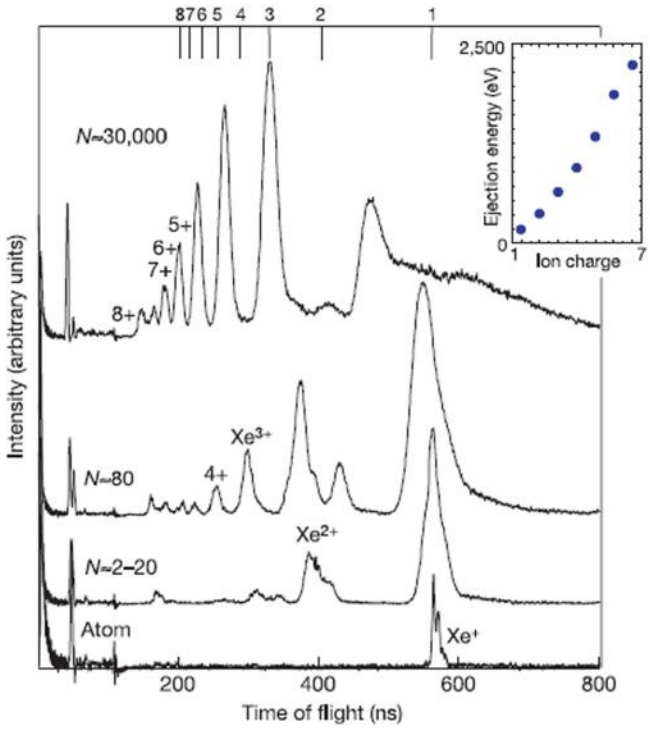

Fig. 33. Time-of-flight (TOF) mass spectra of ionization products of Xe atoms and clusters. The spectra were recorded after ionization with soft X-rays (98 nm wavelength) at an average power density of 2 x 10^{13} W cm^{-2}. The atomic spectrum (bottom trace) shows a splitting into several lines owing to the different isotopes. After irradiation of clusters, highly charged ions are observed. The mass peaks are rather broad and displaced with respect to the calculated flight times indicated by thin vertical lines (different charge states) in the uppermost part of the figure. This indicates that the ions have high kinetic energies. N is the number of atoms per cluster. Insert: the kinetic energy of ions as a function of the charge for N = 1500.
Source: From Wabnitz et al. (2002).

possibility for coherent imaging of matter with atomic resolution and, in a next step, the investigation of the dynamics on femtosecond time scales. Time resolved single-shot single-particle imaging, summarized in the slogan "Take movies instead of pictures", was one of the most popular science drivers for the construction of free-electron X-ray lasers. On one hand it was clear that pulses with about 10^{12} X-ray photons in 50 fs will destroy everything hit by the focused laser beam, but on the other hand already in the 1980ies a way out of this dilemma was discussed (Solem and Baldwin, 1982). If the number of photons in an extremely short pulse is extremely high then one can hope to get an interpretable diffraction pattern from a single shot before the sample is significantly damaged. This is the "diffraction before destruction" method, which is presently only possible at XFELs because of the requirement of exceptionally high intensities. The method allows essentially damage-free diffraction data to be gathered at atomic resolution from individual submicron protein crystals, and, in theory, such high resolutions should also be achievable for non-crystalline objects too, provided that pulses are sufficiently short in duration (Neutze et al., 2000).

4.1.1. First demonstration of single-shot femtosecond diffractive imaging

Femtosecond diffractive imaging was first demonstrated in an experiment at FLASH using an intense 25 fs, 4×10^{13} W cm $^{-2}$ pulse, containing 10^{12} photons at 32 nm wavelength, which produced a coherent diffraction pattern from a nanostructured non-periodic object, before destroying it at 60,000 K (Chapman et al., 2006). The image information encoded in the coherent diffraction pattern is similar to a hologram, except that the object acts as its own scattering reference. Reconstruction from the far-field diffraction pattern was carried out by phase retrieval through oversampling using the iterative transform algorithm, Shrinkwrap (Marchesini et al., 2003). Fig. 34 shows the experimental setup. The object was a micrometer-sized pattern cut through a partially transparent silicon nitride membrane with a focused ion beam (FIB), it is shown in the inset of Fig. 34. The diffraction pattern obtained with a single pulse of FLASH is shown in Fig. 35a. The reconstructed picture shown in Fig. 35c agrees very well with a scanning electron microscopy picture of the original target shown in Fig. 35d. The diffraction pattern obtained with a subsequent pulse 20 s later is shown in Fig. 35b, the inset of Fig. 35d shows the same target after being obliterated by the FEL pulse. This experiment was the first to demonstrate the "diffraction before destruction" technique and let to a series of papers focused on achieving the goal of "single molecule imaging" at higher resolution using harder X-ray energies (Bogan et al., 2008; Loh et al., 2010). These

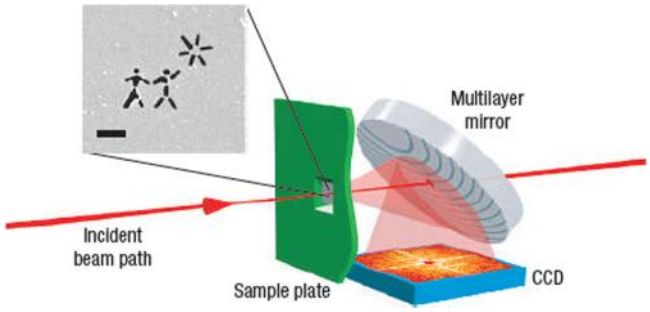

Fig. 34. Schematic diagram of the experimental apparatus. The FEL beam is incident from the left and is focused to a 20 μm spot on the sample, which is a 20-nm-thick transmissive silicon nitride membrane with a picture cut through its entire thickness using a focused ion-beam (FIB) (this is enlarged in the inset, and the scale bar indicates 1 μm). The direct beam passes through the sample window and exits the camera through a hole in a graded multilayer planar mirror. The diffracted light from the sample reflects from this mirror onto a CCD detector. The multilayer mirror also acts as a filter which reduces the amount of background radiation reaching the detector. The on-axis path length from the sample to the detector is 55 mm. For 32 nm radiation and objects smaller than 20 μm, this distance is in the far field, where the diffraction pattern is equal to the Fourier transform of the exit wave.
Source: From Chapman et al. (2006).

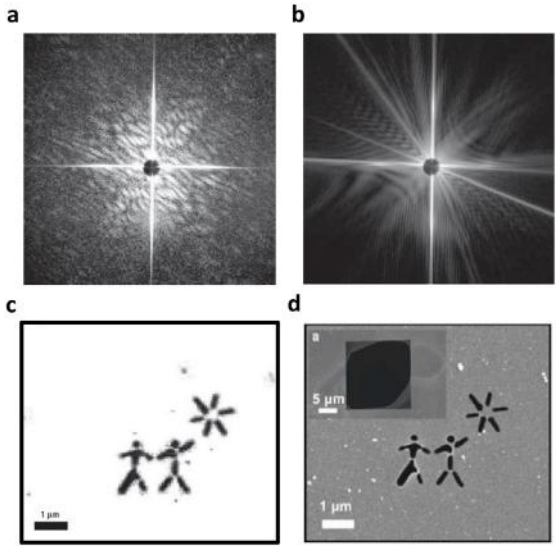

Fig. 35. Coherent diffraction patterns recorded for a single $(4 \pm 2)\times 10^{14}$ W cm^{-2}, 25 ± 5 fs pulse (**a**) and for the subsequent pulse of similar intensity and duration, 20 s later (**b**), showing diffraction from the damage caused by the pulse that formed (**a**). In comparison with an SEM picture of the original pattern (**d**) the reconstructed X-ray image shows no evidence of the damage caused by the first pulse. The inset of (d) shows the square 20 μm window and some silicon nitride after being obliterated by the first FEL pulse. The damage to the silicon support is caused by the non-circular beam.
Source: From Chapman et al. (2006).

papers aimed to develop the diffraction-before-destruction technique for capturing single X-ray images from supposedly "identical" copies of an object in flight through the pulsed XFEL beam, and for orienting the diffraction patterns in 3D space to obtain a 3 dimensional reconstruction of a (supposedly) reproducible object.

The ability to take images in a single shot is key to studying non-repetitive behavior mechanisms. As an example, the transient nanoscale dynamics of materials on femtosecond to picosecond timescales is of great interest in the study of condensed phase dynamics such as crack formation, phase separation and nucleation, and rapid fluctuations in the liquid state or in biologically relevant environments. Barty et al. studied laser ablation on artificial structures imprinted on a Si_3N_4 foil by illuminating the target with an optical laser and capturing time-series snapshots with fs free-electron laser pulses from FLASH using the setup shown in Fig. 34 (Barty et al., 2008). Although the spatial resolution of 50 nm and the temporal resolution of 10 ps are modest this was the first optical pump/X-ray probe coherent imaging experiment and opened the door to a new regime of time-resolved studies of mesoscopic dynamics.

Experiments at FLASH led directly to higher resolution experiments at LCLS, which can achieve higher spatial resolution through shorter wavelength X-rays. In particular, the diffraction-before-destruction technique pioneered at FLASH has

grown into the method of serial femtosecond crystallography, by which hard to crystallize and radiation sensitive proteins can be exposed to X-ray doses far in excess of conventional radiation damage limits at room temperature (Chapman et al., 2011). Although the first high-resolution (2 Å) structures were only demonstrated a few years ago (Boutet et al., 2012), this technique is already having significant impact on structural biology through the study of hard-to-crystallize but medically relevant G protein-coupled receptors (GPCR) at room temperature (Liu et al., 2013), time resolved studies of photochemistry (Barends et al., 2015; Pande et al., 2016) and damage-free studies of photosynthesis (Kern et al., 2014; Kupitz et al., 2014). Single particle imaging has been demonstrated at low resolution (Ekeberg et al., 2015) and progress continues to be made towards higher resolution.

4.1.2. 3-dimensional architecture of free silver nanoparticles from single-shot diffraction patterns

The final goal in single-shot single-particle imaging experiments is the reconstruction of a three-dimensional picture of the object from the one diffraction pattern which can be obtained for each target particle. Barke et al. reached this goal in the special case of a study of the 3D-architecture of individual free silver nanoparticles using 100 fs pulses of 13.5 nm radiation from FLASH (Barke et al., 2015). The authors study the diversity of nanoparticle shapes generated by condensation from gaseous matter which reflects the fundamental competition between thermodynamic equilibration and the persistence of metastable configurations during growth. It is essential to study free clusters instead of particles grown or deposited on substrates. Free particle growth is a statistical process such that a specific combination of shape, orientation and size cannot be repeatedly prepared, which excludes tomographic techniques that rely on multiple measurements of the same object or of equivalent replicas. Because of the diversity of the clusters and their orientation ensemble averaging should be avoided. For these reasons single-shot single particle imaging using free-electron lasers is the technique of choice. Fig. 36 shows the schematics of the wide-angle scattering experiment. Silver particles were produced in a cluster machine and directed into the focus of the FEL beam. The single-shot diffraction patterns were collected in a 2D detector (Bostedt et al., 2012). Reconstruction of wide-angle X-FEL scattering has been advocated by Raines et al. with emphasis on hard X-ray scattering (Raines et al., 2010). Using soft X-rays, where the wave-vectors of the incident and scattered beams are of the same order of magnitude as the momentum transfer, the 3-D information in the wide angle diffraction pattern is much more pronounced. In addition, at a wavelength of 13.5 nm, the detailed atomic structure is averaged out in the scattering image which strongly simplifies the shape analysis of the particles. On the other hand the morphology identification method must account for scattering effects beyond Born approximation, which excludes application of conventional iterative reconstruction techniques. Because parametric geometry models are available for the various shapes of silver clusters Bark et al. could develop a very efficient scheme that allows extracting the relevant 3-D structure information from a single scattering pattern of an individual particle. A total of 25,000 scattering patterns with sufficient intensity have been collected, the results are summarized in Fig. 37. This work paves the way to spectroscopy of well characterized clusters. Time-resolved experiments will allow for investigations of the shape-specific evolution of growth, of structural phase transitions and relaxation phenomena, with implications for various fields including molecular and atmospheric physics, material science, chemistry and astrophysics. Combined with femtosecond pump–probe schemes, single-shot imaging promises new insight into the ultrafast dynamics of free nanoparticles, such as collective electron (Varin et al., 2012) and nuclear (Peltz et al., 2014) motion or non-equilibrium melting processes.

4.1.3. Explosion dynamics of nano-size particles hit by a FEL pulse

To study the explosion dynamics of nano-size particles when hit by FEL X-ray pulses on fs time scales Chapman et al., stimulated by Newton's "dusty mirror" experiment, developed femtosecond time-delay holography (Chapman et al., 2007). The experimental setup is shown in Fig. 38. A membrane carrying the samples is placed near an X-ray mirror; after the pulse traverses the sample, triggering the reaction, it is reflected back onto the sample by the normal-incidence multilayer mirror to probe this reaction. The mirror is also locally destroyed by the pulse energy, but not before reflecting the pulse. For the next measurement at a different delay time the ensemble of mirror and target membrane is translated in direction perpendicular to the incident beam to reach an undamaged region of the mirror and an undamaged particle. Because the target foil is slightly tilted with respect to the mirror this translation changes the path length for the probing pulse and therefore the delay time between initiation of the explosion at its imaging. The delay is encoded in the resulting diffraction pattern to an accuracy of one femtosecond, and the structural change is holographically recorded with high resolution. Chapman et al. apply the technique to monitor the dynamics of polystyrene spheres in intense free-electron-laser pulses, and observe an explosion occurring well after the initial pulse (see Fig. 39).

4.2. Nonlinear light–matter interaction

An in-depth understanding of the interaction of the extremely intense fs VUV/XUV pulses from free-electron lasers was among the prime goals of the early experiments at FLASH. These included gas phase photoionization studies of atoms and molecules. The short pulse duration allowed modification and control of the photoionization process by synchronized intense optical laser. The high pulse energy of the FEL pulses when focused to a diameter of several microns, as well as its quasi-monochromaticity enabled detailed studies of non-linear photoionization such as direct and sequential multiple ionization or resonant multi-photon excitation. The understanding of these basic atomic and molecular processes caused by the interaction with intense short wavelength radiation is of fundamental interest to describe properly the complex electron correlation, but is also a necessary basis for the description of processes in larger systems such as nano-particles or biomolecules, or femtosecond dynamics on condensed matter surfaces.

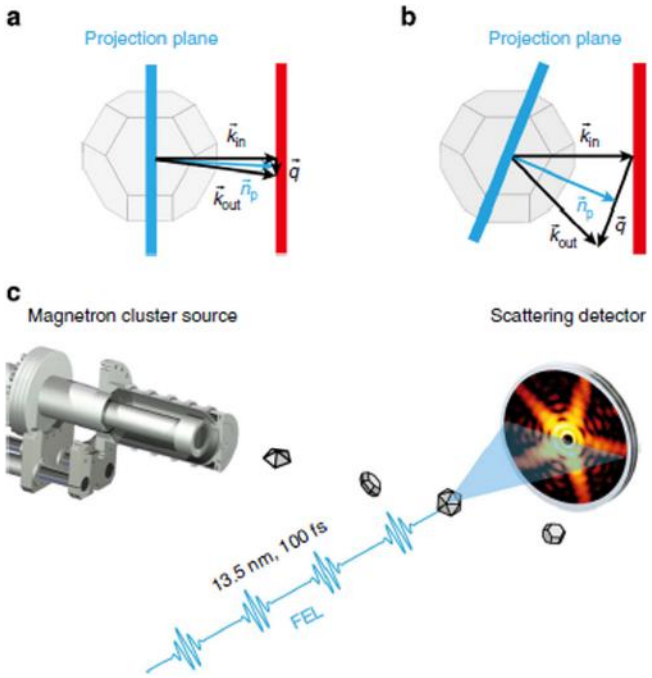

Fig. 36. Schematics of the wide-angle scattering experiment. Scattering of hard X-rays from a nanoparticle is concentrated in the forward direction. It declines with the inverse of the fourth power of the momentum transfer and the diffraction pattern includes information essentially from one projection plane and leads essentially to a 2-D picture (a). For soft X-rays the diffraction pattern includes information from projection planes including a much wider angle and contains significant 3-D information (b). (c) Silver clusters interact with the FEL beam, single-shot single-particle diffraction patterns are recorded with a 2-D detector composed of an imaging quality multichannel plate (MCP) stack, converted into optical photons with a phosphorous screen, and digitized with an out-of-vacuum CCD camera.
Source: From Barke et al. (2015) (Creative Commons Attibution 4.0 International, https://creativecommons.org/licenses/by/4.0/).

4.2.1. Photoelectric effect revisited: "The Xenon surprise"

First photoionization studies on rare gas atoms have already been performed at the TESLA Test Facility using 98 nm radiation at power densities up to 10^{13} W cm^{-2} (Wabnitz et al., 2005). The ionization products of xenon and argon atomic beams were analyzed with time-of-flight mass spectroscopy and multiple charged ions up to Xe^{6+} and Ar^{4+} have been observed. At the power levels reached in the experiment the ionization was attributed to sequential multiphoton processes. The production of multiple charged ions saturated at 5–30 times lower power densities than at wavelengths of 193 or 564 nm, respectively.

A big surprise was met when studying the photoelectric effect again in Xe, but now at FLASH using 13.3 nm (93 eV) radiation at well controlled levels of irradiance between 10^{12} and 10^{16} W cm^{-2} (Sorokin et al., 2007). The pulse duration amounted to (10 ± 2) fs. Fig. 40 shows a sketch of the experimental setup. A horizontal beam stop of 1.5 mm in height divided the incident beam into two halves with an empty slot in the middle which contained the sampling area of an ion time-of-flight (TOF) spectrometer. The radiation was focused under normal incidence by a spherical Si/Mo narrow-band multilayer mirror with a focal length of 200 mm to a focus of (2.6 ± 0.5) μm in diameter into the cylindrical sampling volume of the TOF approximately 2.6 μm in diameter and 350 μm in length. The mirror could be moved by ± 2 cm along the photon beam in order to vary the photon beam cross section A in the sampling area and, by that, the pulse irradiance. The results are shown in Fig. 41. At the highest level of irradiance ionization states of up to Xe^{21+} were observed with the TOF. For the generation of this state a total energy of more than 5 keV must have been absorbed by a single atom within a photon pulse duration of 10 fs, i.e. more than 57 EUV photons of 93 eV energy. People liked to talk about the "Xenon ionization surprise" and discussed the results in terms of perturbative and nonperturbative descriptions. It was speculated that the situation might even be beyond the scope of perturbation theory and the particle picture of light.

In a later study with the same experimental setup the photoionization of different rare gases was compared by applying ion spectroscopy at the photon wavelength of 13.7 nm and irradiance levels of up to 2.0 x 10^{15} W cm^{-2} (Richter et al., 2009). In the case of xenon, the degree of nonlinear photoionization was found to be significantly higher than for neon, argon, and krypton. This target specific behavior could not be explained by the standard theories developed for optical strong-field phenomena. More general the authors conclude that in the extreme ultraviolet the interaction of high-power lasers with matter cannot be described in the same manner as in the optical regime. Nonperturbative theories based on ponderomotive motion of quasifree electrons are not applicable. On the other hand, the inner-shell electron structure, electron correlation, and resonances play a significant role in explaining strong-field phenomena on photoionization in

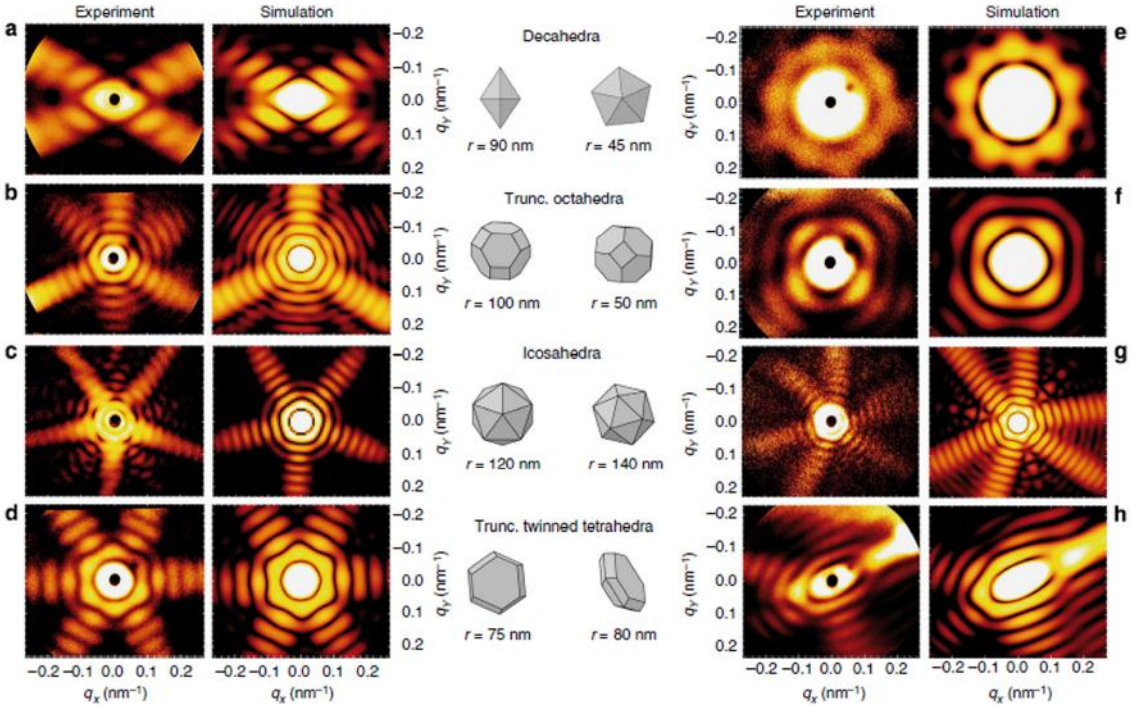

Fig. 37. Comparison of measured and theoretical scattering images. (a–d) Selected experimental scattering patterns of single Ag particles and simulation results for matched geometries. False-color images show the scattering intensity (logarithmic scale) as function of the transverse components of the scattering vector. The dark spot in the center of the experimental data originates from a hole in the detector for direct beam transmission. Cluster shapes are drawn as seen from the direction of the incident beam. The size is given by the radius r of the polyhedra's circumscribed sphere. (e–h) Same cluster shapes as in (a–d) but imaged at different orientations with respect to the incident beam.
Source: From Barke et al. (2015) (Creative Commons Attibution 4.0 International, https://creativecommons.org/licenses/by/4.0/).

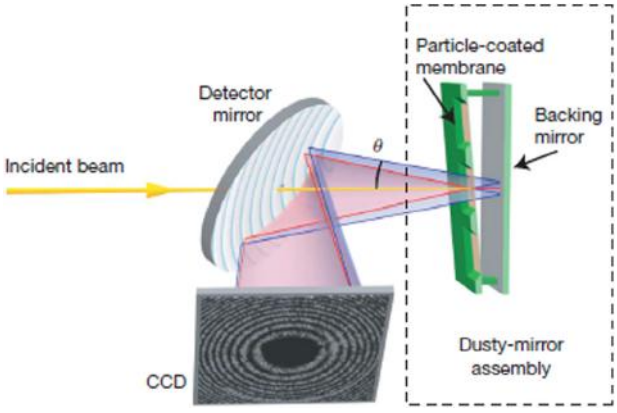

Fig. 38. Diagram of the apparatus, similar to Newton's dusty-mirror experiment. The incident FEL pulse from the left passes through a hole in a multilayer-coated detector mirror. The 'dusty mirror' consists of particles on a 20-nm-thick silicon nitride membrane backed by a multilayer-coated plane mirror. This returns the direct beam back through the hole in the detector mirror, which reflects the diffracted light onto a CCD detector. The prompt diffraction (blue, the reference wave) and delayed diffraction (red, the object wave) interfere to generate the hologram on the CCD detector.
Source: From Chapman et al. (2007).

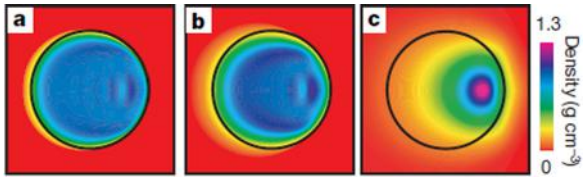

Fig. 39. (a–c) Simulated density profile of an initially uniform 140-nm-diameter polystyrene ball (black circle) irradiated by a 25-fs, 10^{14} W cm^{-2} soft-X-ray FEL pulse from the left, after 0.5 ps (a), 0.9 ps (b) and 3.2 ps (c).
Source: From Chapman et al. (2007).

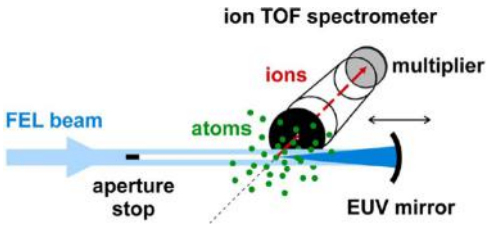

Fig. 40. Experimental setup for the investigation of atoms by ion time-of-flight (TOF) spectroscopy at the FLASH free-electron laser facility. The 13.3 nm radiation is focused under normal incidence by a spherical Si/Mo narrow-band multilayer mirror with a focal length of 200 mm to a focus of (2.6 ± 0.5) μm in diameter. A horizontal beam stop of 1.5 mm in height divides the incident beam into two halves with an empty slot in the middle which contains the sampling area of the TOF defined by its aperture of 0.35 mm parallel and 1.0 mm perpendicular to the FEL beam. The pulse irradiance in the intersection zone was varied by moving the multilayer-mirror along the incident FEL beam and thus changing the effective beam size. To ensure that any interactions between neighboring atoms do not affect the data, the target gas filled the experimental vacuum chamber homogeneously at the low pressure of about 1.1×10^{-4} Pa.
Source: Courtesy M. Richter From (Sorokin et al., 2007).

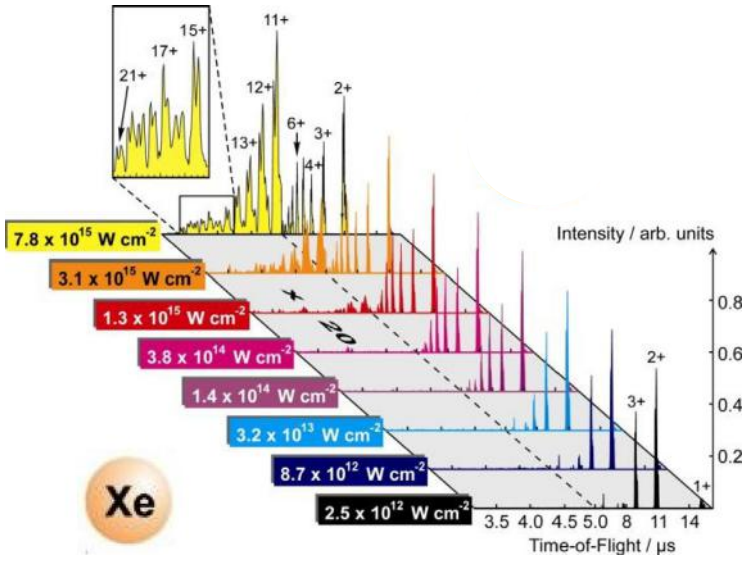

Fig. 41. Ion time-of-flight (TOF) mass/charge spectra of xenon (Xe) taken at a photon energy of 93 eV and different pulse irradiance levels. Each spectrum represents an accumulation over 300 to 500 consecutive FEL shots. In the low TOF regime (below 5 μs), the ion intensities were multiplied by a factor of 20. The multiplet structures of the different ion signals are due to the Xe isotope distribution.
Source: Courtesy M. Richter From (Sorokin et al., 2007).

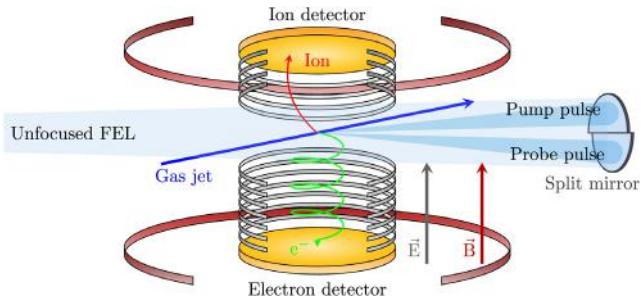

Fig. 42. Reaction microscope (REMI) for the investigation of atomic and molecular collisions with electrons, ions, and single photons in combination with a split-and-delay mirror assembly for focusing and pulse-pair creation. The FEL beam is focused onto a collimated supersonic gas jet in the center of an ultrahigh vacuum chamber (Ullrich et al., 2003). Ions and electrons are guided by means of weak electric and magnetic fields applied along the spectrometer axis onto two position-sensitive and multi-hit capable MCP detectors achieving a detection solid angle close to 4 for all particles of interest. From the measured flight times and positions on the detector, the initial momentum vectors are reconstructed. The REMI allows highly differential or even kinematically complete measurements.
Source: From Schnorr et al. (2015).

the short-wavelength regime of the photoelectric effect. First attempts to theoretically approach the xenon results have been published including discussions of the role of giant resonances and collective effects on photoionization in the high-intensity short wavelength regime (Popruzhenko et al., 2008; Makris et al., 2009; Richter, 2011; Lambropoulos et al., 2011).

4.2.2. First differential cross-sections for double ionization of He and Ne

Theory has been quite successful when describing the interaction of few photons with few electrons. Correlated electron emission in single-photon double or multiple ionization of Helium is a prominent example. By now the problem of single-photon double ionization is considered to be solved. At the other extreme case, in experiments with short-pulse lasers in the IR or visible regime, ionization and excitation of atoms proceed via absorption of several tens of photons, and a solid ab-initio theoretical description of two- or more-electron transitions like e.g. double ionization of Helium, is still out of reach, simply because too many photons being absorbed at the same time. Between these two extreme regimes are cases were only two or three photons are absorbed in double excitation or double ionization reactions. The theoretical treatment of the prototype reaction, two-photon double ionization of He, is challenging but feasible - a large number of theoretical papers on this subject appeared during last 10 years. Corresponding experiments can be done only with intense pulses of short wavelength (VUV or XUV) provided by free-electron lasers. At FLASH the group of J. Ullrich and R. Moshammer from the Max-Planck Institute for Nuclear Physics in Heidelberg succeeded in measuring the first differential cross-sections for double ionization of He and Ne. The group used the Heidelberg reaction microscope (REMI) shown in Fig. 42 in combination with a split-and-delay mirror assembly both for focusing and performing XUV–XUV pump–probe experiments in studies of time-resolved molecular reactions. Differential measurements on two-photon double ionization of Ne and He (Moshammer et al., 2007; Rudenko et al., 2008) provided first evidence for different electron emission characteristics for sequential and direct (non-sequential) two-photon transitions. The very first kinematically complete measurement on two-photon double ionization of Ne at 44 eV could be performed using the REMI at FLASH (Kurka et al., 2009). This comprises the coincident and 3D momentum resolved detection of both electrons together with the doubly charged ion. The data are in accord with the dynamics expected for 'sequential' ionization. The angular asymmetry parameters inferred from the electron angular emission distributions served as benchmark data for theory. In a subsequent study on He the correlated electron dynamics could be extracted and analyzed by inspection of recoil-ion momentum distributions (Kurka et al., 2010). In comparisons with state-of-the-art theoretical models good agreement was achieved within the experimental error bars, with remaining significant differences under certain kinematical conditions.

4.2.3. Pioneering studies of the nature of formation and breaking of molecular bonds

Today, in ultra-fast physics, fundamental questions related to the dynamics of molecules in excited states are mostly studied with table-top ultra-fast lasers like attosecond high-harmonic sources or phase-stabilized few-cycle optical light pulses. The nature of the formation and breaking of molecular bonds are examined by probing the correlated motions of electrons and nuclei in molecules, the motions of nuclei during a chemical reaction, or the redistribution of vibrational-energy along the reaction coordinate, ideally with atomic spatial and temporal resolution. However, because of the limitations of wavelength and time regimes accessible by ultra-fast optical lasers the above mentioned ansatz could only partly provide answers to the questions of high interest in conventional femtochemistry. Progress is expected from using XUV or X-ray radiation provided by modern free-electron Lasers (XUV and X-rays) because probe and pump are typically perturbative single-photon interactions for both, excitation and/or ionization, which make a theoretical treatment of the processes straight forward and keep the perturbation of the investigated atoms and molecules by pump and probe pulses

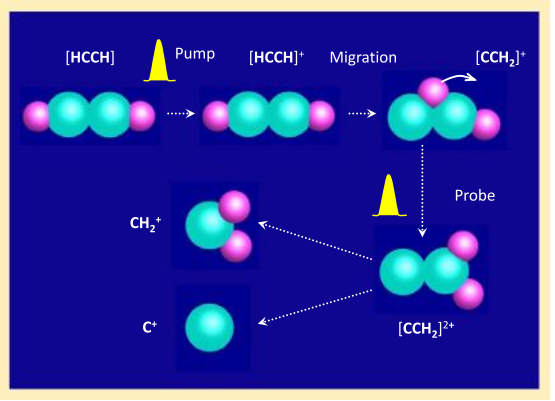

Fig. 43. Schematic presentation of an acetylene–vinylidene reaction observed by an XUV-pump/XUV-probe experiment. After ionization by absorption of a photon out of the pump pulse the originally linear structure of the acetylene molecule changes to the bend structure of the vinyliden molecule. The subsequent probe pulse ionizes the molecule further which leads to a Coulomb explosion. Depending if the molecule is in an acetylene (HCCH)- or vinylidene (CCHH)-modification it will disintegrate into two CH^+-fragments or in a C^+- and a CH_2^+-fragment. The momentum distribution of the fragments is determined with the 2D ion detector of the REMI and allows differentiation between the two modifications of the molecule.
Source: From Moshammer et al. (2013).

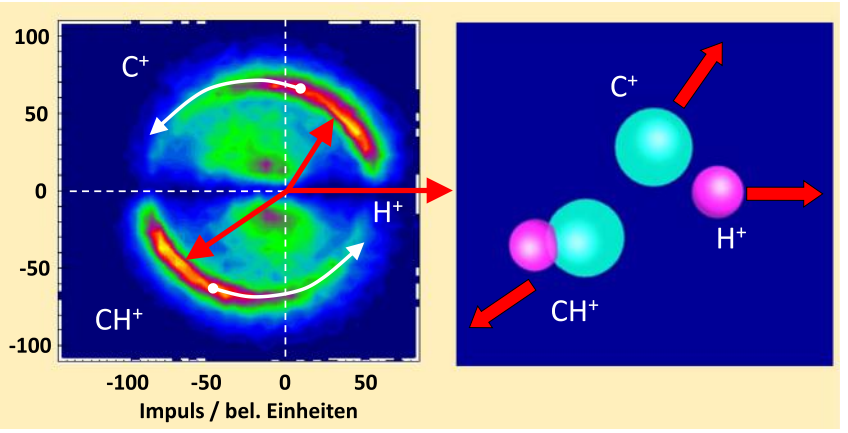

Fig. 44. 2-dimensional momentum distribution of C^+- and CH^+-fragments after a three-particle-Coulomb-explosion removing 2 electrons by the probe pulse. In the data analysis the momentum distribution is oriented such that the momentum of the H^+-fragment always points in the horizontal to the right. The right figure shows the molecular structure deduced from the momentum distribution on the left. With increasing delay between pump and probe pulse the momentum distributions of the C^+- and CH^+-fragments rotate as indicated by the white arrow from which one concludes that the molecular structure approaches more and more the vinylidene modification.
Source: From Moshammer et al. (2013).

small. This makes a big difference compared to conventional measurements with IR or visible laser pulses involving strong-field multi-photon probes or "streaking" scenarios. In addition, highly excited molecular states, relevant for e.g. modeling of interstellar molecular clouds, are easily accessible by absorption of just one photon, and the subsequent molecular dynamics can be probed with FELs. A number of pioneering experiments have been performed at FLASH using the Heidelberg RMI combined with XUV–XUV pump–probe schemes shown in Fig. 42:

- The ultrafast nuclear wave-packet motion in D_2 cations could be resolved with a time resolution of better than 10 fs in excellent agreement with time-dependent quantum calculations (Jiang et al., 2010a). The measurements were the first demonstration for resolving molecular dynamics with sub 10 fs resolution using intense FEL radiation.
- The process of ultrafast isomerization of acetylene molecules C_2H_2 triggered by single photon excitation (Fig. 43), i.e. migration of an H-atom from a HCCH-configuration to a CCHH-configuration, has been investigated (Jiang et al., 2010b). By recording and analyzing coincident ion fragments created by Coulomb-explosion in the probe pulse an isomerization time of 52 +/- 15 fs was found. The results triggered theoretical quantum-chemistry calculations. By analyzing the two-dimensional momentum distribution of C^+ and CH^+- fragments the structure of the molecule at the moment of the Coulomb-explosion could be determined (Fig. 44). By varying the time between pump and probe pulse the structural changes during the isomerization process was visualized. These results may be seen as a

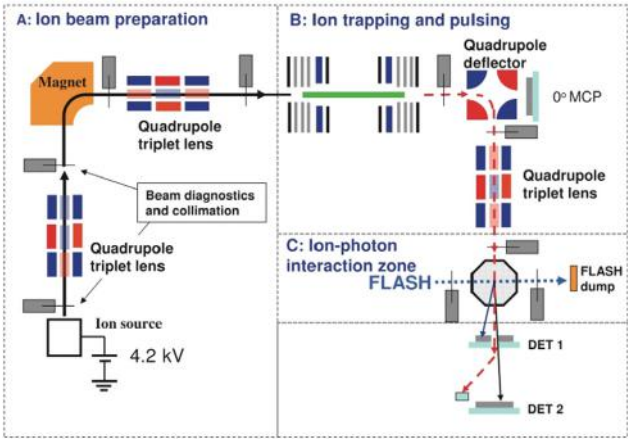

Fig. 45. Scheme of the ion beam infrastructure TIFF installed at FLASH. The solid black line shows the dc ion beam, the thick green (light gray) line shows the optionally trapped beam, and the dashed red (gray) line shows the ion pulses behind the ion trap (Pedersen et al., 2009).

first realization of the old dream to film molecular reactions. A pictorial description of the process is provided by Moshammer, Rudenko and Ullrich (Moshammer et al., 2013).

- The lifetime of interatomic Coulombic decay (ICD) in Ne dimers has been determined for the first time (Schnorr et al., 2013). The experimental value for the ICD-lifetime of 150 +/- 50 fs was found to be in agreement with quantum calculations, but only those that explicitly take into account the intermolecular nuclear motion between the excitation step and the subsequent ICD decay.
- The charge rearrangement in dissociating I_2 molecules, i.e. the transfer of electrons from one site to the other, could be observed in real-time (Schnorr et al., 2014). From the measured fragmentation kinematics the effective internuclear distance between both constituents at the moment of electron exchange was extracted. The results could be explained using a very (surprisingly) simple classical over-the-barrier model for electron transfer, with possible implications for plasma modeling or chemistry applications.

4.2.4. Photo-absorption at XUV photon energies on molecular ions

In addition, highly excited molecular states, relevant for e.g. modeling of interstellar molecular clouds, are easily accessible by absorption of just one photon, and the subsequent molecular dynamics can be probed with FELs.

The intense photon pulses of FLASH make it possible to study photo-absorption at XUV photon energies also on dilute targets like molecular ions. When such experiments are performed with fast moving ion beams, the photo-fragments can be projected onto particle detectors at the high beam velocity. Such interaction conditions allow both charged and, in particular, neutral reaction products to be detected and analyzed with respect to fragmentation energy and break-up geometry. The group of A. Wolf and H.B. Peterson from the Max-Planck Institute for Nuclear Physics in Heidelberg realized at FLASH an ion infrastructure for trapped ion fragmentation named TTIF which allows the characterization of photo-fragmentation processes of molecular ions and radicals after valence shell excitations or ionization within a fast moving ion target (Pedersen et al., 2009). The scheme of the experimental setup is shown in Fig. 45.

With the possibility to perform measurements directly on molecular ions, even systems whose electron shell is particularly stable in ionic form could be studied. In general the protonated versions of stable atoms or molecules belong to this class and the first experiment, which demonstrated that photo-dissociation experiments were possible with an ion beam and XUV photon pulses from a free-electron laser, was performed on protonated helium HeH^+ (Pedersen et al., 2007). Through fragmentation imaging, the photo-fragment momenta were studied below the ionization threshold to HeH^{++}, which revealed the nature of the intermediate excited states of HeH^+ most favorably populated by XUV absorption. The method was extended to study the effects of vibrational levels and to perform more detailed studies of the final atomic states reached after the photodissociation (Pedersen et al., 2010). The measurement gave rise to new theoretical studies (Dumitriu and Saenz, 2009; Loreau et al., 2011) which show that the non-adiabatic effects found in the experiments during the dissociation process are difficult to accurately represent in theoretical calculations today. There is much room for future studies of molecular ion systems of importance in the development of the theory of highly excited molecular states and for understanding processes in astrophysical and atmospheric environments.

The protonated water molecule H_3O^+ (the hydronium ion) is important because of its wide natural occurrence. Water can bind a proton with high proton affinity (about 6 eV). Moreover, once H_3O^+ is formed, either in liquid water or in the gas phase, it can trigger further complex reactions leading to formation of larger protonated water clusters. Here, the interplay of electronic and vibrational excitation is of particular interest and can be sensitively studied by photoionization of valence electrons and the subsequent fragmentation of the di-cation H_3O^{++}. These studies, employing XUV photons,

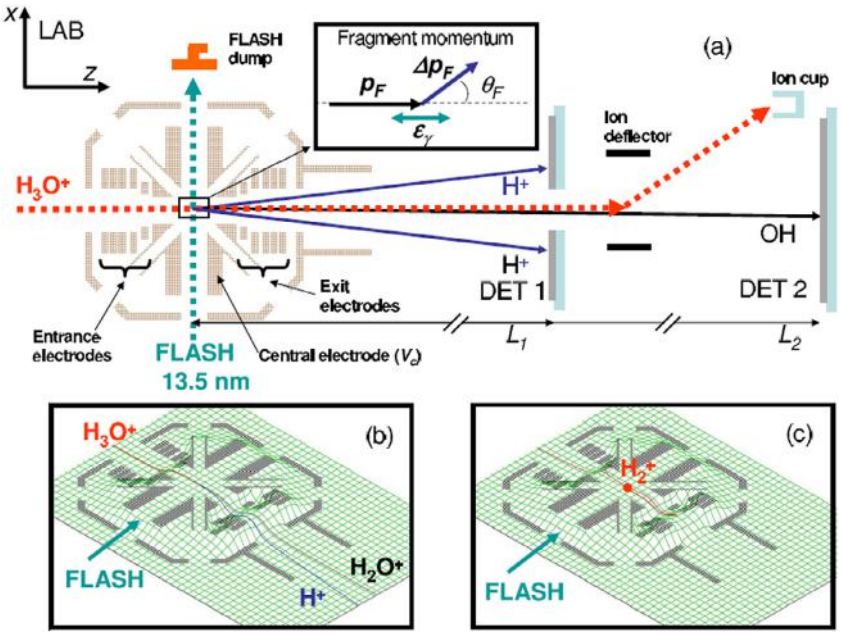

Fig. 46. (a) The ion–photon interaction zone and fragment imaging system (not to scale) indicating the detection of the fragmentation channel OH+2H$^+$. The inset shows the fragment momentum representation with ε_γ being the photon polarization. (b) Electrical potential surface in the interaction region and related ion trajectories for outgoing fragments after an H_3O^+ breakup into H_2O^++H$^+$ with a total kinetic energy release of 5 eV. (c) The same potential surface demonstrating the rejection of a slow (2 eV) H_2^+ produced by FLASH in the residual gas (Pedersen et al., 2009).

require stable targets of protonated ions, which are very dilute. The very intense XUV radiation provided by FLASH made it possible to study the XUV ionization of H_3O^+ ions and small protonated water clusters (Pedersen et al., 2009). The ion–photon interaction zone and the fragment imaging systems used in this experiment are shown in Fig. 46. For H_3O^+, analysis of the photo-fragment momenta after photolysis with FLASH revealed very detailed information on the photoionization and break-up processes:

- Photoionization leads to the production of the water radical ion H_2O^+ in about 70% the cases, mostly (>75%) via the $1e_1$ orbital of H_3O^{++} di-cation.
- Ground-state, neutral OH radicals are produced in about 18% of the cases, via the $1e_1$ valence orbital of H_3O^{++} di-cation.
- Electron detection in coincidence with the dominant H_2O^+ product channel shows that photoionization from outer ($3a_1$ and $1e_1$) valence orbitals by far dominates and shows that a contribution from the $2a_1$ inner valence orbital should be much smaller (only a few percent of the outer valence).
- The H_2O^+ radical cations produced are mostly in an excited state ($\tilde{A}\ ^2A_1$) of linear geometry.

The results could also shed first light on the photoionization of gas-phase H_3O^+ ion via the so far little studied H_3O^{++} di-cation and showed that also electron detection is feasible for XUV experiments with ion beams.

The protonated water cluster $H^+(H_2O)_2$ was found to behave differently in photoionization as the formation of a di-cationic single-water structure with subsequent destruction of one of the water molecules was avoided. Instead, the experiment on photoionizing $H^+(H_2O)_2$ ions with 90 eV FLASH photons showed that the product channel H_3O^+ + H_2O^+ is dominant (Lammich et al., 2010) , in which two ionized water structures are maintained. Soon afterwards, a theoretical explanation of this result was suggested (Li et al., 2013). It showed that a photon-generated valence-shell vacancy would be repelled from the positive charge of the proton in an ultra-fast non-adiabatic molecular coupling mechanism; hence the formation of a di-cationic structure with two positive charges on a single water molecule is strongly suppressed. This ultra-fast non-adiabatic dynamics has recently been extended to photoproduced vacancies also in larger molecular structures (Li and Vendrell, 2016).

Studies of negative ions using fast beam setups at free electron laser facilities hold a huge potential to analyze previously inaccessible molecular processes. In particular, the high pulse intensity available at these facilities enables the favorable crossed photon-ion-beam geometry, from which all photofragments and electrons are universally detectable. With the TIFF setup at FLASH these possibilities were first demonstrated by the study of one and two electron detachment of anionic oxygen (O^-) in 2012 (Harbo et al., 2012), were both electrons, neutral, and single positively charged fragments were observed, revealing for instance a clear dominance of neutral fragments.

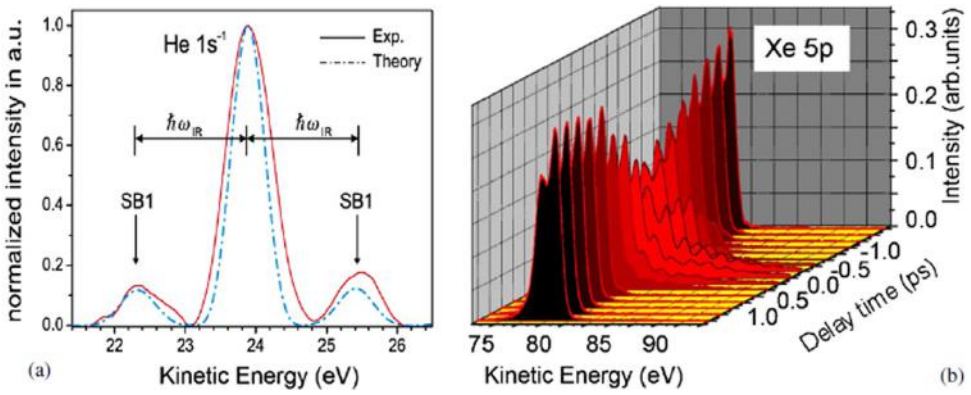

Fig. 47. (a) Typical single-shot photoelectron spectrum of the 1s ionization of atomic He for overlapping FEL and NIR pulses ($h\nu$ (FEL) = 48.5 eV and I (NIR) = 2×10^{11} W cm^{-2}). The theoretical spectrum obtained from TDSE calculations is given as a dashed line for comparison. (b) Series of electron spectra (average of 100 single-shot spectra) of atomic Xe as a function of the temporal delay between the FEL and NIR pulses (($h\nu$ (FEL) = 91.8 eV and I (NIR) = 4×10^{13} W cm^{-2}).
Source: From Meyer et al. (2010a).

4.2.5. Studies of photoionization multiphoton processes in the presence of intense optical fields

Photoionization in the presence of an intense optical field was investigated in experiments combining the XUV-FEL and synchronized optical pulses (Meyer et al., 2006, 2010a,b). The spatial and temporal overlap of both pulses gives rise to additional structures in the photoelectron spectrum, so-called sidebands, which are a clear signature of the interaction with the optical field during the photoionization process. The appearance of the sidebands has been already demonstrated with high-order harmonic generation sources (Glover et al., 1996), but the use of single-wavelength FEL radiation enabled to clearly observe multi-photon processes induced by the optical laser in the ionization continuum and to test the theoretical descriptions of the corresponding free–free transitions (Meyer et al., 2010a,b; Radcliffe et al., 2012). A typical spectrum resulting from two-color above threshold ionization (ATI) is shown in Fig. 47(a). The spectrum was recorded upon photoionization in the 1s shell of atomic He by one single FLASH pulse operating at 25.5 nm (48.5 eV) and by using a NIR dressing field of about 2×10^{11} W cm^{-2} created by a 800 nm, 120 fs, 20 μJ laser pulse. At this intensity of the dressing field, about 20% of the electron signal is transferred from the main photoline into the sidebands, which are energetically displaced from it by 1.55 eV, i.e. by the photon energy of the NIR laser. The process is well understood and the experimental data can be perfectly reproduced by a theoretical analysis using the so-called 'soft-photon' approximation (Maquet and Taïeb, 2007) or by numerically solving the time dependent Schrödinger equation (TDSE) for a single active-electron, three-dimensional model of He (Guyétand et al., 2005). Fig. 47(b) shows a series of sideband measurements at Xe atoms as a function of the degree of temporal overlap.

After having explored the general feasibility of these two-color experiments, attention was given to details of the photoionization process. In particular, the effect of the polarization of the radiation was explored, i.e. experiments measuring the linear dichroism in the integrated or angle-resolved photoemission were performed (Meyer et al., 2008; Richardson et al., 2012; Düsterer et al., 2013). In a proof-of-principle experiment on atomic helium, the dichroism for the simplest case of non-linear processes, the two-photon ionization, was analyzed (Meyer et al., 2008), i.e. the intensity variation of the first sideband was monitored as a function of the relative angle between the linear polarization vector of the XUV and optical radiation, respectively (see Figs. 48–49). The emission of the He 1s electron by a two-photon process is described by the superposition of two outgoing partial waves, characterized by "s" and "d" symmetry, respectively. Both partial waves are differently affected by the relative orientation of the polarization vectors. As a consequence it is possible to determine the relative contribution of the "s" and "d" waves by comparing the experimentally recorded dichroism with the theoretical analysis of the two-photon process. This procedure is well known for experiments involving discrete states, but could not be realized before in the ionization continuum in the non-linear regime. Generally, the final aim of these experiments is the "complete" characterization of the ionization process, i.e. the determination of the amplitudes of the outgoing partial waves and their relative phase, quantities enabling the most profound comparison with theory.

The effect of an intense optical dressing field superimposed to the FEL radiation was also investigated in studies of the relaxation dynamics of inner shell resonances. In this type of experiment the electric field of the optical laser causes a shift of the energy levels in the atom and a modification of the resonance line shape. For the case of the resonant 3d→5p excitation in atomic Kr (Mazza et al., 2012), a displacement of the resonance position of about 100 meV, i.e. in the order of the natural line width, was observed. In addition, the width of the resonance changed as a function of the optical intensity, because the optical laser can also ionize the excited 5p electron, which represents a three-photon process. The 5p ionization competes with the relaxation of the resonance via Auger decay and represents a second decay channel,

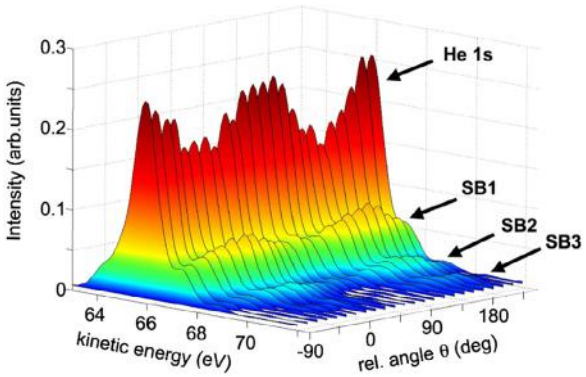

Fig. 48. Photoelectron spectra showing the He 1s photoline and the high energy sidebands for high optical dressing fields (∼6 x 10^{11} W=cm^2) upon photoionization at 90.5 eV. Spectra are presented for different relative orientations θ between the linear polarization vectors of the FEL and the 800 nm laser.
Source: From Meyer et al. (2008).

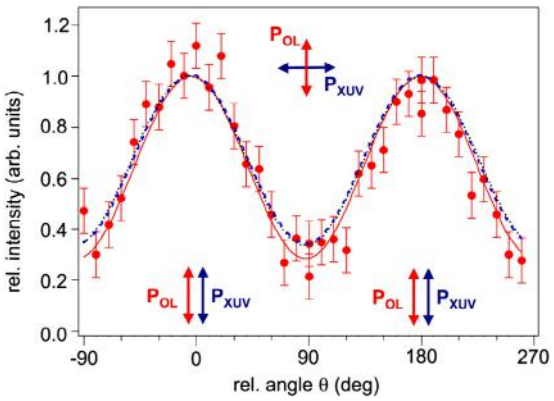

Fig. 49. Variation of the upper sideband yield in the low field regime (∼8 x 10^{10} W/cm^2) for the two-photon ionization in the He 1s shell at 13.7 nm as a function of the relative angle θ between the linear polarization vectors of the FEL and the 800 nm laser. The solid line denotes the fit to the experimental data (circles). The results of time-dependent second-order perturbation theory (dashed line) and soft-photon approximation (dotted line) are almost identical.
Source: From Meyer et al. (2008).

which reduces the lifetime of the resonance and broadens its profile. This experiment is therefore a demonstration of the possibilities for optical control of electronic relaxation processes on the femtosecond time scale. The intense optical laser enabled (i) the change of the absorption strength of a medium for a particular wavelength as function of optical intensity (optical switch) and (ii) the control of the relaxation dynamics passing from a resonant Auger process, which is producing dominantly singly charged ions, towards a normal Auger process resulting mainly in doubly charged ions.

Beside the possibility to initiate the non-linear process by an intense optical field, the high number of photons carried in the short XUV FEL pulses can also induce a multi-photon transition. In general, the two-photon processes are at the considered intensities (10^{13}–10^{14} W/cm^2) several orders of magnitude less efficient than a one-photon process, but for specific cases, e.g. resonant excitations and two-photon above threshold ionization (ATI), the weak two-photon events can easily be separated from the intense one-photon signal. The first study of a two-photon core resonance was realized for the 3d→4d excitation in atomic Kr (Meyer et al., 2010a,b). Due to the dipole selection rules for electronic transitions, the absorption of two photons opens the access to resonances, which are characterized by the same symmetry as the ground state, i.e. resonances forbidden by one-photon excitation. The possibility to excite with the intense FEL radiation these two-photon resonances opens a completely new class of investigations dedicated to resonances and corresponding relaxation dynamics, which were excluded from all previous studies.

Similarly, a direct two-photon transition in the ionization continuum, called above threshold ionization (ATI), was investigated for atomic xenon in the region of the 4d giant resonance. After the first observation of the 4d ATI signal (Richardson et al., 2010), the systematic study of the photon energy dependence of the ATI signal (Mazza et al., 2015) provided new and unique information on the 4d giant resonance. The theoretical description of the two-photon process, which was supported by quantitative agreement with the experiments, demonstrates high sensitivity of the ATI signal to the photon energy. In particular, it emphasizes substructures in the broad 4d giant resonance profile, which are clear

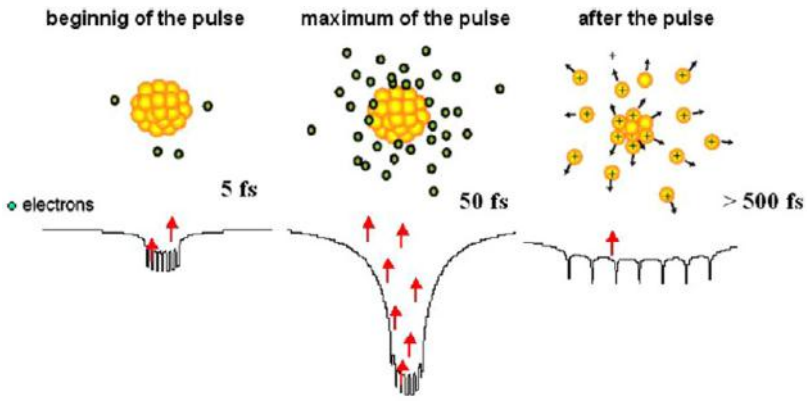

Fig. 50. Schematic illustration of the ionization of Xe clusters and subsequent Coulomb explosion. The Coulomb potential of the clusters is shown at the beginning of the FEL pulse, at its maximum and at the end of the pulse. Photons are indicated by red arrows (Bostedt et al., 2010a).

signatures for collective phenomena. Through this combined experimental and theoretical study of the two-photon signal new insights were obtained in phenomena, which, although extensively studied, remained undiscovered in one-photon excitation experiments. This type of experiments will certainly be further explored and developed in the future, because it provides unique and new information on the photoionization dynamics in the short wavelength regime.

4.3. Clusters

The next logical step in research with FELs are studies of the interaction of intense FEL beams with clusters. These are assemblies of a limited number of atoms and molecules. Clusters are intermediates between atoms and molecules with clearly defined energy states and condensed matter with energy bands. Clusters of variable size can be produced routinely and they are often studied in the gas phase, i.e. no interaction with a surrounding medium. These experiments allow distinguish between inter- and intra-atomic effects and make clusters model systems for the investigation of light–matter interactions. Cluster experiments provide instructive data for benchmarking theoretical models. X-ray based tools can yield information about their structural properties, their electronic structure with chemical sensitivity, their optical and magnetic behavior, as well as their dynamics. Because targets in gas phase experiments are strongly diluted, intense beams of synchrotron radiation with tunable wavelength and arbitrary polarization are most used for such experiments today. In terms of peak brightness, FELs are many orders of magnitude brighter than synchrotron radiation sources and enable new strategies for the investigation of clusters. Single-shot single-particle imaging experiments become possible. The pulse structure and high photon flux in each FEL pulse can be exploited to apply the powerful X-ray spectroscopic tools to ultra-dilute samples like size selected clusters (see Fig. 32). Detailed studies about ionization and disintegration of nanometer-sized samples in intense X-ray pulses become possible. A schematic illustration of the ionization of clusters and subsequent Coulomb explosion in an FEL beam is shown in Fig. 50. For a recent review on X-ray studies of clusters see Bostedt, Gorkhover, Rupp and Möller (Bostedt et al., 2016b).

Already the first experiment with 13 eV radiation from the FEL at the Tesla Test Facility (Wabnitz et al., 2002) demonstrated that clusters, forming the bridge between the gas and the condensed phase of matter, are very well suited to explore the light–matter interaction in the new parameter regime offered by free-electron lasers. Since then rare-gas clusters have revealed a surprising variety of phenomena, changing drastically with the photon energy. Studies include

- Thermionic electron emission (Laarmann et al., 2004) and multi electron dynamics in XUV radiated clusters (Bostedt et al., 2010b)
- Identification of a step-wise, sequential ionization process (Bostedt et al., 2008)
- Identification of recombination processes in clusters (Hoener et al., 2008; Saalmann, 2010; Schroedter et al., 2014; Müller et al., 2015)

4.3.1. Cluster ionization dynamics in intense short-wavelength laser pulses

The first VUV experiments together with a number of theoretical works show that collisional plasma heating through inverse bremsstrahlung is typically the leading high heating process in the 100 nm wavelength range, and electron emission mostly proceeds via thermal evaporation. With increasing photon energy collisional plasma heating processes diminish rapidly and different heating and electron emission processes take the lead. The current understanding of cluster ionization dynamics in intense short-wavelength laser pulses has been summarized by Arbeiter and Fennel (Arbeiter and Fennel, 2011) (see Fig. 51). The authors investigate the wavelength-dependent ionization, heating, and expansion dynamics of medium-sized rare-gas clusters (Ar_{923}) under intense femtosecond short-wavelength free-electron laser

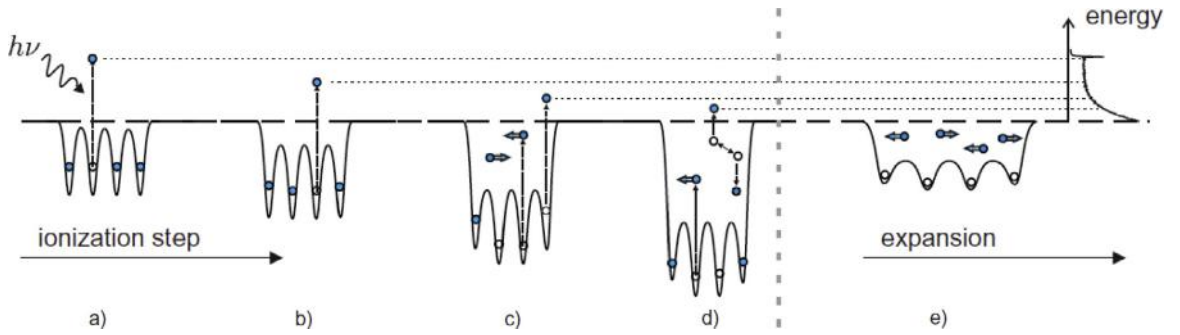

Fig. 51. Schematics of the cluster ionization dynamics in intense short-wavelength laser pulses based on the effective cluster potential. After direct photoemission of the first electron (a), subsequently emitted photoelectrons experience a continuous Coulomb downshift with increasing cluster charge (b). This multistep ionization becomes frustrated at a certain ionization stage and nanoplasma formation sets in (c). Collisions between trapped electrons induce evaporation electron emission (d). Finally, the cluster expands due to charging and hydrodynamic forces (e) (Arbeiter and Fennel, 2011).

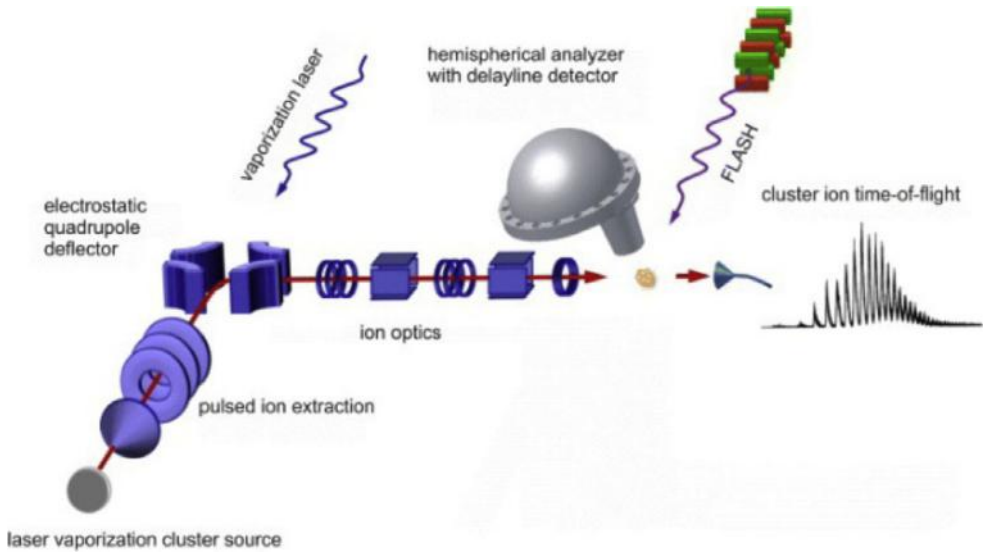

Fig. 52. Schematic view of the experimental setup for conducting soft X-ray PES on mass-selected clusters. The cluster beam is produced by a pulsed laser vaporization source. After acceleration with a 1 kV electric potential the clusters are guided and focused into the interaction region. There, the mass-resolved cluster bunches overlap with radiation from FLASH. A hemispherical analyzer with a maximum detection angle of $\pm 13^{\circ}$ disperses the electrons which are registered in a delay-line detector allowing for time-resolved electron detection. Due to the separation in time it is possible to assign the electron signals to the corresponding cluster sizes (Bahn et al., 2012).

pulses by quasi-classical molecular dynamics simulations. A comparison of the interaction dynamics for photon pulses with $\hbar\omega = 20$, 38 and 90 eV energy at fixed total excitation energy indicates a smooth transition from plasma-driven cluster expansion, where predominantly surface ions are expelled by hydrodynamic forces, to quasi-electrostatic behavior with almost pure Coulomb explosion. Corresponding signatures in the time-dependent cluster dynamics, as well as in the final ion and electron spectra, corroborate that this transition is linked to a crossover in the electron emission processes. The authors conclude that the resulting signatures in the electron spectra are even more reliable for identifying the cluster expansion mechanisms than ion energy spectra.

4.3.2. Inner-shell photoemission spectroscopy on metal clusters with precisely known number of atoms

Changes in the electronic structure of metal clusters as a function of their size have been studied extensively with photo-electron spectroscopy and synchrotron radiation. The investigations on isolated clusters suffer from the fact that only size distributions of the clusters produced in jet expansions could be studied. Spectroscopy on mass-selected clusters suffers from the extremely dilute target densities. However, with the advent of free-electron lasers inner-shell photoemission spectroscopy on clusters with precisely known number of atoms become feasible. Bahn et al. performed Pb 4f photoelectron spectroscopy on mass-selected anionic lead clusters at FLASH (Bahn et al., 2012), the experimental setup is shown in Fig. 52. FLASH provided pulse trains of up to 200 micro-pulses separated by 1 μs at a frequency of 10 Hz, the

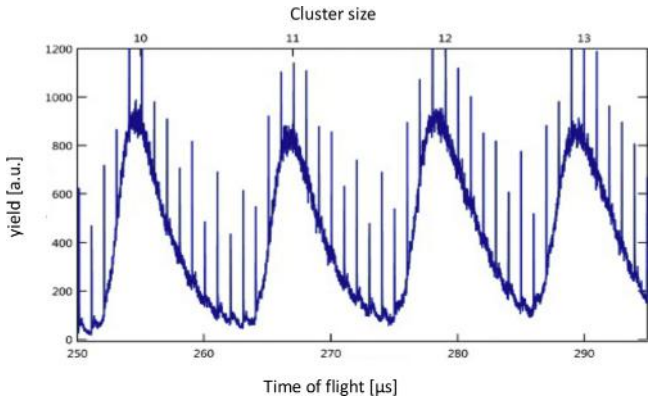

Fig. 53. Timing control of cluster mass peaks (broad features) and the FLASH micro-pulses (narrow features on top of the mass peaks). The channeltron detector registers the cluster ions simultaneously with stray light from FLASH. With the gated electron spectrometer photoelectrons from each single micro-pulse are selectively registered (Bahn et al., 2012).

photon energy was 263.5 eV. The interaction zone was deliberately placed 1.5 m out of the FLASH focal point in order to reduce the peak intensity and illuminate a 1.5 mm spot, which matches the size of the cluster beam. By this a sufficiently large number of clusters were exposed and multi-photon effects could largely be neglected. The ion acceleration and the delay-line detector were triggered by the FLASH clock such that the pulse train overlapped in time with a defined cluster size range (see Fig. 53) and photoelectrons released by each micro-pulse could be assigned to a given cluster size. The ions as well as the FLASH stray light signals were registered simultaneously by the channeltron. Only a few delay settings were necessary to record photoelectron spectra of a wide range of selected clusters, here with the number of atoms in a cluster varying between 10 and 90 atoms. The size dependence in the measured 4f binding energies shows metallic behavior for cluster larger than Pb_{20}, i.e. for clusters containing more than 20 atoms. For smaller clusters a deviation in the 4f binding energies is observed. The authors attribute this finding to a full screening of the core hole which, in agreement with earlier results for the 5d levels, indicates a change in bond character from metallic to non-metallic clusters.

4.3.3. Combining single-shot single-particle imaging and spectroscopy

Free-electron lasers enable single-shot single-particle scattering and spectroscopy experiments. Because size and shape of the individual particles can differ from shot to shot and also groups of particles may interact with the FEL beam, the value of these experiments increases significantly if the target particles can be characterized shot by shot using imaging techniques. The group of Thomas Möller from Technical University Berlin developed such techniques at FLASH. Their first experimental setup is shown in Fig. 54, which is used together with time-of-flight ion and electron spectrometers for studies of ionization dynamics and electron emission (Bostedt et al., 2010a).

The imaging device is based on a multi-channel plate (MCP) in combination with a phosphorous screen as photon amplifier and an out of vacuum CCD camera. The MCP front is pulsed active with a negative voltage for only 50 ns during the arrival of the light pulse. In this way, photoelectrons generated by the laser pulse are deflected from the detector and the MCP is switched off prior to the arrival of ionic fragments from the nanoclusters explosion, resulting in clean scatter photon detection. The X-ray pulse can exit through a 3 mm hole in the detector assembly. This setup allows the detection of scattering angles from $\pm\,3^\circ$ to 50° over 2π covering a large solid angle. The experiments were performed with intense soft X-ray pulses at $\lambda = 13.7$ nm and pulse length of 10–20 fs resulting in power densities up to 5×10^{13} W cm^{-2}. All data are stored shot by shot with a unique pulse identifier so that it can be correlated to the laser parameters in the post analysis. First results are shown in Fig. 55.

In a subsequent study the 2D scattering patterns have been analyzed quantitatively. Scattering profiles were calculated by cutting a slice of 20 degrees out of the 2D diffraction pattern and averaging the measured intensities radially, i.e. over intensities at constant values of momentum transfer. The scattering curves are analyzed within the Mie scattering scheme and provide information about the cluster size as well as the optical constants and thus information about the electronic structure of the particles investigated. Fig. 56 shows typical results of the study on large Xe clusters at different power-densities (Bostedt et al., 2012). The high flux of the X-ray laser induces severe transient changes of the electronic configuration, resulting in a tenfold increase of absorption in the developing nanoplasma. The paper shows that single-shot single-particle scattering on femtosecond time scales yields insight into ultrafast processes in highly excited systems where conventional spectroscopy techniques are inherently blind.

The scattering patterns of single particles contain a very high degree of double cluster structures. Such ‘twin clusters’ are predicted to appear as intermediate states in the cluster growth process and, for the first time, have been studied in detail using an improved imaging device at FLASH, see Fig. 57 (Rupp et al., 2012). Simulated patterns are calculated from estimated 3D and 2D structures and compared to the experimental data. By taking into account a variety of parameters

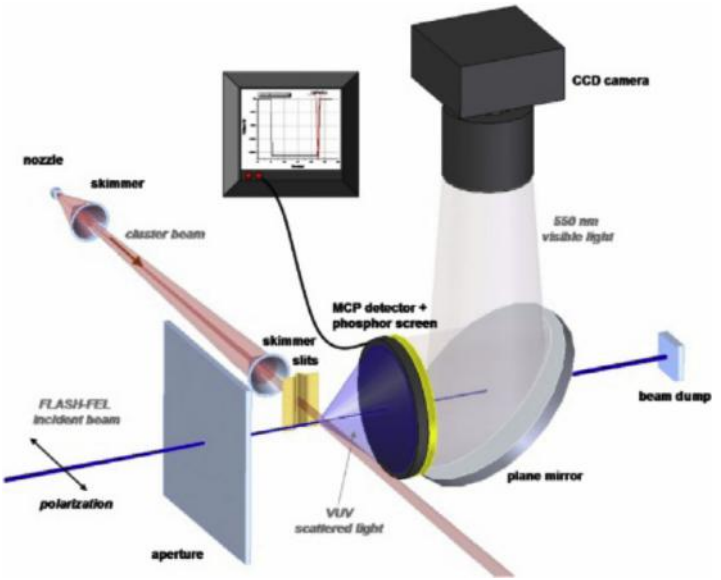

Fig. 54. Schematic illustration of the imaging detector for recording of scattering patterns of clusters (Bostedt et al., 2010a).

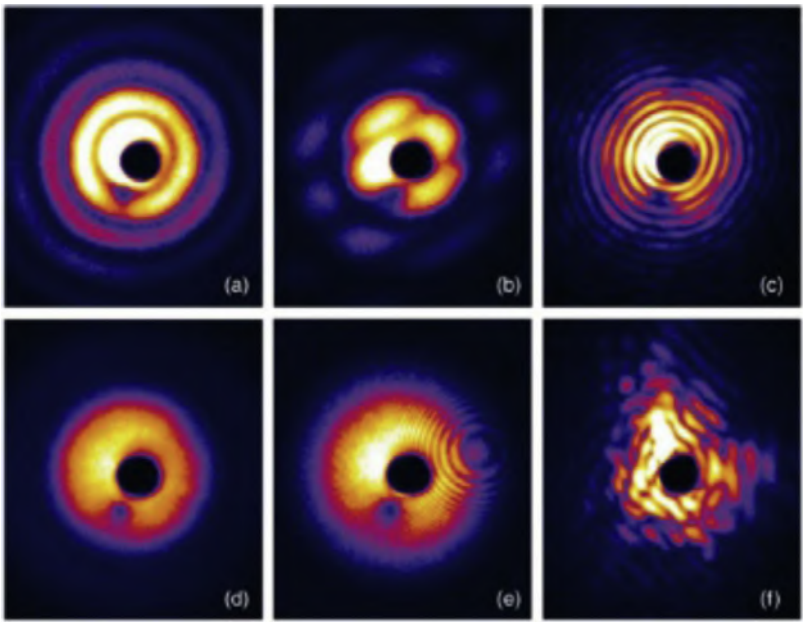

Fig. 55. Single-shot scattering patterns of large Xe clusters. The patterns are recorded with the detector shown in Fig. 23: (a) a single cluster; (b) two clusters in direct contact; (c) a single large cluster; (d) an ensemble of many clusters (more than 10) in the focus; (e) two clusters separated by a large distance; (f) a complex pattern from an ensemble with unknown geometry (Bostedt et al., 2010a).

and by careful comparison with the measured scattering patterns, cluster configurations can be determined. Virtually all detected patterns can be explained by simulations that allow for three degrees of freedom:

- the orientation of the two clusters with respect to the scattering plane,
- the distance between two clusters, i.e. separation in the case of Newton rings (Fig. 24(b)) and fusion for twin clusters,
- sizes of both the particles.

Examples are shown in Fig. 58.

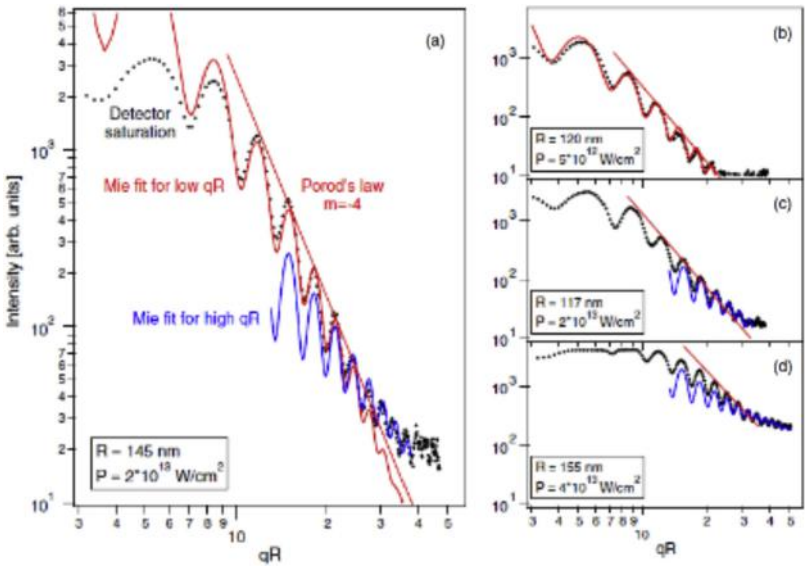

Fig. 56. Single-shot scattering profiles (dotted curves). In (a), the profile of a R ¼ 145 nm cluster and two Mie fits for low and high qR as well as Porod's law are shown. The three panels on the right-hand side show the power-density-dependent changes in the scattering functions. The first maxima, in particular, for the highest power density shot in (d), suffer from detector saturation (Bostedt et al., 2012).

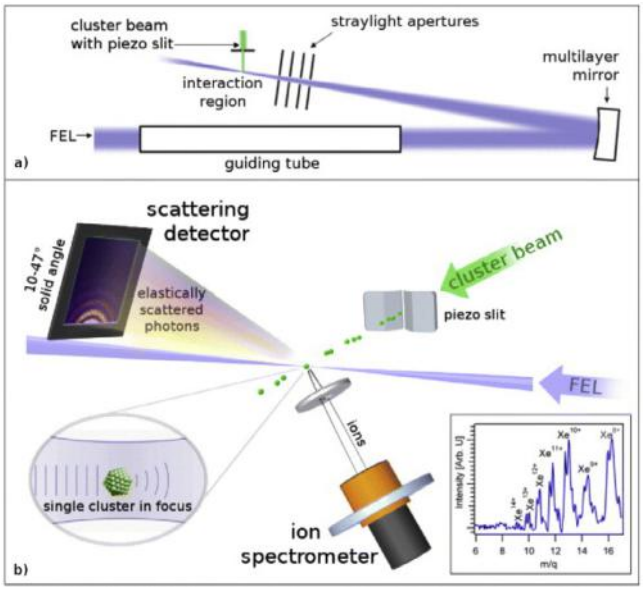

Fig. 57. (a) Optical path of the experimental layout: a guiding tube for the incoming beam and a multilayer-based off-axis back-focusing geometry allow for quasi background-free scattering measurements. (b) Schematic layout of the interaction region: a cluster beam is skimmed down to one cluster in the focal volume by a piezo slit. The micrometer focal spot is optimized using a time-of-flight ion spectrometer. By moving the multilayer mirror along the bisecting line between the incoming and focused FEL beams, power density dependent nonlinear processes in xenon ion spectra can be scanned (displayed for highest power density in the inset). A fast readout pnCCD detector (Strüder et al., 2010) measures the elastically scattered photons from single xenon clusters (Rupp et al., 2012).

4.3.4. Studies of large cluster growth

These imaging techniques at FLASH also allowed the discovery and characterization of Xe clusters in pulsed jets which are by several orders of magnitude larger than predicted by the Hagena scaling law (Rupp et al., 2014). Scanning the time delay between the pulsed cluster source and the intense femtosecond X-ray pulses in the range of up to 14 ms first shows a main plateau with size distributions in line with the scaling laws, which is followed by an after-pulse of

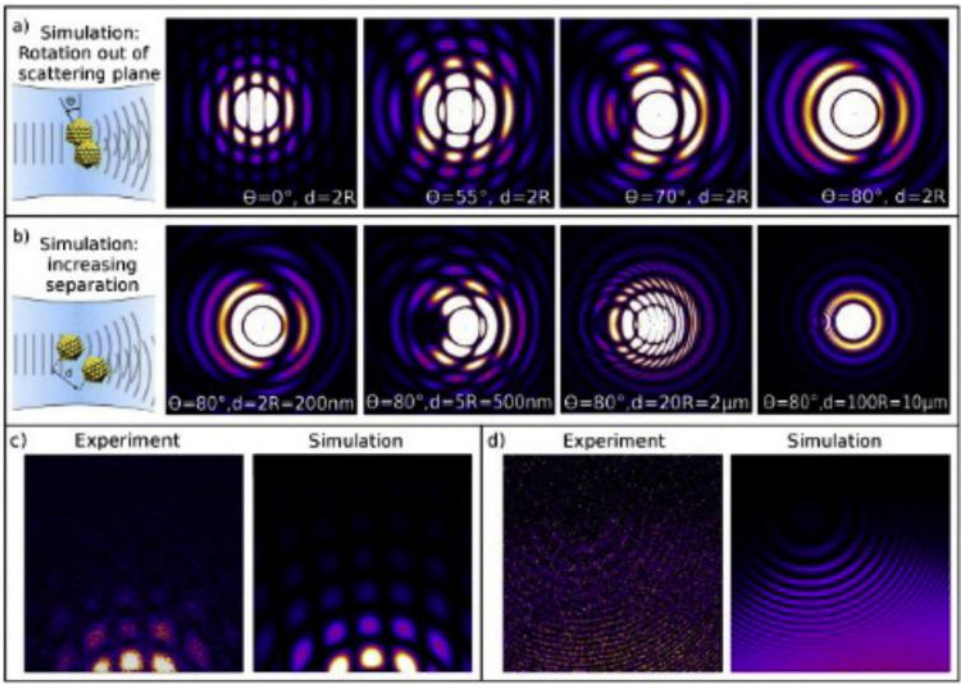

Fig. 58. Simulations for two equally sized clusters (a) in contact and rotated out of the scattering plane and (b) at a fixed angle of 80° with increasing separation. Calculations are done with an adaption of the program ClusScat3 (de Castro et al., 2008). (c) The typical obtained pattern of the 'classical double slit' case can be explained by two similarly sized clusters in direct contact ($R = 65$ nm at 130 nm distance). (d) The typical 'Newton rings' pattern is in good agreement with simulations for one cluster after the other with a 10 μm separation and an axis rotation of 22° (Rupp et al., 2012).

giant clusters. In addition to the cluster size, the single particle images of the clusters reveal fine structure connected to the cluster morphology (see Fig. 59). Clusters up to approximately 100 nm appear mostly spherical with a significant fraction of twinned clusters. For larger clusters of several hundreds of nanometers radius, hailstone-like structures are most abundant. Their grainy shape indicates that the particles which grow by coagulation tend to freeze in non-spherical intermediate structures from a certain grain size on. The discovery and characterization of these giant clusters gives access to a new regime of studies on laser–cluster interaction ranging from infrared to X-rays.

4.3.5. Nanoplasma formation and explosion dynamics of single large xenon clusters

Rupp et al. studied the nanoplasma formation and explosion dynamics of single large xenon clusters in ultrashort, intense X-ray free-electron laser pulses via ion spectroscopy (Rupp et al., 2016). FLASH pulses of about 100 fs duration and intensities of $I \leq 5 \times 10^{14}$ W/cm^2 at photon energy of 91 eV were used. The cluster size varied between 180 and 600 nm in diameter. The simultaneous measurement of single-shot diffraction images enabled a single-cluster analysis that is free from any averaging over the cluster size and laser intensity distributions. The measured charge-state-resolved ion energy spectra show narrow distributions with peak positions that scale linearly with final ion charge state (see Fig. 60), and average ion energies well beyond the values expected for pure hydrodynamic nanoplasma formation and explosion dynamics of single large xenon clusters expansion. These two distinct signatures are attributed to highly efficient recombination that eventually leads to the dominant formation of neutral atoms in the cluster. The measured mean ion energies exceed the value expected without recombination by more than an order of magnitude, indicating that the energy release resulting from electron–ion recombination constitutes a previously unnoticed nanoplasma heating process. The observed nanoplasma expansion dynamics have direct implications for the physics of plasma expansion at surfaces and provide an important benchmark scenario for theory. The single shot capability of combined ion spectroscopy and X-ray imaging experiments will enable a deeper understanding of plasma expansion dynamics in weakly and strongly coupled plasmas. Including this novel acceleration mechanism into theoretical modeling will be important for experiments in a broad field from matter under extreme conditions to biophysics, aerosol science, and X-ray imaging of nanoparticles.

With the single-shot single-particle imaging techniques in hand the time evolution of laser-induced nanoplasma in large clusters and its neutral residuals was investigated by means of pump–probe experiments at FLASH (Flückiger et al., 2016). Light induced dynamics in clusters proceeds on several time scales depending on cluster size and the power of the pump pulse. Flückiger et al. studied very large, individual Xe clusters with radii larger than 700 nm using 800 nm pump

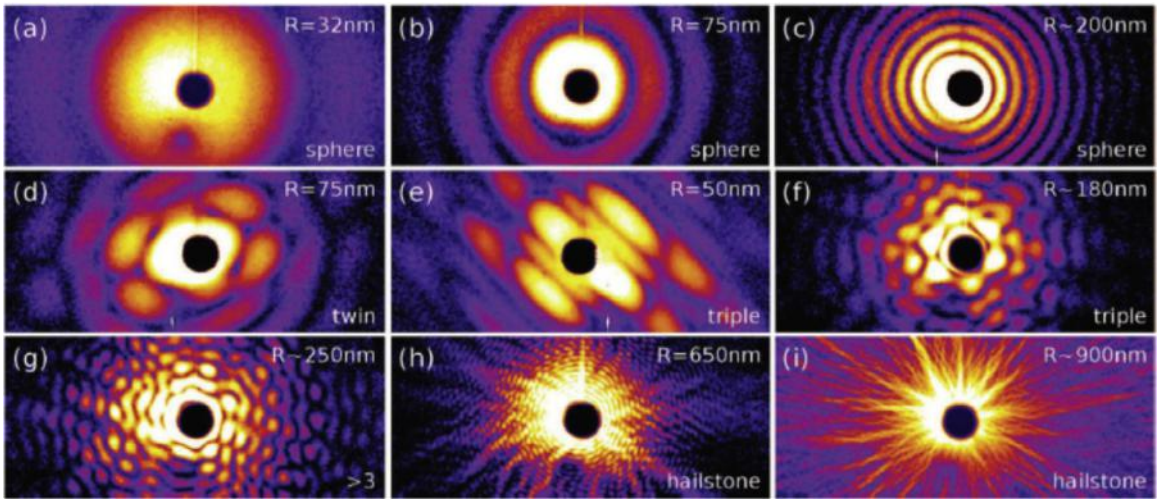

Fig. 59. Examples of single-cluster scattering patterns measured in the after pulse for varying delay times between the trigger of the valve of the cluster source and the arrival time of the FEL pulse. The typical shape of clusters changes with increasing size from spherical over twin and triple structures to grainy hailstones (Rupp et al., 2014).

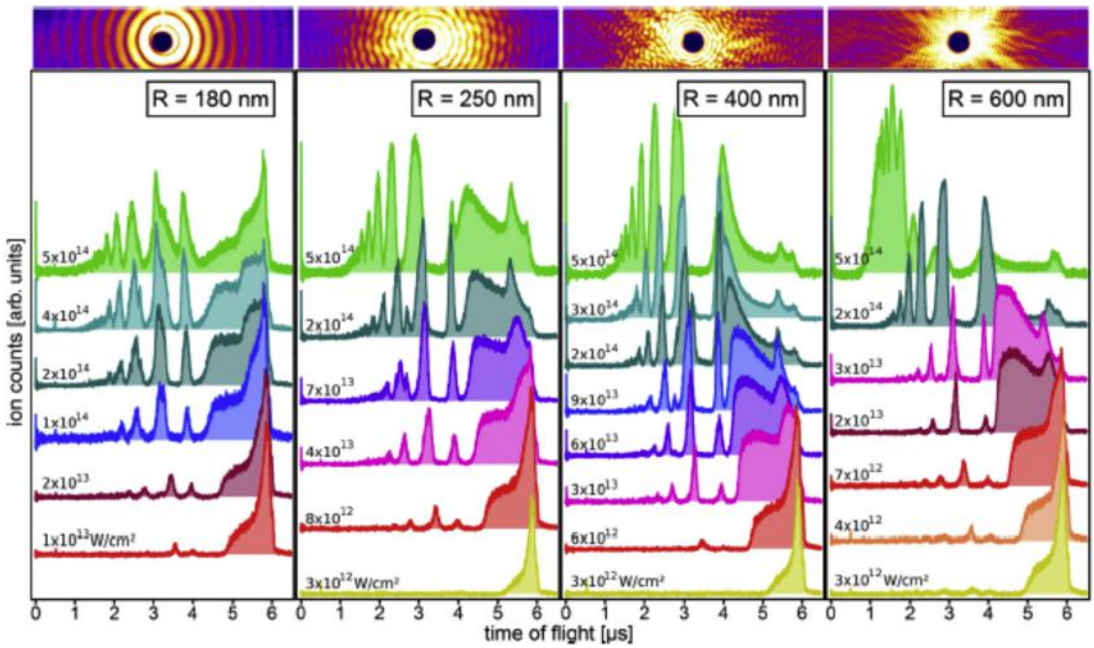

Fig. 60. Ion time-of-flight spectra of single large clusters [radii of 180(±30) nm, 250(±40) nm, 400(±50) nm, and 600(±50) nm] sorted by cluster size and laser intensity, derived by comparison with Mie simulations;. The FEL intensity values experienced by the clusters, as indicated in the figure, have to be considered as orientation only, as the intensity assignment may be compromised by detector nonlinearities and intensity-dependent ultrafast electronic changes in the cluster (Rupp et al., 2016).

and 13.6 nm probe pulses with power densities of 10^{14} and 4×10^{14} W cm^{-2}, respectively. The time delay between IR pump and VUV probe pulse varied from ps to ns. Fig. 61 shows typical single-shot scattering patterns taken at a sample which is not pumped, and at 4 samples after different delay times.

Model calculations based on recent theoretical work show a radius of at least 700 nm for the original cluster. The key observation in a quantitative analysis of the diffraction patterns shown in Fig. 61 is that the envelope slopes of the scattering signal at small angles get steeper with increasing delay time. Such observation has also been made in a recent experiment at LCLS in Stanford studying a different size regime of xenon clusters (Gorkhover et al., 2016) and

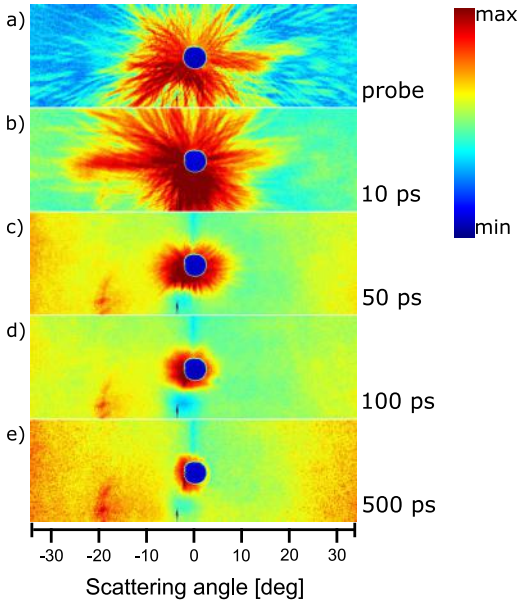

Fig. 61. Scattering patterns from xenon clusters imaged with the soft X-ray pulse without pre-irradiation (a), and at several delay times after the IR pulse excitation (b)–(e). Each pattern is the most intense out of all images recorded at the indicated delay time. Exclusive probe pulse imaging (a) shows an intact particle with radius larger than 700 nm. In pump–probe configuration (b)–(e) with increasing delay time the information at lower scattering angles is blurred revealing proceeding particle surface ablation. The blue dots in the center correspond to blind areas due to the hole in the center of the detector preventing damage by the FEL beam. The bright diffuse spot at around -20° on the left side of the scattering patterns is an artifact. Striking is the growth of diffuse scattering at larger scattering angles for delay times of 50 ps and larger (Flückiger et al., 2016) (Creative Commons Attibution 3.0 Unported, https://creativecommons.org/licenses/by/3.0/).

is well explained by theoretical calculations on hydrogen clusters (Peltz et al., 2014). The effect is attributed to surface ablation. By analyzing the diffuse scattering at high momentum transfer, which shows characteristic speckle patterns, the development of the structure of the recombined inner part of the cluster has been studied next.

Fig. 62 shows typical speckle patterns recorded 0.5 and $\sim$1.5 ns after irradiation with the Ir pulse together with the corresponding azimuthally integrated speckle intensities. A detailed analysis of such speckle patterns can provide information on particle shape and density. The mean size of speckles is inversely proportional to the average radius of the overall object and the slope of a speckle distribution is correlated with the average characteristic length scale of the internal structure which induces the scattering. For references see (Flückiger et al., 2016). The analysis of the data is very much hindered due to the missing information in the angular range of $\pm 4^\circ$. Nevertheless, after systematic calculations of the speckle patterns of model systems the measured diffraction patterns could be reproduced by simulations which assumed that the cluster expands with pronounced internal density fluctuations hundreds of ps after IR excitation. For samples I to III in Fig. 62 a change of slope in the amplitude envelope is found at approximately 20°. This corresponds to about 25 nm range in density fluctuations, which is mimicked by a sub-cluster radius of 25 nm in simulations whose results are shown in Fig. 63.

In summary, Flückiger et al. explored cluster evolution by snapshotting time-slices of laser induced disintegration in pump–probe configuration, pushing to extreme time regimes from several ps up to 1.5 ns. After initiation of the expansion with an intense IR laser pulse, xenon clusters in the size range of several ten to hundred nanometers in radius were imaged with a soft-X-ray FEL pulse in single-shot single-particle mode. Two different kinds of scattering patterns on different time scales were identified: fringe patterns, where the scattering signal vanishes at high scattering angles with increasing delay time within tens of picoseconds, as well as speckle patterns, which appear from 500 picoseconds onwards.

The authors attribute these two types of patterns to different stages of the expansion:

- Following strong particle excitation and subsequent electron trapping in the deepening Coulomb potential a quasi-neutral nanoplasma is formed. Its surface ions undergo hydrodynamic expansion due to the pressure of the plasma electrons. The expansion evolves on a picosecond timescale layer-wise from the outside towards the cluster center. This surface softening is mirrored by a decrease in scattering signal at high scattering angles.
- Meanwhile the majority of excited electrons recombines and consequently the expansion driven by plasma electrons finally stops. The remaining neutral cluster core stays in the interaction region up to nanoseconds. Its density decreases slowly and density fluctuations occur, leading to speckle patterns with intensity modulations.

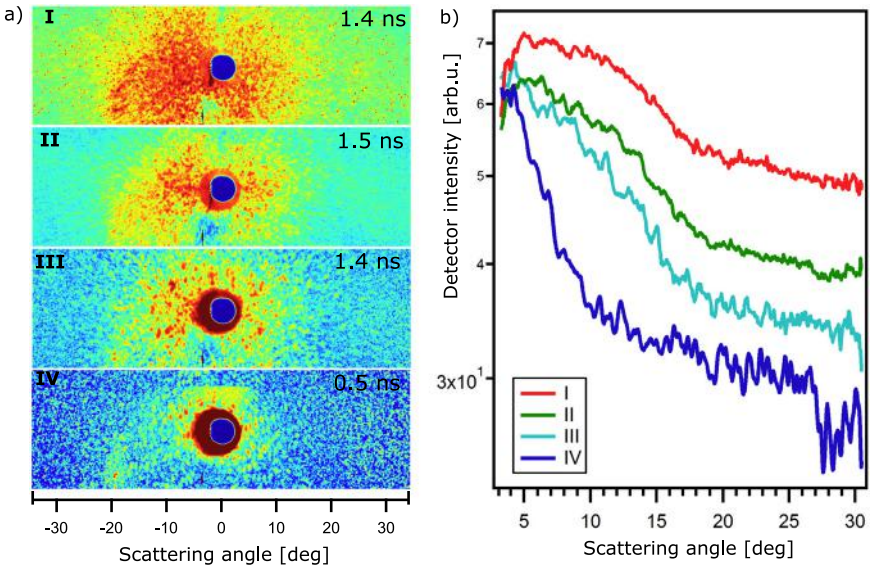

Fig. 62. (a) Characteristic speckle patterns measured with soft X-ray FEL radiation at large Xe clusters 0.5 and ∼1.5 ns after irradiation with a strong IR pulse. (b) Corresponding azimuthally integrated scattering intensities showing a modulation in the amplitude envelope with change of slope at around 20° scattering angle and lower. The angular range of ±4° is not considered because it contains the hole in the detector and is affected by stray light from the incident FEL beam (Flückiger et al., 2016) (Creative Commons Attibution 3.0 Unported, https://creativecommons.org/licenses/by/3.0/).

It is shown that simple image analysis of the recorded speckle patterns has the potential to determine the overall size and internal density fluctuation range of the examined object. These findings from dynamic diffraction imaging extend the picture of laser–matter interaction into the nanosecond time scale, where structural signatures up to date not explored in homogeneous clusters could be identified.

4.4. Plasmas and warm dense matter

From early on, studies of high energy density plasmas and warm dense matter have been one of the most prominent research fields in building the scientific case for X-ray free-electron lasers (Lee et al., 2003). Theoretically, such matter is difficult to handle because electrostatic and thermal energies are at the same order of magnitude, rather than one being a perturbation of the other, as in solid state physics or classical plasma physics (Ziaja et al., 2007). A good understanding of this complex regime between cold solids and hot dilute plasmas is important for high pressure studies, applied materials studies, inertial fusion, and planetary interiors. Free-electron lasers providing extremely intense XUV and/or hard X-ray pulses of some tens of fs duration open a new window in warm dense matter (WDM) research. The photon energy can be higher than the plasma frequency ω_p, so that the penetration of the radiation into the sample is not limited to the surface but results in volumetric photo absorption and consequent heating. In addition, compared to optical heating, irradiation with intense fs XUV radiation is a relatively clean excitation/heating process because photo absorption is the dominant radiation–matter interaction. While in the astrophysical context WDM states exist in a stable phase, in laboratory experiments they occur as transient states following non-equilibrium paths in the phase diagram. In general, the cold sample system is excited into a non-equilibrium, two-temperature state with $T_{ion} \ll T_{electron}$ immediately after heating (<50 fs). In a next step the system develops into a local thermal equilibrium WDM state (after 1–2 ps) from where it further cools down by isentropic expansion (>2 ps after irradiation). Due to its ultrashort pulse duration (∼15–50 fs) and high penetration power, X-ray FEL radiation is well suited for experiments probing these states in a time resolving manner.

In addition to high beam power, extreme focusing of the FEL beams is necessary to reach the power densities essential for warm dense matter studies. In a large international effort at FLASH a beam of 13.5 nm wavelength could be focused down to sub-micron size reaching a power density of 10^{18} W cm $^{-2}$ in the focus using a multilayer-coated 27-cm focal length parabola in normal incidence (Bajt et al., 2009; Nelson et al., 2009). Beam imprints on poly methyl methacrylate (PMMA) were used to determine the focus (Chalupský et al., 2010) and the focused beam could then be used to create isochoric heating of various slab targets. The optics survived the very intense beam. XUV spectroscopy (Zastrau et al., 2012) and Thomson scattering (Höll et al., 2007; Glenzer and Redmer, 2009) are applied for accurate determination of plasma temperatures and densities.

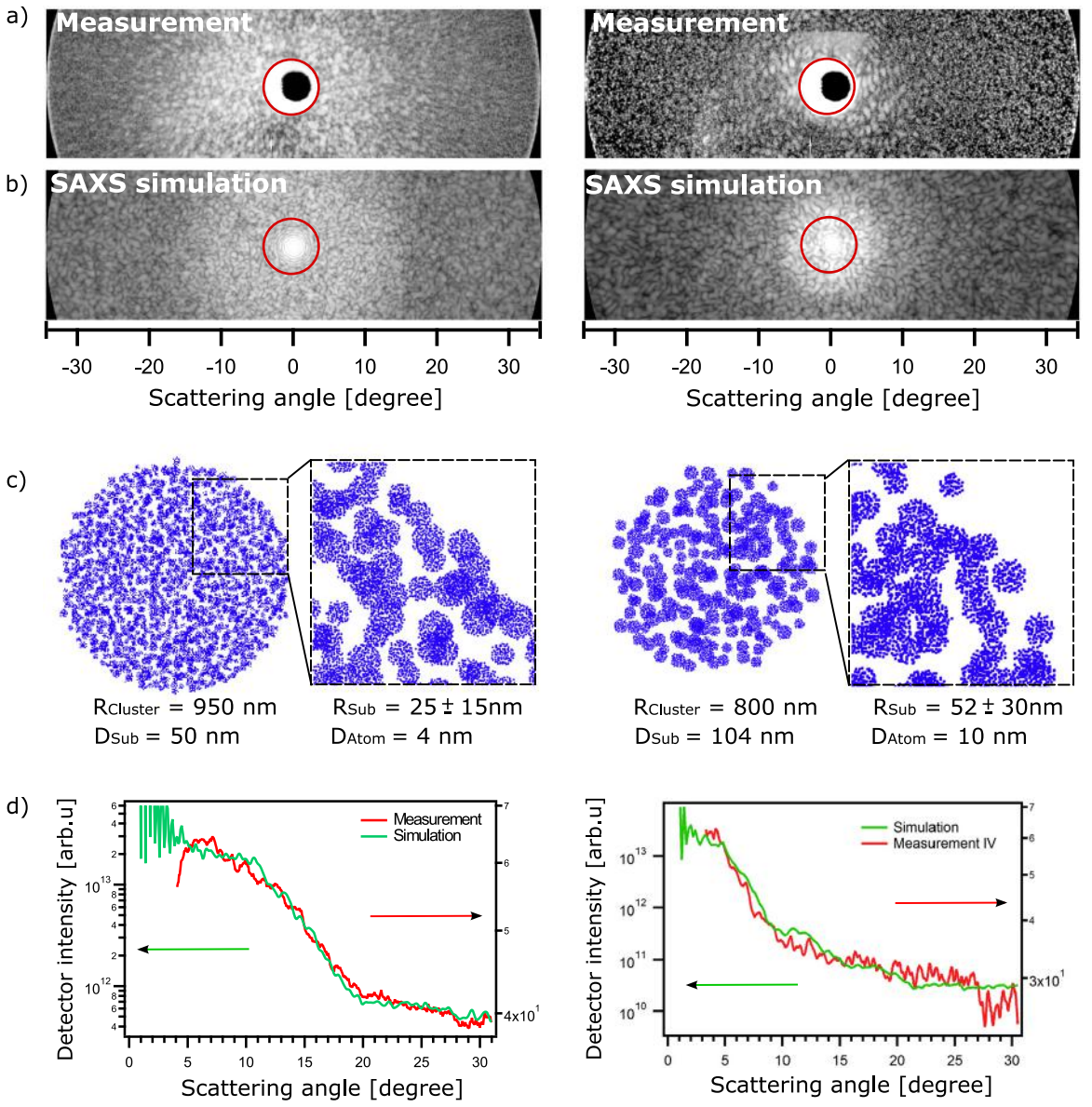

Fig. 63. (a) Typical speckle diffraction patterns recorded 1.4 ns (II) and 0.5 ns (IV) after IR laser impingement. (b) Simulated patterns calculated in scalar numerical small angle X-ray scattering approach from a $R_{cluster} = 950$ nm dilute gas ball with internal density fluctuations on a size range of $R_{Sub} = (25 \pm 15)$ nm, and a cluster with $R_{cluster} = 800$ nm and $R_{Sub} = (52 \pm 30)$ nm, respectively. (c) Visualization of the model clusters used to calculate (b). Atomic distances are set to $D_{Atom} = 4$ nm and sub-cluster distances to $D_{Sub} = 50$ nm, and $D_{Atom} = 10$ nm and $D_{Sub} = 104$ nm, respectively. (d) Radial profiles of measured and simulated data show the elaborateness of input values. The intensity scale for measured and simulated data varies due to the ambiguous linearity of the detector (Flückiger et al., 2016) (Creative Commons Attibution 3.0 Unported, https://creativecommons.org/licenses/by/3.0/).

The kinematics of a Thomson scattering experiment determines if collective electron excitations or non-collective properties are probed. In the examples discussed later the probed length scales are larger than the Debye screening length and as a consequence primarily collective scattering is accessible. This collective scattering probes the existence of plasmons which are down- and up-shifted in energy, relative to the elastic scattering at the incoming photon energy. From the energy difference of these resonances with respect to the FEL probe pulse the electron density can be estimated. The slope of the peak heights of the resonances allows an independent estimate of the electron temperature. Fig. 64 shows the idealized result expected from a Thomson scattering experiment at a homogeneous and stationary WDM target performed with XUV radiation.

The measurement of plasma parameters such as temperature, free-electron density or ionization is required for the investigation of equation-of-state properties, the main goal in WDM research. In the following, pioneering FLASH

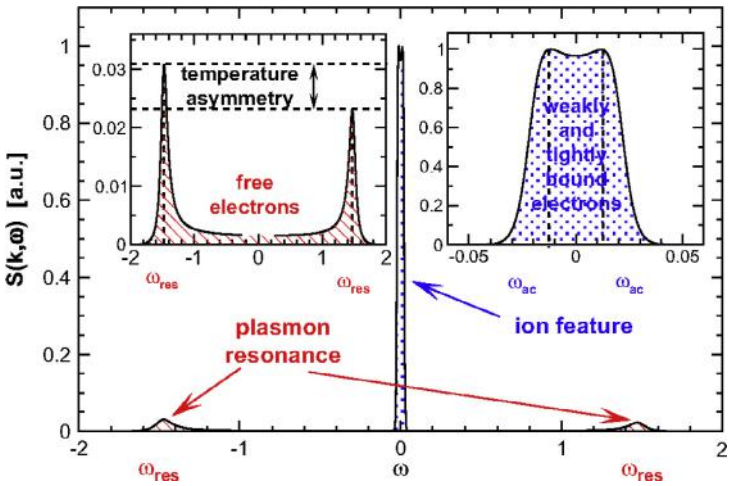

Fig. 64. Schematic view of the dynamical structure factor S(k, ω) as a function of the frequency shift ω in the collective scattering regime. The high resonance collective mode (plasmons) is shown as a red hatched region. At low frequency shifts, the ion feature due to weakly and tightly bound electrons is shown as the blue dotted region. The plasmon and ion acoustic resonance frequency, ω_{res} and ω_{ac}, respectively, are shown. The insets on the upper left and right show magnifications of the plasmon resonance and the ion feature, respectively (Höll et al., 2007).

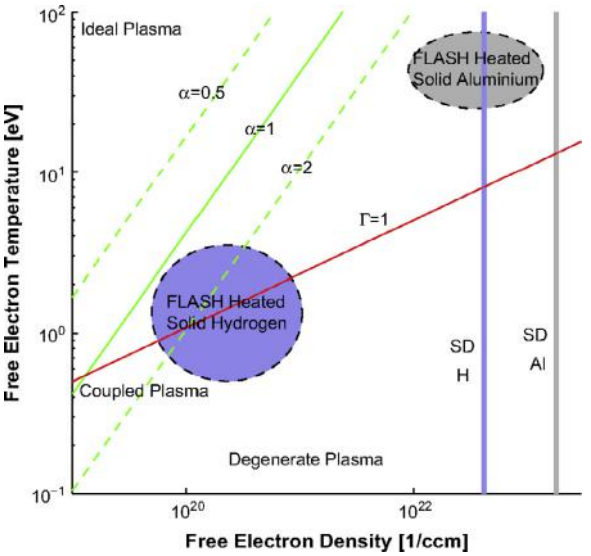

Fig. 65. Phase space representation for electron density n_e and temperature T_e; probing photon energy $\hbar\omega = 92$ eV and scattering angle $\theta = 90°$. The coupling parameter Γ is the ratio of the interatomic potential energy to the thermal energy; the scattering parameter α is the ratio between the inverse momentum transfer in the scattering experiment and the Debye screening length. Both quantities are functions of free electron temperature and free electron density and the green and red lines show their relationship for fixed values of α and Γ. Densities of cold hydrogen and aluminum are indicated. For details see Toleikis et al. (2010a).

experiments at warm dense aluminum and warm dense hydrogen will be discussed. Fig. 65 shows the temperature-density diagram for both systems with the filled areas indicating the regions of the parameter space accessible with Thompson scattering using 92 eV radiation.

4.4.1. First observation of saturable absorption of an L-shell transition in aluminum

Based on extensive preparatory work by the so called "Peak-Brightness-Collaboration" at FLASH, saturable absorption of an L-shell transition in aluminum could be observed for the first time in the soft X-ray regime of the electro-magnetic spectrum (Nagler et al., 2009). Saturable absorption, the decrease in the absorption of light with increasing intensity, is a well-known effect in the visible and near-visible region of the electromagnetic spectrum, and is a widely exploited phenomenon in laser technology. However, the effect had never been observed before with XUV radiation because of the short lifetime of the excited states involved and the high intensities of the soft X-rays needed. The transmission of a

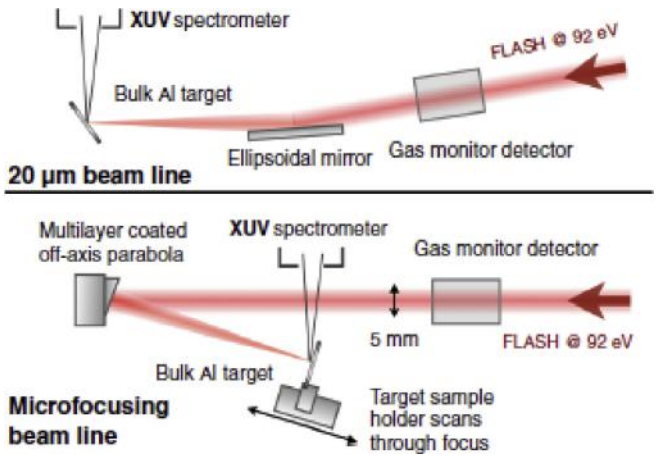

Fig. 66. Schematic view of two experimental setups at FLASH to access a range of power densities between 10^{13} and 10^{16} W/cm^2 (Vinko et al., 2010). 20 μm **beamline**: Experimental setup for lower power densities. The power density is varied using a gas attenuator providing between 1–50 μJ on target in a constant spot size of 20 x 30 μm^2 (Zastrau et al., 2008). **Microfocus beamline:** FLASH beam is focused using a Si/Mo-multilayer-coated off-axis parabola (Nelson et al., 2009). At constant intensity of the incident beam the power density is varied by changing the position of the target with respect to the focus leading to effective spot sizes between 1–10 μm. (Zastrau et al., 2012).

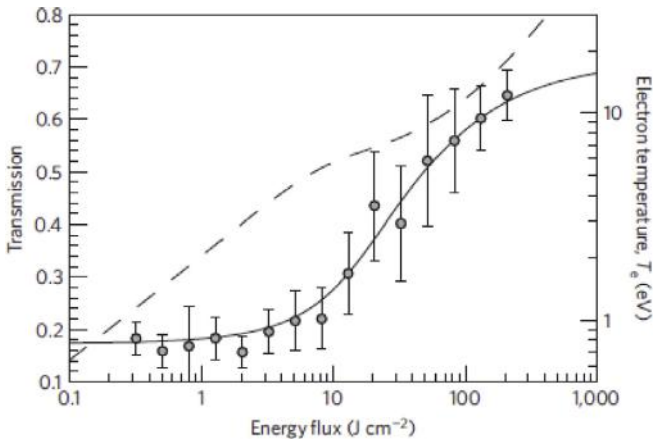

Fig. 67. Transmission of an aluminum target as a function of fluence. The circles are the experimental data points with a 1σ error bar; the solid line is a theoretical prediction. The dashed curve is the predicted electron temperature in electronvolts (right y axis) in the valence band after the FEL pulse has passed, but before the L-shell holes are filled and the Auger recombination heats the band further (Nagler et al., 2009).

53 nm thick Al foil was measured using 92 eV (wavelength 13.5 nm) FLASH pulses of about 15 fs duration. By moving the target through the focal area of the FLASH micro-focus beamline the power density could be varied by 3 orders of magnitude reaching record intensities over 10^{16} W/cm^2. The experimental setup is shown in Fig. 66.

For photons of 92 eV almost all of the absorption in aluminum is due to photoionization of L-shell electrons. At high intensities, the fraction of aluminum atoms with photo ionized L-shell electrons is high, leading to depletion of L-shell absorption: after an electron is ejected from the L-shell of an atom, the L-edge of that particular atom will increase owing to reduced screening. The energy needed to eject a second L-shell electron is calculated to be 93 eV, which is confirmed by measurements of Auger energies. Therefore, the FEL (at 92.5 eV) will not be able to create a second L-shell hole; the photoionization quenches and the absorption coefficient is heavily reduced to the value of the free–free absorption, i.e. due to the valence electrons. Once an electron is ejected from the L-shell, the hole will be refilled by means of either radiative decay or the dominant Auger decay.

However, the total lifetime of such an L-shell vacancy (which is much shorter than the radiative lifetime) is estimated to be around 40 fs, that is, long compared with the FLASH pulse length of 15 fs, but still short compared with any electron–phonon coupling time, or hydrodynamic motion. Thus, the loss of L-shell electrons during the initial part of the FLASH pulse results in reduced absorption during the rest of the pulse, an effect that is negligible at previously accessible soft X-ray intensities (see Fig. 67).

For the same experimental conditions Vinko et al. showed that soft-X-ray emission spectroscopy measurements, supported by detailed calculations of the electronic structure based on finite-temperature density functional theory, can

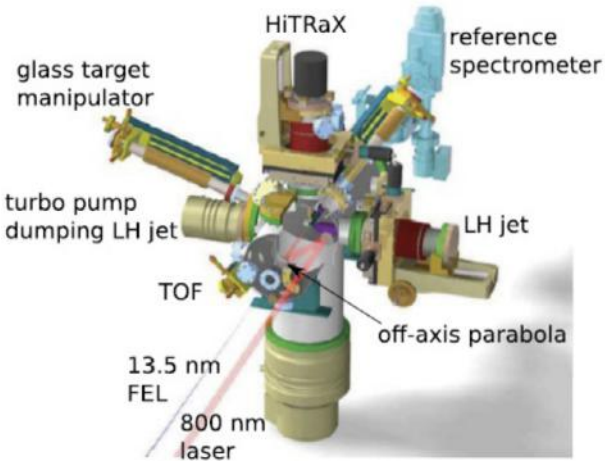

Fig. 68. Experimental setup to study warm dense hydrogen using Thomson scattering at FLASH. HiTRax is a compact soft X-ray spectrograph combining high efficiency and resolution for Thomson scattering plasma diagnostics. (For a detailed description see Fäustlin et al. (2010a).
Source: Toleikis et al. (2010b).

reveal the electronic temperature and density of this highly excited state of matter in solid-density aluminum immediately after the excitation pulse (Vinko et al., 2010). A similar paper by Medvedev et al. improves the understanding of non-equilibrium electron dynamics of the experimental spectra measured by Vinko et al. by means of ultrafast Monte-Carlo electron kinetics simulations (Medvedev et al., 2011). Galtier et al. analyzed the plasma emission lines measured at the same system and estimated the electron temperature and density just after decay of crystalline order and to characterize the early time evolution (Galtier et al., 2011).

4.4.2. Pioneering studies of warm dense hydrogen

The investigation of warm dense hydrogen has been one of the core areas of research in the early years of FLASH operation. Focus was on the experimental setup including target station, WDM diagnostics and synchronization with external optical laser (Toleikis et al., 2010a). The vacuum chamber is shown in Fig. 68. The FEL beam passes horizontally through the chamber aligned such that the focal point is located in the center of the chamber. At the focus the hydrogen pellet source horizontally injects a continuous liquid hydrogen jet or liquid hydrogen droplets depending on the operation mode. The FEL beam at FLASH is horizontally polarized and in order not to decrease the scattered power the soft X-ray spectrometer is mounted vertically at a scattering angle of $\theta = 90°$. In addition a reference spectrograph is mounted in the transmission direction to monitor the reference wavelength of the incident FEL beam for a later comparison with the scattering spectra recorded at 90°. The liquid hydrogen jet which is horizontally injected is dumped in a turbo-molecular pump to reduce the gas ballast in the chamber. The optical pump laser at an 800 nm wavelength is guided and reflected onto an off-axis parabolic mirror which has a hole to let pass the FEL beam, allowing on the one hand to collinearly overlap both beams and on the other hand to focus the optical laser to the same focal spot as the FEL beam.

To provide a free standing target of near-solid density hydrogen in the focus of the FEL beam, the use of cryogenic liquid or solid hydrogen as a target is mandatory. A fluid is pressed through a small orifice into the vacuum in a way that a continuous liquid filament is formed. Such a cylindrical liquid is unstable against its surface tension, small fluctuations will grow and the Rayleigh breakup process will produce almost monodisperse droplets. By introducing an artificial perturbance to the liquid, the breakup process can be stabilized and the tuning of the droplet size becomes possible. The produced droplets freeze by evaporational cooling in the vacuum and form solid pellets after several millimetres in flight. In the present setup a temperature-controlled helium flow cryostat is used to cool down a nozzle holder and the hydrogen to the needed temperature in the range of 20 K. A picture of the hydrogen liquid jet and pellet source and a sketch of the cold head are shown in Fig. 69. The cryostat is mounted on a three-dimensional manipulator to provide the alignment to the focus area. The source can be operated in different modes. At higher temperatures, smaller droplets in a divergent jet are generated. In the Rayleigh regime, a well-collimated stream of droplets is produced. The piezo actuator can be used to modulate the Rayleigh breakup process with frequencies between 25 and about 100 kHz which provides a limited size control and the possibility of synchronizing the droplets in the focus area with the optical laser and the FLASH pulse.

The experiments on warm dense hydrogen have been performed using a photon energy of 91.8 eV. FEL radiation with 5 Hz pulse repetition rate, average pulse energy on target of 15 μJ and duration of ∼40 fs is focused to a 25 μm spot yielding intensities of $\sim 8 \times 10^{13}$ W cm^{-2}. The energy of 91,8 eV has been chosen in order to be in a regime where the photon energy is well above the plasma frequency for liquid density hydrogen ($\hbar\omega = 7.6$ eV) and to match the large penetration depth of 9.4 μm to the target radius (10 μm). While at this photon energy attenuation via photoabsorption

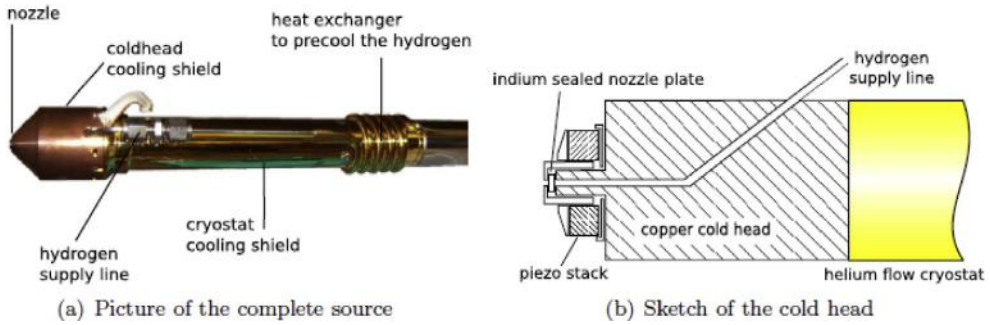

Fig. 69. (a) A picture of the hydrogen pellet source used to study WDM at FLASH. It utilizes a cryostat to control the temperature of a cold head holding the nozzle and the piezo transducers. Details of the cold head are shown in (b) (Toleikis et al., 2010b).

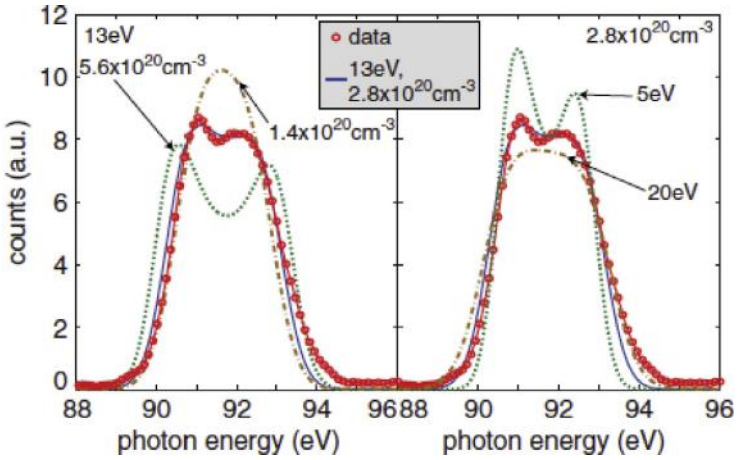

Fig. 70. Thompson scattering at warm dense hydrogen (red circles) measured over 15 min integration time is shown together with a best fit (solid blue line) of a calculated spectrum with a free-electron density of ne $= 2.8 \times 10^{20}$ cm^{-3} and an electron temperature of $T_e = 13$ eV. The results of calculations using different values of n_e (left) and T_e (right) are shown for comparison. The error in the fitting procedure is estimated to 25% for the electron temperature and 7% for the density (Fäustlin et al., 2010a).

has the highest cross section, a small fraction of the incident radiation is Thomson scattered. Thus, the FEL pulses deposit energy in the liquid hydrogen while simultaneously probing the system, which leads to gradients in the free-electron density n_e and the electron temperature T_e across the target. This so called self-Thomson scattering has been simulated with the result that ignoring the gradients in the target can lead to errors in the determined electron density n_e and temperature T_e of the order of 10% (Fortmann et al., 2009). The effect is much stronger in an optical pump XUV probe experiment leading to a very inhomogeneous target (Thiele et al., 2010). The result of the FLASH experiment on warm dense hydrogen is shown in Fig. 70. The scattering pattern is composed of asymmetric peaks (plasmons) equally blue and red shifted from the incident photon energy by 0.65 eV. The measured spectrum is mainly broadened by the incident FEL bandwidth (1.1 eV full width at half maximum, mainly Gaussian). Further source broadening effects, like 0.2 eV due to the 20 μm source diameter, are not significant. From a comparison with theoretical calculations it is concluded that the hydrogen plasma has been driven to a nonthermal state with an electron temperature of 13 eV and an ion temperature below 0.1 eV, while the free-electron density is 2.8×10^{20} cm^{-3} (Fäustlin et al., 2010b). It is suggested that the electronic subsystem is thermalized within the duration of the FEL pulse, but no equilibrium has been reached between the other components explaining the combination of low degree of ionization and high electron temperature (Fäustlin et al., 2010b). Pump–probe techniques available at FLASH (Mitzner et al., 2009) allow the investigation of the time scales for the subsequent relaxation channels via electron–ion collision and equilibration, which determine the microscopic properties of matter related to reflectivity and thermal conductivity.

For investigations of dynamic processes of uniform samples of warm dense hydrogen on all relevant time scales, dual-pulse experiments are necessary, where the first XUV FEL pulse generates an excited state that is subsequently probed by a second XUV FEL pulse. Fig. 71 shows the schematic layout of such a pump–probe experiment at FLASH for investigations of the dynamics of ultrafast heating in cryogenic hydrogen. (Zastrau et al., 2014a,b)

FLASH was operated with a repetition rate of 10 Hz and at photon energy of 92 eV to be in a regime where the photon energy is well above the plasma frequency for liquid-density hydrogen ($\hbar\omega_P \sim 8$ eV). This leads to a high penetration

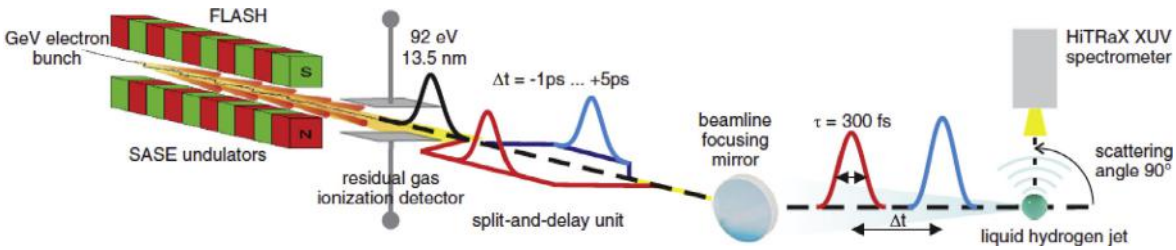

Fig. 71. Schematic layout of the pump–probe experiment at FLASH for investigations of the dynamics of ultrafast heating in cryogenic hydrogen. Soft X-ray pulses are split and delayed before they are focused onto a cryogenic hydrogen jet. Scattering at 90° is observed with an XUV spectrometer. (Zastrau et al., 2014b).

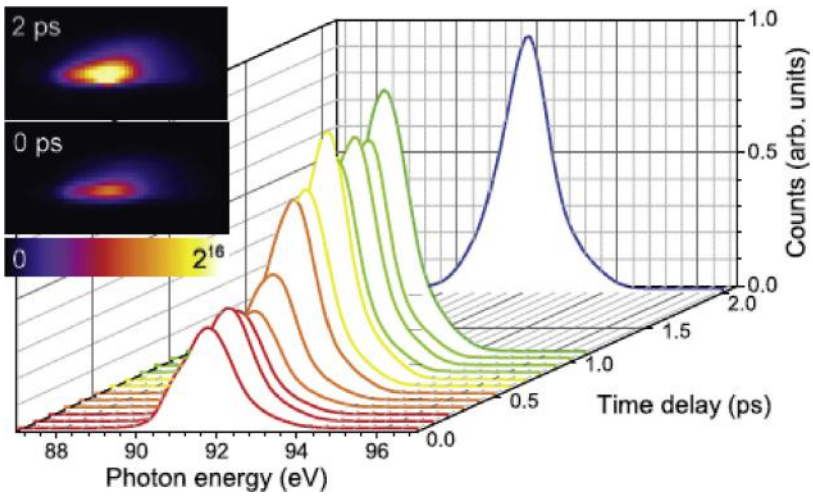

Fig. 72. Experimental scattering spectra as function of time delay. The inset shows two raw spectra, each 25 × 50 pixels of $(13.5\ \mu m)^2$ size. The scattering data are obtained after integration over the vertical axis (Zastrau et al., 2014b).

depth with an absorption length $l_{abs} = 11\ \mu m$, comparable to the hydrogen jet radius of ∼9 μm. The average spectral bandwidth was measured to be $\Delta E/E \approx 1.6\%$. An upper limit for the FEL pulse duration was estimated from the measured electron bunch duration (∼300 fs FWHM), and individual pulse energies have been recorded by a residual gas ionization detector, yielding an average pulse energy of (200 ± 50) μJ. The horizontally polarized FEL radiation is geometrically divided by a split-and-delay unit (Wöstmann et al., 2013) which allows adjustment of the delay times between pump and probe pulse of up to 15 ps with a precision of a few fs. The pulses are subsequently focused to a (20 x 30) μm^2 spot yielding intensities up to 27 ± 0.6 TW/cm^2 for the variable delay branch and 19 ± 0.4 TW/cm^2 for the fixed branch. In the focus, the FEL pulses hit a (9 ± 2)-μm-radius cryogenic hydrogen jet with mass density of 0.08 g/cm^3 (5×10^{22} cm^{-3}) and temperature of 20 K, prepared in a liquid-helium-cooled cryostat (Toleikis et al., 2010b). With a 60 m/s flow velocity each FLASH pulse scatters from an unperturbed sample.

Fig. 72 shows a series of scattering patterns as a function of delay times between 0 and 2 ps. The momentum transfer k is very small in this experiment and the measured scattering represents the sum of all short and long range electron correlations. For these conditions the probed length scale is about 100 times larger than the mean inter-particle distance so that the collective behavior of a large number of particles is probed in the experiment. Fig. 73 shows the transition of the scattering measured with the probe pulse from dense cryogenic molecular hydrogen to a nearly uncorrelated plasma-like structure together with the results of various theoretical simulations of this process. The indicated electron–ion equilibration time is (0.9 ± 0.2) ps. This result agrees with hydrodynamics simulations based on a conductivity model for partially ionized plasma that is validated by a two-temperature density-functional theory (Zastrau et al., 2014a,b, 2015).

4.5. Condensed matter science

4.5.1. Magnetization dynamics

An area of very intense research with FELs in general and with FLASH in particular is ultra-fast magnetization dynamics using coherent imaging and scattering techniques in an attempt to combine fs-temporal and nm-spatial resolution. The fundamental physics behind ultra-fast optical switching of magnetic domains is an open question ever since the

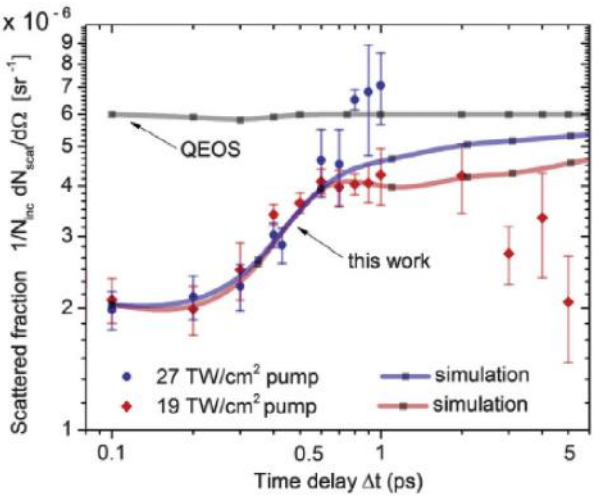

Fig. 73. Transition of dense cryogenic molecular hydrogen to a nearly uncorrelated plasma-like structure. A total of 300 exposures were grouped together by delay, and their errors resemble their root mean square deviations. For the blue diamonds, ranging from $\Delta t = 0$ to 1 ps only, the more intense 27-TW/cm^2 pulse pumps the target, while it is probed by the 19-TW/cm^2 pulse. The red points, ranging from $\Delta t =$ to 5 ps, resemble the inverse case where the pump was less intense (19 TW/cm^2) than the probe (27 TW/cm^2). In both cases the signal increases within 1 ps and for the more intense pump the amplitude is larger. The lines represent the scattered fraction simulated with the HELIOS code (MacFarlane et al., 2006), the red and blue (lower) ones using a Saha-like ionization model — and the gray (upper) one using a Thomas–Fermi model implemented in the quotidian equation of state (QEOS), a general-purpose equation of state model for use in hydrodynamic simulation of high-pressure phenomena More et al. (1988).
Source: Zastrau et al. (2014a).

pioneering work by Beaurepaire et al. which showed that ultra-fast demagnetization induced by an ultra-short optical laser pulse occurs on femtosecond timescales (Beaurepaire et al., 1996). More recent studies demonstrating that with circular polarized femtosecond laser pulses reversible all-optical switching of the magnetization can be realized in certain materials have led to an even increased interest in ultra-fast magnetization dynamics because of the relevance for application in magnetic data storage (Stanciu et al., 2007).

First experiments at FLASH demonstrated the possibility to record single-shot resonant magnetic scattering images with FELs. These experiments were performed on CoPt multilayer sample with the images taken with linear polarized XUV pulses at the Co $M_{2,3}$-edges (Gutt et al., 2010) (see Fig. 74). The first time-resolved demagnetization study using a pump–probe approach with an IR-pump pulse and an XUV probe pulse to record a resonant magnetic scattering pattern as a function of pump–probe delay was also performed at FLASH (see Fig. 75) (Pfau et al., 2012). In this experiment reduction of the magnetic scattering signal on less than 300 fs was observed accompanied by an apparent increase in magnetic correlation length. This increase in correlation length has been attributed to softening of the domain walls due to super-diffusive spin currents across the domain walls. The study represents the first experiment were correlations between fs-demagnetization and nm-scale structure changes have been recorded.

While most of the experiments use rather indirect measures to determine the change in spin state of the electrons, time-, spin- and energy-resolved photoelectron spectroscopy would provide direct access to the changes in spin dependent electronic structure during the ultrafast demagnetization process. However, such experiments require intense short soft X-ray pulses from a high repetition rate source to become feasible. At FLASH a first experiment in this direction was successfully performed by a group lead by Yves Acremann from ETH Zürich (Fognini et al., 2014). Fig. 76 shows the schematics of the experiment. The secondary electron cascade from a magnetic material which originates from inelastic scattering of outgoing photoelectrons is spin polarized and reflects the spin polarization of the unoccupied electronic states above the vacuum level E_{vac}. Hence, the measured spin polarization can be used as a direct measure of the spin state of the sample. By monitoring the spin polarization of energy resolved secondary electrons as a function of time after an optical excitation, Fognini et al. were able to follow the demagnetization of an iron film showing that the total magnetization is reduced within less than 200 fs.

4.5.2. Towards electronic structure movies

Free-Electron Lasers such as FLASH provide ultrashort, extremely powerful short wavelength pulses in the XUV and soft X-ray regime. Hence they offer the possibility to extend the well-established X-ray spectroscopic techniques for the investigation of the static electronic structure of matter to probing the evolution of the electronic structure after controlled excitation in the time domain. Many pioneering experiments in this direction have been performed at FLASH and examples will be given in the following sections.

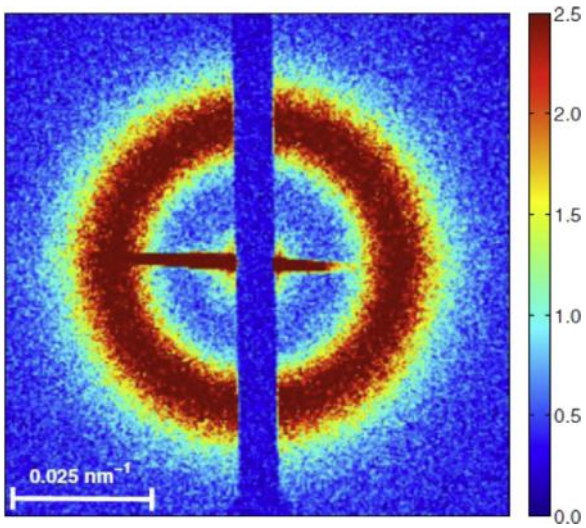

Fig. 74. Resonant magnetic small-angle scattering pattern of a Co/Pt multilayer recorded with a single 30 fs FEL pulse of 1.3×10^{11} W cm $^{-2}$. The photon wavelength was in resonance with the Co $M_{2,3}$ edge @ 20.8 nm providing magnetic scattering contrast. The color scales indicate the number of scattered photons per pixel (4×4 binned image) (Gutt et al., 2010).

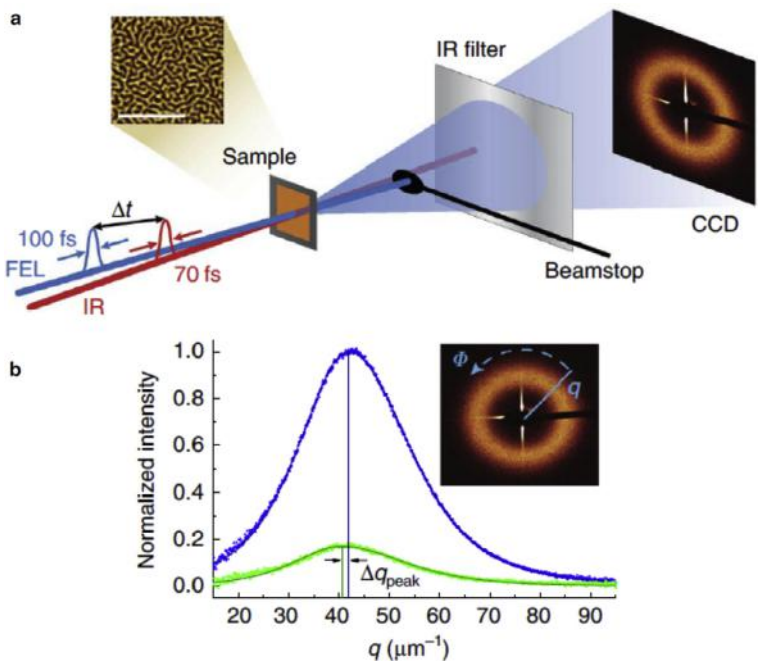

Fig. 75. (**a**) The magnetic multilayer sample is pumped by an optical laser pulse and probed by a delayed X-ray pulse produced by the FEL. The magnetic SAXS pattern is recorded on an IR-protected (CCD) camera while the intense directly transmitted radiation is blocked by a beamstop. The inset shows a typical magnetic force micrograph of the sample in the probed labyrinth-domain state. The scale bar in the micrograph corresponds to 2 μm distance. (**b**) By fitting the azimuthally integrated (see inset) SAXS intensity, the intensity maximum is determined. A decrease in the intensity and a shift of the peak position Δq_{peak}, when comparing unpumped (blue) and pumped (green) spectra (pump fluence: 14.2 mJ cm^{-2}, time delay: 1.3 ps) is observed (Pfau et al., 2012).

4.5.2.1. Time resolved photoelectron spectroscopy. Time resolved photoelectron spectroscopy (TR-PES) is a very powerful tool to study non-equilibrium electron dynamics of condensed matter systems. If performed in an angle-resolved way (TR-ARPES) it offers the possibility to study the evolution of the valence electronic structure energy- and momentum resolved, i.e. to follow the dynamics of the full band structure of a material. Time resolved core level photoemission (TR-XPS) with its element specificity on the other hand provides information on the dynamics of the local charge state around a specific center. Both techniques benefit from high-repetition sources since the typical count rates per pulse have

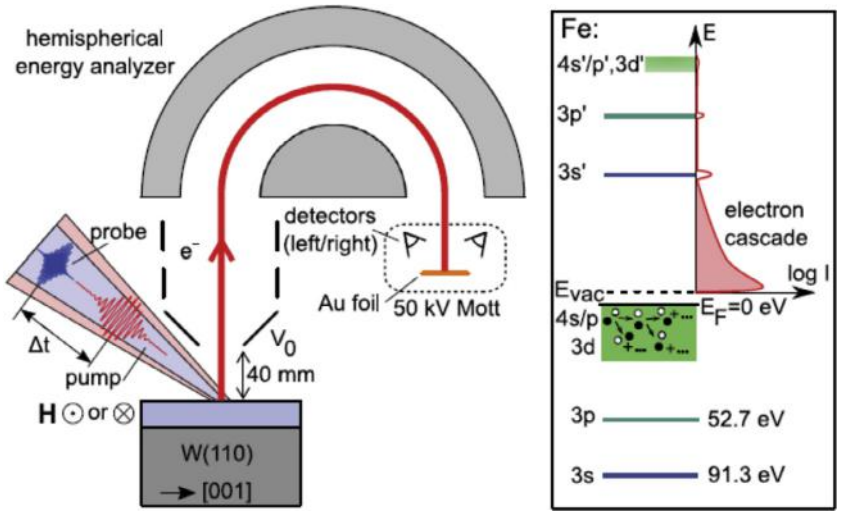

Fig. 76. Experimental overview: The iron film is excited by an 800 nm pump laser. The subsequent FEL probe pulse generates an electron cascade which passes through a hemispherical energy analyzer. The spin polarization is measured with a Mott detector. An electric field of 2.5 kV/m is applied between the sample and the first lens element to accelerate the electrons towards the electron optics. The inset shows the energy levels involved and the generation of the electron cascade with the electron yield denoted as I (Fognini et al., 2014).

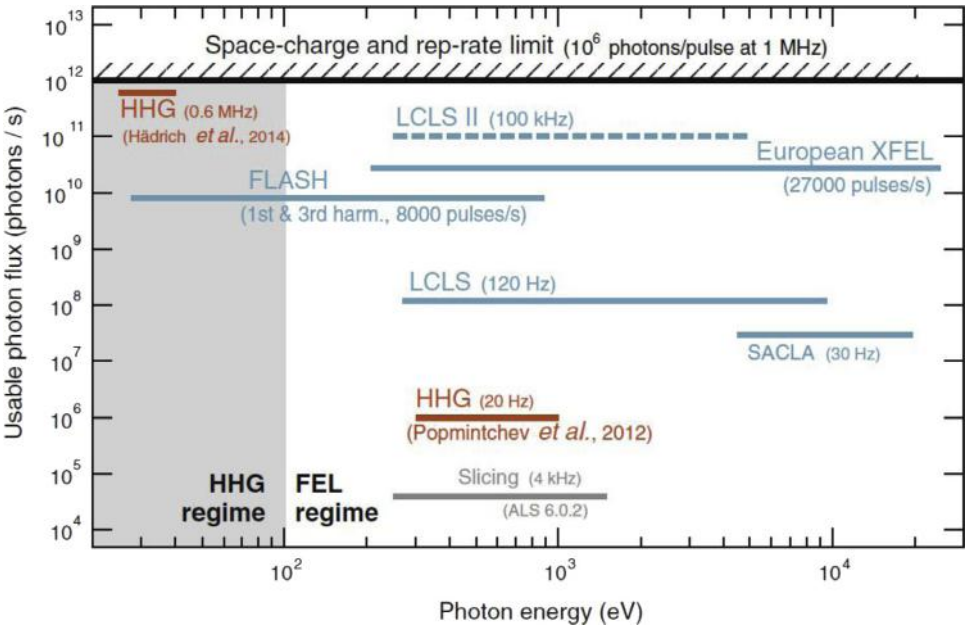

Fig. 77. The figure shows a comparison of the usable photon flux in time-resolved photoelectron spectroscopy experiments on solid density targets assuming a space-charge limit of 10^6 photons/pulse for different HHG laser sources and FELs (for LCLS II which is currently under construction 100 kHz operation has been assumed). Above 100 eV photon energy high repetition rate FELs are clearly the sources of choice for such experiments (Oloff et al., 2016).

to be kept small. In TR-PES experiments on high density (e.g. solid) targets this is a consequence of space charge effects in the outgoing electron cloud which limits the number of photoelectrons that can be emitted per pulse. The signal-to-noise ratio in TR-PES experiments on solids and surfaces is governed by the detection efficiency for the photoelectrons and the repetition rate of the photon source. Even so space charge effects prevent the use of the full power of FELs in such experiments high repetition rate FELs such as FLASH are by far superior to HHG laser sources for TR-PES if photon energies above 100 eV and pulse duration below 100 fs are considered (see Fig. 77).

Statistical fluctuations of SASE FELs such as FLASH require single shot detection for ultimate time- and energy resolution. Since the SASE spectral band width is typically not sufficient for TR-PES the PG2 monochromator beamline

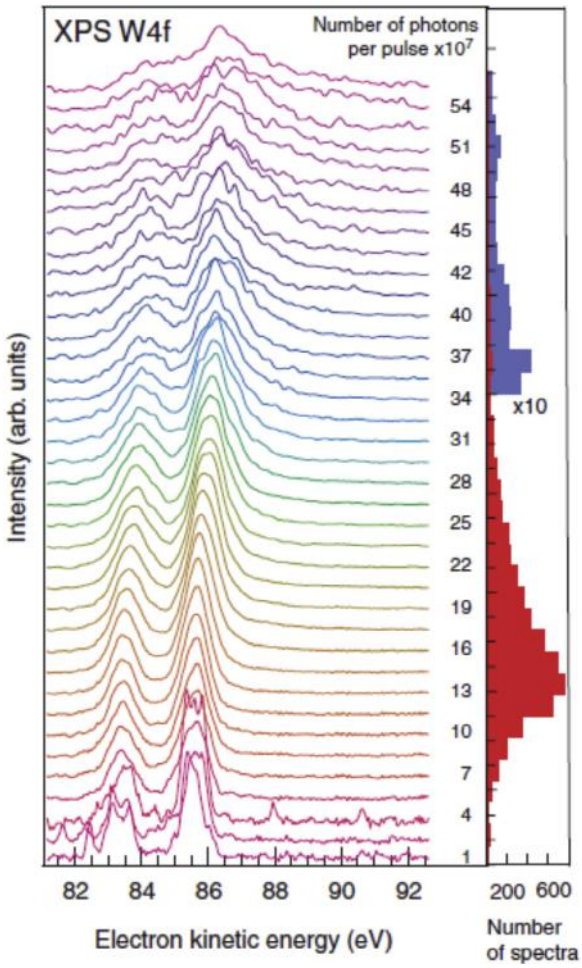

Fig. 78. W4f photoemission as a function of incident X-ray intensity (photon energy 118.5 eV, pulse duration 30 fs). Focal size $395 \pm 23 \times 274 \pm 14\ \mu m^2$. On the right the number of spectra measured at a given photon energy is shown (Pietzsch et al., 2008).

is used for these experiments at FLASH. To make optimum use of the unique properties of high-repetition rate FEL's new analyzer and detection concepts are necessary which are under constant development.

The first experiments on TR-PES at FLASH have been targeted at TR-XPS studies. Pietzsch et al. performed a pioneering study where they investigated space charge limits by measuring the 4f core levels of a tungsten sample as a function of the incoming intensity from FLASH (Pietzsch et al., 2008). The experiment was performed at the monochromator beamline PG2 using the third harmonic of FLASH at 118.5 eV with the fundamental set to 38.5 eV. Burst mode operation with 50 bunches per bunch train with a repetition rate of 5 Hz was used at that time. To determine the number of monochromatic X-ray photons impinging onto the sample on a shot-to-shot basis a calibrated MCP detector (Bittner et al., 2007) was used, which detected a fraction of the incoming photons reflected from a Au mesh (transmission 65%) behind the exit slit. The MCP detector was cross-calibrated against a facility gas monitor detector (Richter et al., 2003) taking into account beamline transmission (Wellhöfer et al., 2007), reflectivity at the mesh and quantum efficiency at the MCP. The evolution of the spectra with increasing number of photons clearly shows the FEL-induced space charge effects which lead to a shift to higher kinetic energy and a significant broadening of the peaks (see Fig. 78).

In the same study also a first cross-correlation experiment was realized. Overlapping an IR laser field in the photoemission process leads to the phenomenon of laser assisted photoemission and the appearance of sidebands. In the experiment a decrease of the photoemission main line was observed which could be used to determine the temporal width of the cross correlation of optical laser and FEL. The temporal width was determined to $\sim$440 fs which resulted mainly from the fairly large jitter between the optical laser and the FEL in the earlier days of FLASH user operation. Another important feature of the observed sideband formation is that it allows to determine time zero in laser pump FEL probe TR-PES experiments (see Fig. 79).

The progress in FEL performance (400 bunches with 10 Hz repetition rate, higher spectral and temporal stability across the bunchtrain) and improved instrumentation (use of time-of-flight electron spectrometers which have a higher

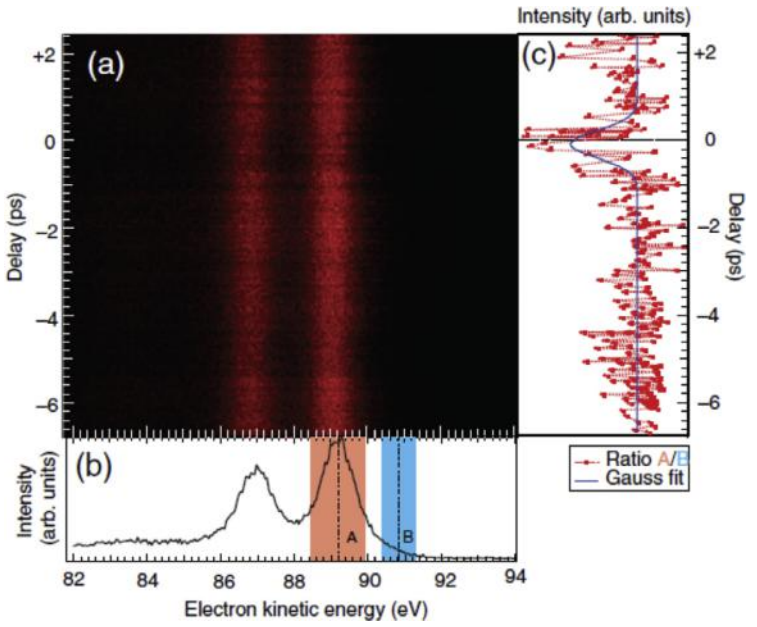

Fig. 79. (a) W 4f photoemission spectra for different delays between optical and XUV pulses. (b) Single W4f spectrum. The energy range of the sidebands is marked (B) together with the reference range (A). (c) Evolution of the ratio A/B as a function of the delay between pump and probe pulse. A weak dip at delay t = 0 indicates the appearance of sidebands. A Gaussian fit gives a width of 440 ± 90 fs (Pietzsch et al., 2008).

transmission in comparison to hemispherical analyzers used in the earlier experiment by Pietzsch et al. can be seen in Fig. 80 where results of a laser assisted photoemission experiment on tungsten are shown which has been performed in 2017 at FLASH by Wenthaus et al. (Wenthaus, 2018).

A first proof of the unique capabilities of high repetition rate FELs like FLASH for TR-XPS was a joint experiment by a group from the Christian-Albrechts Universität Kiel and a group from the Universität Hamburg (Hellmann et al., 2010). Hellmann et al. investigated the photoinduced dynamics of the Mott insulator 1T-TaS_2 . They prepared the sample in the low temperature insulating phase where 1T-TaS_2 exhibits a charge density wave which is commensurate with the lattice. This commensurate charge density wave (CCDW) results in a David-star cluster arrangement of Ta atoms in different charge states. In the XPS spectra of the Ta 4f levels the charge inequality of the tantalum atoms results in two peaks split by ∼0.6 eV (Δ_{CDW}) (see Fig. 81).

After photoexcitation with an 800 nm laser pulse with fluences of 1.8 and 2.5 mJ cm^{-2}, respectively, a rapid decrease of the splitting of the Ta 4f levels on a sub-picosecond time scale and afterwards a partial recovery on a picosecond lifetime into a quasi-equilibrium state with a lifetime longer than 10 ps is observed. On an even longer time scale of ns heat diffusion out of the interaction volume leads to a full recovery of the original CCDW state (Hellmann et al., 2012). The fastest time scale is due to the electronic melting of the CCDW state followed by electron–phonon coupling which leads to transfer of energy from the electronic system to the lattice and a partial melting of the periodic lattice distortions which accompanies the periodic charge arrangement in the CCDW phase. The Fig. 82 shows the temporal evolution of the Ta 4f spectra during the different phases of the dynamic evolution of the sample. The spectra were again measured at the PG2 beamline using the third harmonic of FLASH at a photon energy of 156 eV. They were recorded in macrobunch mode at a master frequency of 5 Hz with each macrobunch consisting of 30 FEL pulses repeated at a period of 4 μs. Each spectrum was accumulated for about 3min.

In a more recent experiment by Dell'Angela et al. photoinduced changes in the electron distribution in the top-most layer of an iridium single crystal were detected by TR-XPS. The experiment was performed with a photon energy of 198 eV in 30 bunch mode with a bunch train repetition rate of 10 Hz. In this photon energy range it is possible to separate surface and bulk contributions in the Ir 4f levels with sufficient instrumental resolution. The surface core level shift of 550 meV allows to distinguish between photoinduced changes of the bulk and surface core level.

Careful evaluation of the measured delay scans reveals that the photoinduced change in the local charge distribution around the iridium atoms induced by the 800 nm laser pulse is concentrated in the surface layer while the bulk signal shows no significant changes (see Fig. 83). In the delay scans a clear asymmetry is visible which can be attributed to the equilibration of the electron gas with the lattice due to electron–phonon coupling (Dell'Angela et al., 2016).

While all these studies were performed with less than the maximum number of possible bunches in a bunch train more recent experiments (not yet published) all have used 400 microbunches which is currently the maximum number of bunches which can be pumped by the burst mode laser in a pump–probe experiment. In combination with novel

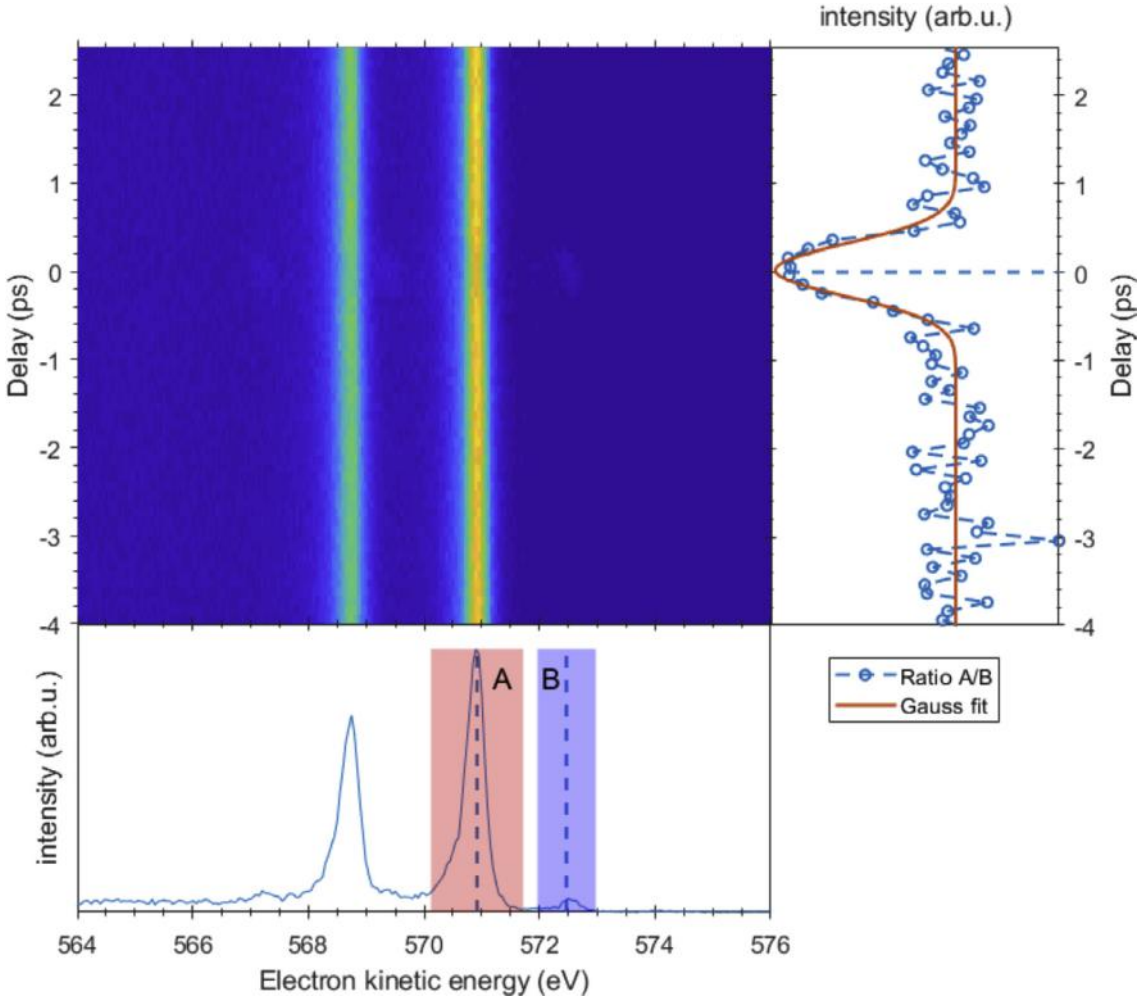

Fig. 80. The figure shows experimental results similar to those depicted in Fig. 79 obtained in 2017. (a) W 4f photoemission spectra for different delays between optical and XUV pulses. (b) Single W4f spectrum. The energy range of the sidebands which can now be clearly resolved is marked (B) together with the reference range (A). (c) Evolution of the ratio A/B as a function of the delay between pump and probe pulse. A pronounced dip at delay t = 0 shows the appearance of sidebands and can be used as a cross-correlation of optical laser and FEL. A Gaussian fit gives a width of 350 fs (Wenthaus, 2018).

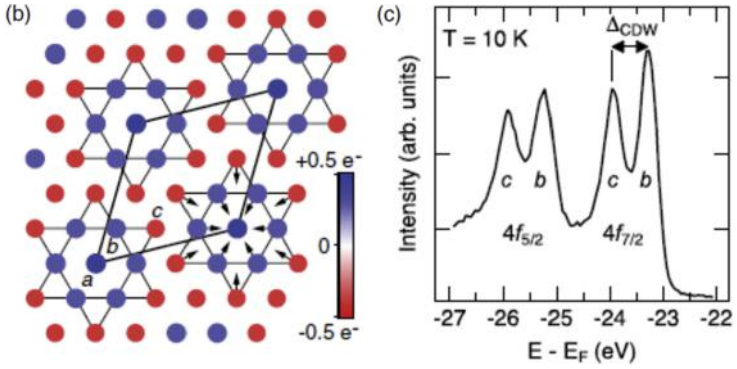

Fig. 81. (left) Sketch of the CCDW showing David-star clusters with inequivalent a, b, and c Ta atoms. The arrows indicate the displacement of the Ta atoms from their original positions. The electron density increases towards the center of the cluster. (right) Ta 4f photoemission spectrum measured with a photon energy of 156 eV. Each Ta 4f level is split into two peaks associated with sites b and c, separated by Δ_{CDW} (Hellmann et al. (2010).

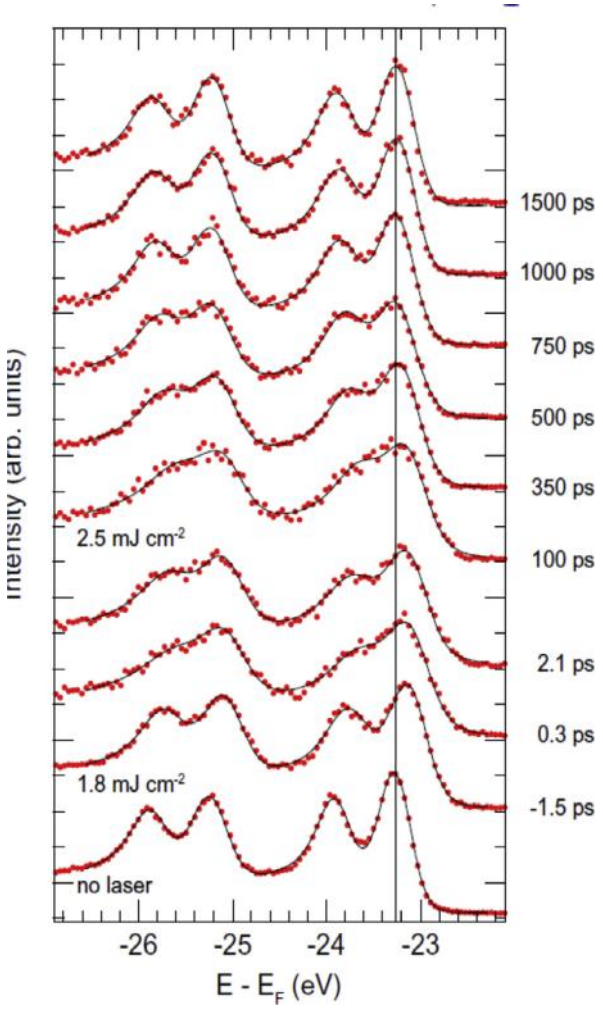

Fig. 82. Time-resolved Ta 4f photoemission spectra of 1T-TaS2 for various pump–probe delays and two incident pump fluences of 1.8 and 2.5 mJ cm −2, recorded at an equilibrium temperature of 10 K. Red dots represent the experimental data and the solid black curves are fits to the spectra using a model function described in the paper. The spectra reveal a transient rigid shift towards lower binding energies, a transient reduction of the CDW-induced Ta 4f splitting and a complete recovery within 1500 ps (Hellmann et al., 2012).

time-of flight electron spectrometers with enhanced angular acceptance this allows to take a full delay scan over a range of 10ps with a step size of 100 fs in about 1 h (Wenthaus, 2018) as demonstrated in Fig. 80.

4.5.2.2. Spectroscopy using photon-in photon-out techniques. As mentioned above the extreme brightness combined with the ultrashort pulses as well as the high average brightness of high repetition rate FELs such as FLASH make such XUV and soft X-ray sources ideally suited to perform X-ray spectroscopy and scattering techniques in a time-resolved fashion which allows to follow the light induced dynamics of materials, but also statically, where high average brightness is mandatory to achieve ultimate spectroscopic resolution.

Among the powerful X-ray spectroscopic techniques which are used statically to investigate the electronic structure of materials X-ray absorption and emission spectroscopy are the most widely used ones giving access to the unoccupied and the occupied valence electronic states, respectively.

X-ray absorption spectroscopy with an FEL is a demanding experiment since it is normally required to scan the wavelength over certain element specific resonances. With the variable gap undulators at FLASH2 this is now possible at FLASH. However, before start of operation of FLASH2 tuning the wavelength always implied a change of electron energy in the accelerator which generally takes quite some time. Hence, at FLASH1 it was considered very difficult to perform X-ray absorption experiments.

However, in a pioneering experiment it was demonstrated that using the PG2 beamline in spectrometer mode and inserting a sample in the dispersed beam after the grating in the exit slit plane while monitoring the transmission through the sample with a CCD camera it is possible to take single shot near edge X-ray absorption fine structure (NEXAFS) spectra

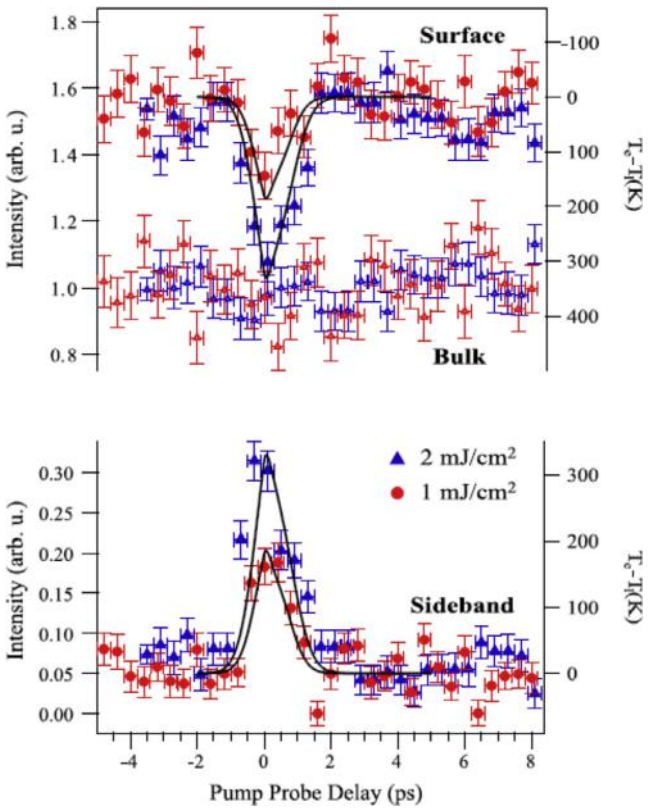

Fig. 83. Intensity as a function of pump–probe delay of the surface (upper trace), bulk (middle trace) and sideband (bottom trace) components from the fit of the delay scans for 1 mJ/cm^2 (red) and 2 mJ/cm^2 (blue) pump fluence. At each fluence the intensity traces have been normalized to the respective average bulk component intensity. The solid lines plotted to the right scale are the difference of electron temperature and lattice temperature calculated by means of the two temperature model (Dell'Angela et al., 2016).

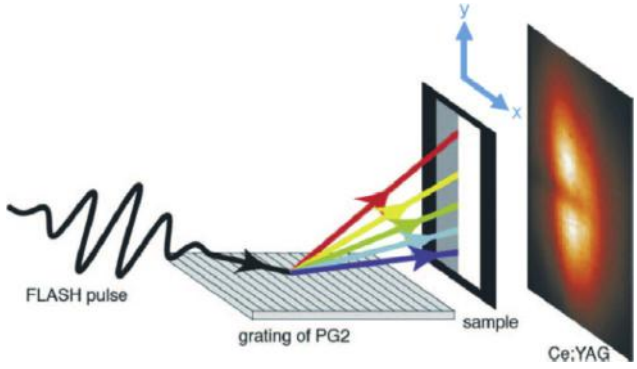

Fig. 84. Cartoon of NEXAFS in single shot spectrograph detection at FLASH. Femtosecond X-ray pulses from the SASE undulator disperse on the monochromator grating and pass through the sample. The sample is two-parted for simultaneous measurement of the absorption in the thin-film sample and the unmodified reference spectral distribution for single shot normalization. The transmitted X-rays are converted into visible light on a Ce:YAG crystal and imaged with an ICCD (Bernstein et al., 2009).

(Bernstein et al., 2009). The schematics of the experiment which utilizes the natural spectral bandwidth of a SASE pulse is shown in Fig. 84.

In combination with photoexcitation the setup would allow to perform transient absorption spectroscopy experiments.

In a more conventional approach Beye et al. performed the first time-resolved X-ray emission spectroscopy (XES) experiment at FLASH (Beye et al., 2010). In this experiment non-thermal melting of a silicon sample was achieved by absorption of 400 nm laser pulses with fluences that lead to electron–hole pair creation for about 25% of the atoms. Such excitation densities would be thermally reached only for temperatures beyond 7000 K far above the melting temperature

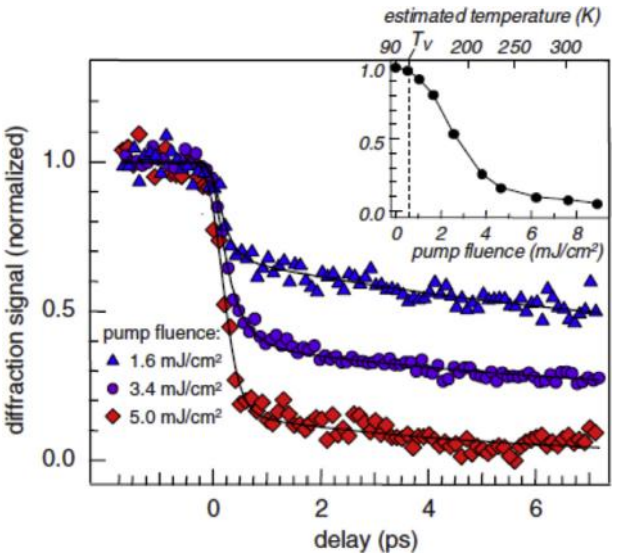

Fig. 85. Time-dependent oxygen K-edge (0,0,1/2) RSXD signal vs. laser pump and X-ray probe time-delay for three different fs-laser pulse fluences (symbols). The lines represent double exponential fits. The inset shows the fluence dependence of the (0,0,1/2) RSXD signal measured at 200 ps time delay measured at BESSY II (Pontius et al., 2011).

of silicon. However, the high excitation density in the electronic system which changes the potential landscape for the silicon atoms and induces non-thermal melting exists only in the first picoseconds before the energy is gradually transferred to the lattice and equilibration takes place. In the X-ray emission spectra taken for different time steps after the photoexcitation by ionizing the Si2p level with a delayed FLASH pulse and spectrally resolving the X-ray fluorescence the transient changes in the electronic structure become visible. From a comparison of the observed valence electronic structure at different times after the photoexcitation it became obvious that in the melting process in the first few ps a non-equilibrium low density liquid state is reached. Only after further transfer of energy from the electronic system to the lattice after about 4 ps the equilibrium metallic high-density liquid state is reached. The existence of a metastable low density liquid state had been postulated for many systems that show tetragonal bonding in the crystalline phase like water for example, but spectroscopically the time-resolved silicon XES data taken at FLASH showed this for the first time.

Another powerful soft X-ray tool which combines information on the electronic or spin state of materials with information on the ordering of the electronic degrees of freedom is resonant soft X-ray scattering (RSXS). Also here the first time-resolved RSXS experiment on a complex material has been performed at FLASH (Pontius et al., 2011). In the experiment the famous Verwey transition in magnetite was photoinduced by an 800 nm laser pulse with different fluences. The intensity of the (0,0,1/2) diffraction peak at 529.4 eV (the peak maximum when scanning the photon energy around the oxygen–edge) representative for the charge ordered insulating low-temperature state was measured with a fast avalanche photodiode. The intensity showed a pronounced fast fluence dependent drop indicative of a loss of charge order upon photoexcitation within the first few hundred femtoseconds (see Fig. 85).

To complete the set of powerful X-ray photon-in photon out spectroscopy tools finally a resonant inelastic X-ray scattering (RIXS) experiment shall be discussed which was performed at the PG1 Raman spectrometer (Rusydi et al., 2014). The off-axis parabolic double-monochromator Raman spectrometer is designed to provide an ultimate resolution below 10 meV (see e.g. Dziarzhytski et al., 2018). In the aforementioned experiment the resolution was set to 24 meV and the low energy excitations of quasi-one-dimensional spin-ladder compounds (SLCs) such as $(La; Sr)_{14-x}Ca_xCu_{24}O_{41}$ were studied after resonant excitation at the Cu M-edges as ideal examples to investigate electronic screening effects for correlation energies. It is expected that correlation energies are lower when electronic screening of Coulomb interactions is present. From the polarization dependent RIXS measurements which here only make use of the high average brightness of FLASH exceeding even powerful storage ring sources, it was possible to obtain the effective Coulomb on-site repulsion energy U_{pd}, superexchange energies J, and estimate anisotropic hopping matrix elements t along the leg and the rung of the ladder for the SLCs. This experiment demonstrates the power of static RIXS at high repetition rate FELs and paves the way for dynamic RIXS studies after photoexcitation of complex materials.

4.5.2.3. Nonlinear light–matter interaction in condensed matter systems. Nonlinear spectroscopy with optical lasers is a very powerful tool to study dynamics in solids and liquids. The first demonstration of nonlinear light–matter interaction in a condensed matter system with an FEL was achieved in an experiment at FLASH where a silicon sample was ionized with FLASH pulses with a photon energy above the Si 2p threshold and the resulting X-ray emission spectra were recorded as a function of the fluence of the FEL pulses (Beye et al., 2013). Under certain geometries an enhancement

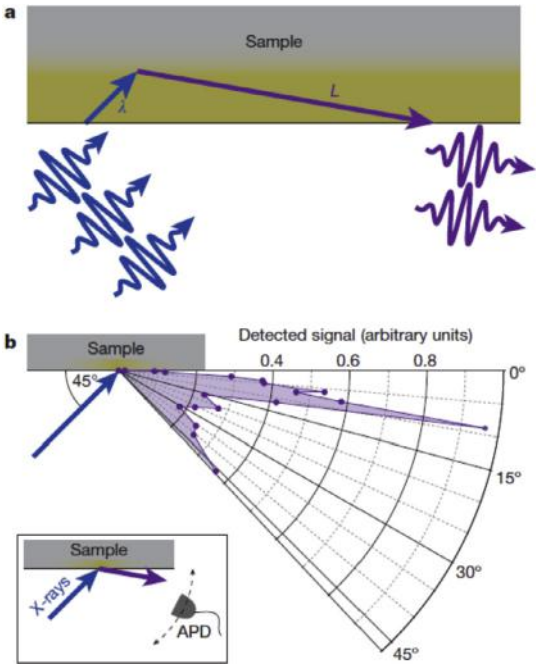

Fig. 86. Geometry to observe spontaneously stimulated X-ray emission from solids. **a**, X-rays create core excitations in the solid (yellow). A cascade of stimulated emission builds up in a direction where the penetration depth λ of incoming photons is balanced by the absorption length L for emission. **b**, The total emission is detected as a function of glancing angle at fluences where stimulated emission saturates. An enhancement is observed for shallow angles, where the interaction length for emitted photons is longest. This direction is far away from the specular reflection increase around 45°. The inset displays the layout of the experiment. APD, avalanche photodiode (Beye et al., 2013).

of the emission signal was observed (see Fig. 86) which is caused by amplified spontaneous emission through stimulated emission processes.

Even so this experiment was only a first step towards nonlinear X-ray spectroscopy it has created a lot of interest and stimulated activities at different FELs which have resulted in a number of demonstration experiments for nonlinear X-ray spectroscopy such as for example sum frequency generation at LCLS (Glover et al., 2012), second harmonic generation (SHG) (Lam et al., 2018) and Transient Grating Spectroscopy (Bencivenga et al., 2015) at FERMI, recently.

5. Outlook

For almost five years FLASH was the only short wavelength free-electron laser facility worldwide. Hence, most of the technological developments as well as the scientific experiments performed by the user community were new and unique as outlined above. FLASH was driving FEL science and technology and paved the way for many new ideas. The original concept of providing only open ports at the end of the beamlines proved to be very successful because it allowed the user community to test new concepts in instrumentation for FEL science and explore which research areas could benefit the most from the novel photon source. Pioneering experiments in AMO science, Coherent Diffractive Imaging and Nonlinear Light–Matter Interaction proved that some of the original science drivers for the development of short wavelength FELs became reality. Early results from cluster studies and warm dense matter experiments at FLASH demonstrated the ability to use FEL pulses to create extreme states of matter. However, it was also shown at FLASH that the high time-resolution of an FEL can be very successfully used to reversibly probe the ultrafast dynamics of materials. Hence, from the success of FLASH, it became obvious that there was an increasing demand for additional free-electron laser facilities in the soft as well as in the hard X-ray regime.

In 2009 the Linac Coherent Light Source in Stanford came into operation where based on the use of part of the old SLAC Linac higher electron beam energies and hence shorter wavelength down to the Angstrom range became accessible (Emma et al., 2010). Concepts developed at FLASH such as single shot coherent imaging (Chapman et al., 2006) were now for the first time applied to solving problems in structural biology and the new field of serial femtosecond crystallography pioneered by Henry Chapman and his collaborators took off at LCLS (Chapman et al., 2011).

Soon after the start of LCLS user operation two more FEL facilities produced first light, SACLA at Harima in Japan, another hard X-ray FEL (Ishikawa et al., 2012), and the first fully seeded FEL, FERMI at Trieste in Italy targeting fully coherent XUV and soft X-ray pulses (Allaria et al., 2012). In the meantime, four more facilities started user operation: the seeded VUV FEL in Dalian, China (Wang, 2017), and the three hard X-ray FELs, PAL FEL in Pohang, Korea (Kang et al.,

2017), the European XFEL in Hamburg, Germany (Tschentscher et al., 2017) and most recently the SwissFEL at the Paul Scherrer Institute in Switzerland (Milne et al., 2017). Another soft X-ray facility – SXFEL – which will also include a seeded FEL line will soon start user operation in Shanghai, China.

Looking at the landscape of FEL facilities there are besides the wavelength range two main distinguishing features between the different facilities. FLASH and the European XFEL are based on superconducting accelerator technology thus being able to provide up to a few 10 000 pulses/s. All the other facilities in operation run with normal conducting Linacs which leads to significantly lower repetition rates in the range from 50 to a few 100 pulses/s. The advantage in higher average brightness of the superconducting machines enables experiments on targets with a very low target density such as molecular ions in astro- and atmospheric chemistry research. Similarly low hit rate experiments like single molecule imaging would not be possible otherwise due to beamtime limits. This has recently been nicely demonstrated in the first publications from user experiments at European XFEL (Grünbein et al., 2018; Wiedorn et al., 2018). A second class of experiments which is only possible with the high repetition rates the superconducting machines can provide are experiments which require or suffer from a low count rate per pulse. Typical examples are time-resolved photoemission spectroscopy on solid targets, which has signal constraints based on space charge effects in the photoemitted electron cloud, or time-resolved inelastic X-ray scattering experiments as well as coincidence experiments, where a low count rate per pulse is intrinsic to the experimental techniques.

The increasing demand for high repetition rate FELs has led to the proposal of new facilities such as LCLS II now being built in Stanford and expected to go online 2020/21 and the SHINE project in Shanghai, which will push the superconducting technology away from the burst mode operation realized at FLASH and the European XFEL to a quasi-continuous wave (cw-) operation with evenly spaced pulses in time and repetition rates up to a MHz. Also, at DESY – DESY2030 – the strategy for the future development of the lab foresees to eventually turn the European XFEL into a cw-FEL.

The second major distinguishing factor between the different facilities is the application of external seeding. Currently there are only two fully externally seeded FELs, FERMI in Trieste operating in the XUV and soft X-ray regime and the new VUV FEL in Dalian. Seeding provides an obvious reduction in pulse-to-pulse fluctuations in parameters such as the arrival time jitter, the spectral content and to a lesser degree the intensity in comparison to a SASE machine. More importantly external seeding enables fully coherent FEL pulses and hence the ability to not only control the temporal shape but also the phase of the pulses. This has recently enabled new classes of experiments such as coherent control e.g. over ionization processes (Prince et al., 2016) and the use of higher-order nonlinear processes such as e.g. four-wave mixing to probe relaxation processes in solids (Bencivenga et al., 2015). It is anticipated that in particular the concepts in multidimensional spectroscopy developed in the optical laser community can be transferred into the XUV and soft X-ray regime with externally seeded FELs such as FERMI. Currently, externally seeded FELs are limited to the XUV and soft X-ray range and even with novel concepts such as echo-enabled harmonic generation (Zhao et al., 2012) it is not expected that the hard X-ray regime can be reached. Seeding in the hard X-ray regime is therefore in the moment restricted to self-seeding with less control over the phase of the pulses (Amann et al., 2012). Since external seeding requires a certain seed laser power in the UV seeding of high repetition rate FELs such as FLASH will require significant developments on the seed laser side towards higher average power.

In the framework of the DESY strategy process for the next decade – DESY2030 – several long-term goals for the future of FLASH have been defined which are in-line with user wishes expressed at a workshop in September 2017 for an upgraded future high repetition rate XUV and soft X-ray FEL facility at DESY.

The resulting FLASH strategy – FLASH2020+ – is based on an ambitious development program of the two FEL lines and the accelerator which includes maintaining the operation of two independent FEL lines (FLASH1 and FLASH2), however, both with tunable undulators being able to deliver photon pulses with variable polarization. One of the two FEL lines shall be fully externally seeded with the full repetition rate that FLASH can provide in burst mode. The other line shall exploit novel lasing concepts based on variable undulator configurations as already in certain aspects e.g. harmonic lasing self-seeding (Schneidmiller et al., 2017), in the moment tested and implemented at FLASH2. Together with a small increase in electron beam energy to 1.3 GeV this would also allow the extension of the wavelength range of the fundamental to the oxygen K-edge, in order to cover the important elements for energy research and the whole water window for biological questions. An important request by the user community for a facility such as FLASH, where 80+% of the experiments are time-resolved and run in some kind of pump/probe scheme, is to provide pump pulses with a large flexibility in wavelength range. While the condensed matter community is asking for THz and mid-IR pump pulses, experiments targeting molecular reactions would like to have tunable pump sources from the visible to the UV and even VUV. Similar to the requirements for seeding at high repetition rate this needs considerable efforts in the development of fully synchronized high average power lasers.

There is a strong push from the user side not only at FLASH but also at the other facilities to provide ever shorter pulses even down to the attosecond regime. Single-spike SASE FEL pulses have been realized recently at FLASH and at LCLS pushing the limits in time-resolution towards the few fs and sub-fs regime (Rönsch-Schulenburg et al., 2014; Huang et al., 2017). Here improved synchronization and timing stabilization of the FELs with respect to external lasers as being developed currently at FLASH will be of key importance for experiments. However, reaching few hundred attoseconds requires in particular in the XUV and soft X-ray regime the realization of new concepts based on laser manipulation of the electron bunches. For FLASH simulations have predicted below 100as pulses with nJ pulse energies down to a few nm

in wavelength. If this could be achieved with the necessary stability in particular the high repetition rate FELs would be below 10 nm very competitive sources in comparison to lab-based laser sources which rely on high-harmonic generation and have certain limits in average power (Heyl et al., 2017).

To conclude, while FLASH has paved the way for FEL science in the early days there are clear trends in the development of FEL technology towards high repetition rate quasi-cw FELs, towards FELs that provide fully coherent photon pulses with phase control and towards the production of shorter pulses in the sub-fs or even attosecond range. At FLASH concepts are currently developed to ensure that the facility stays at the forefront of FEL science and technology.

Acknowledgments

FLASH, the free-electron laser at DESY in Hamburg played a key role in the development and construction of free-electron lasers, and pioneered the ongoing revolution in X-ray science. This success was due to the big efforts made by many colleagues at DESY and the international accelerator and photon science user communities. We want to thank them all and especially the colleagues who provided material for this review and shared with us their views on current and future work with FELs: Anton Barty, Martin Beye, Christoph Bostedt, Henry N. Chapman, Markus Drescher, Stefan Düsterer, Bart Faatz, Alexander Föhlisch, Gerhard Grübel, Igor Isaev, Michel Meyer, Robert Moshammer, Thomas Möller, Hendrik B. Pederson, Elke Plönjes, Kay Rehlich, Mathias Richter, Juliane Rönsch-Schulenburg, Daniela Rupp, Holger Schlarb, Siegfried Schreiber, Frank Stephan, Sven Toleikis, Rolf Treusch, Joachim Ullrich, Mathias Vogt, Hans Weise, Ivan Vartaniants, Andreas Wolf, Igor Zagorodnov, Ulf Zastrau. Financial support by the Accelerator Research and Development Program within the Helmholtz Association, by the Federal Ministry of Education and Research of Germany, by the DFG graduate school program, and by EUROFEL is gratefully acknowledged.

Personal note added in proof. About a month after this review paper became available online, on May 8, 2019, Wilfried Wurth, former corresponding author of the paper, died unexpectedly at the age of 62 on a business trip to Sweden. This was a shock for his family and his many friends all around the world, especially at DESY and at the Universität Hamburg. We all lost a great, visionary scientist and academic teacher, and a wonderful personality. Leading by example, he had enormous impact on developments at DESY, on the education of students at the physics department, and on the synchrotron radiation community at large.

From the beginning, Wilfried Wurth was heavily engaged in realizing the world's first VUV/soft X-ray free-electron laser named FLASH in 2005, and in building beamlines and novel instruments for the best possible science with this revolutionary facility. Most recently, Wilfried led the work on the Conceptual Design Report for further development of FLASH to FLASH2020+. He was also instrumental in setting up the Center for Free-Electron Laser Science CFEL, which is another milestone in the development of DESY.

Wilfried Wurth was a dear friend of us and we are grateful that we could write this review paper together: it includes a lot of his scientific legacy. Through his students, Wilfried will continue advance photon science.

Jörg Rossbach and Jochen Schneider

References

Åberg, T., et al., 1995. A VUV Free-Electron Laser At the TESLA Test Facility At DESY. DESY-Report TESLA-FEL 95-03.
Ackermann, W., Asova, G., Ayvazyan, V., Azima, A., Baboi, N., Bähr, J., Balandin, V., Beutner, B., Brandt, A., Bolzmann, A., et al., 2007. Nature Photon. 1, 336.
Ackermann, S., Azima, A., Bajt, S., Bödewadt, J., Curbis, F., Dachraoui, H., Delsim-Hashemi, H., Drescher, M., Düsterer, S., Faatz, B., et al., 2013. Phys. Rev. Lett. 111, 114801.
Allaria, E., Appio, R., Badano, L., Barletta, W.A., Bassanese, S., Biedron, S.G., Borga, A., Busetto, E., Castronovo, D., Cinquegrana, P., et al., 2012. Nature Photon. 6, 699.
Allaria, E., Castronovo, D., Cinquegrana, P., Craievich, P., Dal Forno, M., Danailov, M.B., D'Auria, G., Demidovich, A., De Ninno, G., Di Mitri, S., et al., 2013. Nature Photon. 7, 913.
Allaria, E., et al., 2019. private communication.
Altarelli, M., Brinkmann, R., Chergui, M., et al., 2006. Technical Design Report of the European XFEL. DESY-Report 2006-097, ISBN: 3-935702-17-5.
Amann, J., Berg, W., Blank, V., Decker, F.-J., Ding, Y., Emma, P., Feng, Y., Frisch, J., Fritz, D., Hastings, J., et al., 2012. Nature Photon. 6, 693.
Andruszkow, J., Aune, B., Ayvazyan, V., Baboi, N., Bakker, R., Balakin, V., Barni, D., Bazhan, A., Bernard, M., Bosotti, A., et al., 2000. Phys. Rev. Lett. 85, 3825.
Arbeiter, M., Fennel, T., 2011. New J. Phys. 13, 053022.
Asova, G., Boyanov, K., Tsakov, I., Baehr, J.W., Boulware, C.H., Grabosch, H.-J., Hakobyan, L.H., Hänel, M., Khodyachykh, S., Korepanov, S.A., et al., 2007. Measurement of the projected normalized transverse emittance at PITZ. In: Proc. Intern. FEL 2007 Conf. Novosibirsk, Russia, pp. 138–141.
Ayvazyan, V., Baboi, N., Bähr, J., Balandin, V., Beutner, B., Brandt, A., Bohnet, I., Bolzmann, A., Brinkmann, R., Brovko, O.I., et al., 2006. Eur. Phys. J. D 37, 297.
Ayvazyan, V., Baboi, N., Bohnet, I., Brinkmann, R., Castellano, M., Castro, P., Catani, L., Choroba, S., Cianchi, A., Dohlus, M., et al., 2002a. Phys. Rev. Lett. 88, 104802.
Ayvazyan, V., Baboi, N., Bohnet, I., Brinkmann, R., Castellano, M., Castro, P., Catani, L., Choroba, S., Cianchi, A., Dohlus, M., et al., 2002b. Eur. Phys. J. D 20, 149.
Bahn, J., Oelßner, P., Köther, M., Braun, C., Senz, V., Palutke, S., Martins, M., Rühl, E., Ganteför, G., Möller, T., et al., 2012. New J. Phys. 14, 075008.
Bajt, S., Chapman, H.N., Nelson, A.J., Lee, R.W., Toleikis, S., Mirkarimi, P., Alameda, J.B., Bakerc, S.L., Vollmer, H., Graff, R.T., et al., 2009. Proc. SPIE 7361, 73610J.
Barends, T.R.M., Foucar, L., Ardevol, A., Nass, K., Aquila, A., Botha, S., Doak, R.B., Falahati, K., Hartmann, E., Hilpert, M., et al., 2015. Science 350, 445.

Barke, I., Hartmann, H., Rupp, D., Flückiger, L., Sauppe, M., Adolph, M., Schorb, S., Bostedt, C., Treusch, R., Peltz, C., Bartling, S., et al., 2015. Nature Commun. 6, 6187.
Barty, A., Boutet, S., Bogan, M.J., Hau-Riege, S., Marchesini, S., Sokolowski-Tinten, K., Stojanovic. R. Tobey, N., Ehrke, H., Cavalleri, A., et al., 2008. Nature Photon. 2, 415.
Beaurepaire, E., Merle, J.-C., Daunois, A., Bigot, J.-Y., 1996. Phys. Rev. Lett. 76, 4250.
Bencivenga, F., Cucini, R., Capotondi, F., Battistoni, A., Mincigrucci, R., Giangrisostomi, E., Gessini, A., Manfredda, M., Nikolov, I.P., Pedersoli, E., et al., 2015. Nature 520, 205.
Bernstein, D.P., Acremann, Y., Scherz, A., Burkhardt, M., Stöhr, J., Beye, M., Schlotter, W.F., Beeck, T., Sorgenfrei, F., Pietzsch, A., et al., 2009. Appl. Phys. Lett. 95, 134102.
Beye, M., Schreck, S., Sorgenfrei, F., Trabant, C., Pontius, N., Schüßler-Langeheine, C., Wurth, W., Föhlisch, A., 2013. Nature 501, 191.
Beye, M., Sorgenfrei, F., Schlotter, W.F., Wurth, W., Föhlisch, A., 2010. Proc. Natl. Acad. Sci. USA 107, 16772.
Bittner, L., Feldhaus, J., Hahn, U., Hesse, M., Jastrow, U., Kocharyan, V., Radcliffe, P., Saldin, E.L., Schneidmiller, E.A., et al., 2007. MCP-based photon detector with extended wavelength range for FLASH. In: Proceedings of FEL 2007, Novosibirsk, Russia, p. 334.
Bogan, M.J., Benner, W.H., Boutet, S., Rohner, U., Frank, M., Barty, A., Seibert, M.M., Maia, F., Marchesini, S., Bajt, S., et al., 2008. Nano Lett. 8, 310.
Bonifacio, R., Pellegrini, C., Narducci, L., 1984. Opt.Commun. 50, 373.
Bostedt, C., Adolph, M., Eremina, E., Hoener, M., Rupp, D., Schorb, S., Thomas, H., de Castro, A.R.B., Möller, T., 2010a. J. Phys. B: At. Mol. Opt. Phys. 43, 194011.
Bostedt, C., Boutet, S., Fritz, D.M., Huang, Z., Lee, H.J., Lemke, H.T., Robert, A., Schlotter, W.F., Turner, J.J., Williams, G.J., 2016a. Rev. Modern Phys. 88, 015007.
Bostedt, C., Eremina, E., Rupp, D., Adolph, M., Thomas, H., Hoener, M., de Castro, A.R.B., Tiggesbäumker, J., Meiwes-Broer, K.-H., Laarmann, T., et al., 2012. Phys. Rev. Lett. 108, 093401.
Bostedt, C., Gorkhover, T., Rupp, D., Möller, T., 2016b. In: Jaeschke, E.J., Khan, S., Schneider, J.R., Hastings, J.B. (Eds.), Synchrotron Light Sources and Free-Electron Lasers. Springer International, pp. 1232–1364.
Bostedt, C., Thomas, H., Hoener, M., Eremina, E., Fennel, T., Meiwes-Broer, K.-H., Wabnitz, H., Kuhlmann, M., Plönjes, E., Tiedtke, K., et al., 2008. Phys. Rev. Lett. 100, 133401.
Bostedt, C., Thomas, H., Hoener, M., Möller, T., Saalmann, U., Georgescu, I., Gnodtke, C., Rost, J.-M., 2010b. New J. Phys. 12, 083004.
Boutet, S., Lomb, L., Williams, G.J., Barends, T.R.M., Aquila, A., Doak, R.B., Weierstall, U., DePonte, D.P., Steinbrener, J., Shoeman, R.L., Messerschmidt, M., et al., 2012. Science 337, 362.
Braune, M., Brenner, G., Dziarzhytski, S., Juranic, P., Sorokin, A., Tiedtke, K., 2016. J. Synchrotron Rad. 23, 10.
Brenner, G., Kapitzki, S., Kuhlmann, M., Ploenjes, E., Noll, T., Siewert, F., Treusch, R., Tiedtke, K., Reininger, R., Roper, M.D., et al., 2011. Nucl. Instrum. Methods A 635, S99.
Brinkmann, R., Materlik, G., Rossbach, J., Wagner, A., 1997. Conceptual Design of a 500 GeV E^+E^- Linear Collider with Integrated X-Ray Laser Facility. DESY-Report 1997-048.
Brunken, M., Genz, H., Hessler, C., Loos, H., Richter, A., Göttlicher, P., Hüning, M., Schlarb, H., Simrock, S., Schmüser, P., et al., 2003. Electro-Optic Sampling At the TESLA Test Accelerator: Experimental Setup and First Results. DESY-Report TESLA 2003-11.
Burian, T., Hájková, V., Chalupský, J., Vyšín, L., Boháček, P., Přeček, M., Wild, J., Özkan, C., Coppola, N., Farahani, S.D., et al., 2015. Opt. Mater. Express 5, 254.
Chalupský, J., Hájková, V., Altapova, V., Burian, T., Gleeson, A.J., Juha, L., Jurek, M., Sinn, H., Störmer, M., Sobierajski, R., et al., 2009a. Appl. Phys. Lett. 95, 031111.
Chalupský, J., Juha, L., Hájková, V., Cihelka, J., Vyšín, L., Gautier, J., Hajdu, J., Hau-Riege, S.P., Jurek, M., Krzywinski, J., et al., 2009b. Opt. Express 17, 208.
Chalupský, J., Juha, L., Kuba, J., Cihelka, J., Hájková, V., Koptyaev, S., Krása, J., Velyhan, A., Bergh, M., Caleman, C., et al., 2007. Opt. Express 15, 6036.
Chalupský, J., Krzywinski, J., Juha, L., Hájková, V., Cihelka, J., Burian, T., Vyšín, L., Gaudin, J., Gleeson, A., Jurek, M., et al., 2010. Opt. Express 18, 27836.
Chapman, H.N., Barty, A., Bogan, M.L., Boutet, S., Frank, M., Hau-Riege, S.P., Marchesini, S., Woods, B.W., Bajt, S., Brenner, W.H., et al., 2006. Nat. Phys. 2, 839.
Chapman, H.N., Fromme, P., Barty, A., White, T.A., Kirian, R.A., Aquila, A., Hunter, M.S., Schulz, J., DePonte, D.P., Weierstall, U., et al., 2011. Nature 470, 73.
Chapman, H.N., Hau-Riege, S.P., Bogan, M.J., Bajt, S., Barty, A., Boutet, S., Marchesini, S., Frank, M., Woods, B.W., Benner, W.H., et al., 2007. Nature 448, 676.
Cornacchia, M., Winick, H. (Eds.), 1992. Report on the Workshop on Fourth Generation Light Sources. SSRL-Report 92/02.
DastjaniFarahani, Sh., Chalupsky, J., Burian, T., Chapman, Henry, Gleeson, A.J., Hajkoya, V., Juha, L., Jurek, M., Klinger, Dorota, Sinn, Harald, et al., 2011. Nucl. Instrum. Methods A 635, S39.
de Castro, A.R.B., Ereminac, E., Bostedtc, C., Hoenerc, M., Thomas, H., Möller, T., 2008. J. Electron Spectrosc. Relat. Phenom. 166–167, 21.
Deacon, D.A.G., Elias, L.R., Madey, J.M.J., Ramian, G.J., Schwettman, H.A., Smith, T.I., 1977. Phys. Rev. Lett. 38, 892.
Dell'Angela, M., Hieke, F., Sorgenfrei, F., Gerken, N., Beye, M., Gerasimova, N., Redlin, H., Wurth, W., 2016. Surf. Sci. 643, 197.
Delsim-Hashemi, H., Grimm, O., Rossbach, J., Schlarb, H., Schmidt, B., Schmüser, P., van der Meer, A.F.G., 2005. Broadband single shot spectrometer. In: Proc. Intern. FEL 2005 Conf. Stanford, USA, pp. 514–517.
Derbenev, Ya.S., Rossbach, J., Saldin, E.L., Shiltsev, V.D., 1995. Microbunching Radiative Tail-Head Interaction. DESY-Report TESLA-FEL 95-05.
Derbenev, Ya. S., Saldin, E.L., Shiltsev, V.D., 1996. Microbunch emittance growth due to radiative interaction. In: Proc. EPAC 96.
DiMauro, L., Doyuran, A., Graves, W., Heese, R., Johnson, E.D., Krinsky, S., Loos, H., Murphy, J.B., Rakowsky, G., Rose, J., et al., 2003. Nucl. Instrum. Methods A 507, 15.
Dumitriu, I., Saenz, A., 2009. J. Phys. B: At. Mol. Opt. Phys. 42, 165101.
Düsterer, S., Radcliffe, P., Geloni, G., Jastrow, U., Kuhlmann, M., Plönjes, E., Tiedtke, K., Treusch, R., Feldhaus, J., Nicolosi, P., et al., 2006. Opt. Lett. 31, 1750.
Düsterer, S., Rading, L., Johnsson, P., Rouzée, A., Hundertmark, A., Vrakking, M.J.J., Radcliffe, P., Meyer, M., Kazansky, A.K., Kabachnik, N.M., 2013. J. Phys. B: At. Mol. Opt. Phys. 46, 164026.
Düsterer, S., Rehders, M., Al-Shemmary, A., Behrens, C., Brenner, G., Brovko, O., DellAngela, M., Drescher, M., Faatz, B., Feldhaus, J., et al., 2014. Phys. Rev. STAB 17, 120702.
Dziarzhytski, S., Gerasimova, N., Goderich, R., Mey, T., Reininger, R., Rübhausen, M., Siewert, F., Weigelt, H., Brenner, G., 2016. J. Synchrotron Rad. 23, 123.
Dziarzhytski, S., Siewert, F., Sokolov, A., Gwalt, G., Seliger, T., Rübhausen, M., Weigelt, H., Brenner, G., 2018. J. Synchrotron Rad. 25, 138.
Edwards, H.T., for the TESLA Collaboration, 1993. Progress report on the TESLA test facility. In: Corneliussen, S.T., Carlton, L. (Eds.), Proc. PAC 1993. pp. 537–539.
Edwards, D.A. (Ed.), 1995. TESLA Test Facility Linac – Design Report, DESY-Report TESLA 1995-01.

Ekeberg, T., Svenda, M., Abergel, C., Maia, F.R.N.C., Seltzer, V., Claverie, J.-M., Hantke, M., Jönsson, O., Nettelblad, C., van der Schot, G., et al., 2015. Phy. Rev. Lett. 114, 098102.
Emma, P., Akre, R., Arthur, J., Bionta, R., Bostedt, C., Bozek, J., Brachmann, A., Bucksbaum, P., Coffee, R., Decker, F.-J., et al., 2010. Nature Photon. 4, 641.
Engel, R., Düsterer, S., Brenner, G., Teubner, U., 2016. J. Synchrotron Rad. 23, 118.
Faatz, B., Plönjes, E., Ackermann, S., Agababyan, A., Asgekar, V., Ayvazyan, V., Baark, S., Baboi, N., Balandin, V., Bargen, N., et al., 2016. New J. Phys. 18, 062002.
Faatz, B., et al., 2017. Appl. Sci. 7, 1114.
Fäustlin, R.R., Bornath, Th., Döppner, T., Düsterer, S., Förster, E., Fortmann, C., Glenzer, S.H., Göde, S., Gregori, G., Irsig, R., et al., 2010a. Phys. Rev. Lett. 104, 125002.
Fäustlin, R.R., Zastrau, U., Toleikis, S., Uschmann, I., Förster, E., Tschentscher, Th., 2010b. J. Instrum. 5, P2004.
Feldhaus, J., Saldin, E.L., Schneider, J.R., Schneidmiller, E.A., Yurkov, M.V., 1997. Opt. Commun. 140, 341.
Ferray, M., L'Huillier, A., Li, X.F., Lompré, L.A., Mainfray, G., Manus, C., 1988. J. Phys. B: At. Mol. Opt. Phys. 21, L31.
Flöter, B., Juranic, P., Kapitzki, S., Keitel, B., Mann, K., Plönjes, E., Schäfer, B., Tiedtke, K., 2010. New J. Phys. 12, 083015.
Flückiger, L., Rupp, D., Adolph, M., Gorkhover, T., Krikunova, M., Müller, M., Oelze, T., Ovcharenko, Y., Sauppe, M., Schorb, S., et al., 2016. New J. Phys. 18, 043017.
Fognini, A., Michlmayr, T.U., Salvatella, G., Wetli, C., Ramsperger, U., Bähler, T., Sorgenfrei, F., Beye, M., Eschenlohr, A., Pontius, N., et al., 2014. Appl. Phys. Lett. 104, 032402.
Fortmann, C., Thiele, R., Fäustlin, R.R., Bornath, Th., Holst, B., Kraeft, W.-D., Schwarz, V., Toleikis, S., Tschentscher, Th., Redmer, R., 2009. High Energy Density Phys. 5, 208.
Fraser, J.S., Sheffield, R.L., Gray, E.R., 1986. Nucl. Instrum. Methods 250, 71.
Frassetto, F., Coraggia, S., Gerasimova, N., Dziarzhytski, S., Golz, T., Weigelt, H., Poletto, L., 2011. Nucl. Instrum. Methods A 635, S94.
Frassetto, F., Coraggia, S., Poletto, L., Guerassimova, N., Dziarzhytski, S., Ploenjes, E., Weigelt, H., 2010. Compact spectrometer for the analysis of high-harmonics content of extreme-ultraviolet free-electron laser radiation. In: Proc. of SPIE 7802, p. 780209.
Fröhlich, L., 2009. Machine Protection for FLASH and the European XFEL, DESY-THESIS 2009-012.
Frühling, U., Wieland, M., Gensch, M., Gebert, T., Schütte, B., Krikunova, M., Kalms, R., Budzyn, F., Grimm, O., Rossbach, J., et al., 2009. Nature Photon. 3, 523.
Gahl, C., Azima M. Beye, A., Deppe, M., Döbrich, K., Hasslinger, U., Hennies, F., Melnikov, A., Nagasono, M., et al., 2008. Nature Photon. 2, 165.
Galtier, E., Rosmej, F.B., Dzelzainis, T., Riley, D., Khattak, F.Y., Heimann, P., Lee, R.W., Nelson, A.J., Vinko, S.M., Whitcher, T., et al., 2011. Phys. Rev. Lett. 106, 164801.
Gensch, M., Bittner, L., Chesnov, A., Delsim-Hashemi, H., Drescher, M., Faatz, B., Feldhaus, J., Fruehling, U., Geloni, G.A., Gerth, Ch., et al., 2008. Infrared Phys. Technol. 51, 423.
Gerasimova, N., Dziarzhytski, S., Feldhaus, J., 2011. J. Mod. Opt. 58, 1480.
Glenzer, S.H., Redmer, R., 2009. Rev. Modern Phys. 81, 1625.
Glover, T.E., Fritz, D.M., Cammarata, M., Allison, T.K., Coh, S., Feldkamp, J.M., Lemke, H., Zhu, D., Feng, Y., Coffee, R.N., et al., 2012. Nature 488, 603.
Glover, T.E., Schoenlein, R.W., Chin, A.H., Shank, C.V., 1996. Phys. Rev. Lett. 76, 2468.
Gorkhover, T., Schorb, S., Coffee, R., Adolph, M., Foucar, L., Rupp, D., Aquila, A., Bozek, J.D., Epp, S.W., Erk, B., et al., 2016. Nature Photon. 10, 93.
Gorobtsov, O.Y., Mercurio, G., Capotondi, F., Skopintsev, P., Lazarev, S., Zaluzhnyy, I.A., Danailov, M.B., Dell'Angela, M., Manfredda, M., Pedersoli, E., et al., 2018. Nature Commun. 9, 4498.
Grimm, O., Morozov, N., Chesnov, A., Holler, Y., Matushevsky, E., Petrov, D., Rossbach, J., Syresin, E., Yurkov, M., 2010. Nucl. Instrum. Methods A 615, 105.
Grimm, O., Rossbach, J., Kocharyan, V., 2007. Numerical calculations of the radiation emitted from the FLASH infrared undulator. In: Proc. of Intern. FEL 2007 Conf. Novosibirsk, Russia, pp. 322–325.
Grünbein, M.L., Bielecki, J., Gorel, A., Stricker, M., Bean, R., Cammarata, M., Dörner, K., Fröhlich, L., Hartmann, E., Hauf, S., et al., 2018. Nature Commun. http://dx.doi.org/10.1038/s41467-018-05953-4.
Gutt, C.L.-M., Stadler, Streit-Nierobisch, S., Mancuso, A.P., Schropp, A., Pfau, B., Günther, C.M., Könnecke, R., Gulden, J., Reime, B., Feldhaus, J., et al., 2009. Phys. Rev. B 79, 212406.
Gutt, C., Streit-Nierobisch, S., Stadler, L.-M., Pfau, B., Günther, C.M., Könnecke, R., Frömter, R., Kobs, A., Stickler, D., Oepen, H.P., et al., 2010. Phys. Rev. B 81, 100401.
Guyétand, O., Gisselbrecht, M., Huetz, A., Agostini, P., Taïeb, R., Véniard, V., Maquet, A., Antonucci, L., Boyko, O., Valentin, C., Douillet, D., 2005. J. Phys. B: At. Mol. Opt. Phys. 38, L357.
Hacker, K., Khan, S., Molo, R., Ackermann, S., Assmann, R.W., Bödewadt, J., Ekanayake, N., Faatz, B., Hartl, I., Ivanov, R., et al., 2015. First lasing of an HGHG seeded FEL at FLASH. In: Proc. Intern. FEL 2015 Conf. Daejeon, Korea, pp. 646–649.
Hahn, U., Tiedtke, K., 2007. The gas attenuator of FLASH at DESY in syncrotron radiation instrumentation. AIP Conf. Proc. 879, 276.
Harbo, L.S., Becker, A., Dziarzhytski, S., Domesle, C., Guerassimova, N., Wolf, A., Pedersen, H.B., 2012. Phys. Rev. A 86, 023409.
Harms, E., Edwards, H., Hüning, M., Vogel, E., 2010. Commissioning and early operation experience of the FLASH third harmonic rf system. In: Proc. Intern. Linac Conf. 2010, Tsukuba, Japan, pp. 422–424.
Hau-Riege, S.P., Chapman, H.N., Krzywinski, J., Sobierajski, R., Bajt, S., London, R.A., Bergh, M., Caleman, C., Nietubyc, R., Juha, L., et al., 2007a. Phys. Rev. Lett. 98, 145502.
Hau-Riege, S.P., London, R.A., Bionta, R.M., McKernan, M.A., Baker, S.L., Krzywinski, J., Sobierajski, R., Nietubyc, R., Pelka, J.B., Jurek, M., et al., 2007b. Appl. Phys. Lett. 90, 173128.
Hau-Riege, S.P., London, R.A., Bionta, R.M., Ryutov, D., Soufli, R., Bajt, S., McKernan, M.A., Baker, S.L., Krzywinski, J., Sobierajski, R., et al., 2009. Appl. Phys. Lett. 95, 111104.
Hellmann, S., Beye, M., Sohrt, C., Rohwer, T., Sorgenfrei, F., Redlin, H., Kalläne, M., Marczynski-Bühlow, M., Hennies, F., Bauer, M., et al., 2010. Phys. Rev. Lett. 105, 187401.
Hellmann, S., Sohrt, C., Beye, M., Rohwer, T., Sorgenfrei, F., Marczynski-Bühlow, M., Kallane, M., Redlin, H., Hennies, F., Bauer, M., et al., 2012. New J. Phys. 14, 013062.
Hemsing, E., Dunning, M., Garcia, B., Hast, C., Raubenheimer, T., Stupakov, G., Xiang, D., 2016. Nature Photon. 10, 512.
Hergott, J.-F., Kovacev, M., Merdji, H., Hubert, C., Mairesse, Y., Jean, E., Breger, P., Agostini, P., Carré, B., Salières, P., 2002. Phys. Rev. A 66, 021801(R).
Heyl, C.M., Arnold, C.L., Couairon, A., L'Huillier, A., 2017. J. Phys. B: At. Mol. Opt. Phys. 50, 013001.
Hoener, M., Bostedt, C., Thomas, H., Landt, L., Eremina, E., Wabnitz, H., Laarmann, T., Treusch, R., de Castro, A.R.B., Möller, T., 2008. J. Phys. B: At. Mol. Opt. Phys. 41, 181001.
Höll, A., Bornath, Th., Cao, L., Döppner, T., Düsterer, S., Förster, E., Fortmann, C., Glenzer, S.H., Gregori, G., et al., 2007. High Energy Density Phys. 3, 120.

Honkavaara, K., Faatz, B., Feldhaus, J., Schreiber, S., Treusch, R., Vogt, M., 2015. Status of the soft X-ray user facility FLASH. In: Proc. Intern. FEL 2015 Conf. Daejeong, Korea, pp. 61–65.
Huang, S., Ding, Y., Feng, Y., Hemsing, E., Huang, Z., Krzywinski, J., Lutman, A.A., Marinelli, A., Maxwell, T.J., Zhu, D., 2017. Phys. Rev. Lett. 119, 154801.
Huang, Z., Kim, K.-J., 2001. Nucl. Instrum. Methods A 475, 59.
Hüning, M., Bolzmann, A., Schlarb, H., Frisch, J., McCormick, D., Ross, M., Smith, T., Rossbach, J., 2005. Observation of Femtosecond Bunch Length Using a Transverse Deflecting Structure. In: Proc. Intern. FEL 2005 Conf. Stanford, USA, pp. 538–540.
Ischebeck, R., Feldhaus, J., Gerth, Ch., Saldin, E., Schmüser, P., Schneidmiller, E., Steeg, B., Tiedtke, K., Tonutti, M., Treusch, R., Yurkov, M., 2003. Nucl. Instrum. Methods A 507, 175.
Ishikawa, T., Aoyagi, H., Asaka, T., Asano, Y., Azumi, N., Bizen, T., Ego, H., Fukami, K., Fukui, T., Furukawa, Y., et al., 2012. Nature Photon. 6, 540.
Ivanov, R., Liu, J., Brenner, G., Brachmanski, M., Düsterer, S., 2018. J. Synchrotron Rad. 25, 26.
Jiang, Y.H., Rudenko, A., Herrwerth, O., Foucar, L., Kurka, M., Kühnel, K.U., Lezius, M., Kling, M.F., van Tilborg, J., Belkacem, A., et al., 2010a. Phys. Rev. Lett. 105, 263002.
Jiang, Y.H., Rudenko, A., Pérez-Torres, J.F., Herrwerth, O., Foucar, L., Kurka, M., Kühnel, K.U., Toppin, M., Plésiat, E., Morales, F., et al., 2010b. Phys. Rev. A 81, 051402(R).
Kang, H.-S., Min, C.-K., Heo, H., Kim, C., Yang, H., Kim, G., Nam, I., Baek, S.Y., Choi, H.-J., Mun, G., et al., 2017. Nature Photon. 11, 708.
Keitel, B., Plönjes, E., Kreis, S., Kuhlmann, M., Tiedtke, K., Mey, T., Schäfer, B., Mann, K., 2016. J. Synchrotron Rad. 23, 43.
Kern, J., Tran, R., Alonso-Mori, R., Koroidov, S., Echols, N., Hattne, J., Ibrahim, M., Gul, S., Laksmono, H., Sierra, R.G., et al., 2014. Nature Commun. 5, 4371.
Khorsand, A.R., Sobierajski, R., Louis, E., Bruijn, S., van Hattum, E.D., van de Kruijs, R.W.E., Jurek, M., Klinger, D., Pelka, J.B., Juha, L., et al., 2010. Opt. Express 18, 700.
Kim, J., Chen, J., Zhang, Z., Wong, F.N.C., Kärtner, F.X., Loehl, F., Schlarb, H., 2007. Opt. Lett. 32, 9.
Kirkpatrick, D.A., Bekefi, G., Dirienzo, A.C., Freund, H.P., Ganguly, A.K., 1989. Nucl. Instrum. Methods A 285, 43.
Kondratenko, A., Saldin, E., 1980. Part. Accel. 10, 207.
Krasilnikov, M., Stephan, F., Asova, G., Grabosch, H.-J., Groß, M., Hakobyan, L., Isaev, I., Ivanisenko, Y., Jachmann, L., Khojoyan, M., et al., 2012. Phys. Rev. ST Accel. Beams 15, 100701.
Krzywinski, J., Andrejczuk, A., Bionta, R.M., Burian, T., Chalupsky, J., Jurek, M., Kirm V. Nagirnyi, M., Sobierajski, R., Tiedtke, K., et al., 2017. Opt. Mater. Express 7, 665.
Krzywinski, J., Sobierajski, R., Jurek, M., Nietubyc, R., Pelka, J.B., Juha, L., Bittner, M., Létal, V., Vorlíček, V., Andrejczuk, A., et al., 2007. J. Appl. Phys. 101, 043107.
Kupitz, C., Basu, S., Grotjohann, I., Fromme, R., Zatsepin, N.A., Rendek, K.N., Hunter, M.S., Shoeman, R.L., White, T.A., Wang, D., et al., 2014. Nature 513, 261.
Kurka, M., Feist, J., Horner, D.A., Rudenko, A., Jiang, Y.H., Kühnel, K.U., Foucar, L., Rescigno, T.N., McCurdy, C.W., Pazourek, R., et al., 2010. New J. Phys. 12, 073035.
Kurka, M., Rudenko, A., Foucar, L., Kühnel, K.U., Jian, Y.H., Th. Ergler, Havermeier, T., Smolarski, M., Schössler, S., Cole, K., et al., 2009. J. Phys. B: At. Mol. Opt. Phys. 42, 141002.
Laarmann, T., de Castro, A.R.B., Gürtler, P., Laasch, W., Schulz, J., Wabnitz, H., Möller, T., 2004. Phys. Rev. Lett. 92, 143401.
Lai, R., Sievers, A.J., 1997. Nucl. Instrum. Methods A 397, 221.
Lam, R.K., Raj, S.L., Pascal, T.A., Pemmaraju, C.D., Foglia, L., Simoncig, A., Fabris, N., Miotti, P., Hull, C.J., Rizzuto, A.M., et al., 2018. Phys. Rev. Lett. 120, 023901.
Lambropoulos, P., Papamihail, K.G., Decleva, P., 2011. J. Phys. B: At. Mol. Opt. Phys. 44, 175402.
Lammich, L., Domesle, C., Jordon-Thaden, B., Förstel, M., Arion, T., Lischke, T., Heber, O., Klumpp, S., Martins, M., Guerassimova, N., et al., 2010. Phys. Rev. Lett. 105, 253003.
Lee, R.W., Moon, S.J., Chung, H.-K., Rozmus, W., Baldis, H.A., Gregori, G., Cauble, R.C., Landen, O.L., Wark, J.S., Ng, A., et al., 2003. J. Opt. Soc. Amer. B 20, 770.
Li, Z., Madjet, M.E.A., Vendrell, O., Santra, R., 2013. Phys. Rev. Lett. 110, 38302.
Li, Z., Vendrell, O., 2016. Struct. Dyn. 3, 43203.
Limberg, T., Piot, P., Stulle, F., 2002. Design and performance simulation of the TTF-FEL II bunch compressors. In: Proc. EPAC 2002 Conf. Paris, France, pp. 811–813.
Liu, W., Wacker, D., Gati, C., Han, G.W., James, D., Wang, D., Nelson, G., Weierstall, U., Katritch, V., Barty, A., et al., 2013. Science 342, 1521.
Loh, N.D., Bogan, M.J., Elser, V., Barty, A., Boutet, S., Bajt, S., Hajdu, J., Ekeberg, T., Maia, F.R.N.C., Schulz, J., et al., 2010. Phys. Rev. Lett. 104, 225501.
Löhl, F., 2005. Measurements of the Transverse Emittance At the VUV-FEL. DESY-Report TESLA-FEL 2005-03.
Löhl, F., Arsov, V., Felber, M., Hacker, K., Jalmuzna, W., Lorbeer, B., Ludwig, F., Matthiesen, K.-H., Schlarb, H., Schmidt, B., et al., 2010. Phys. Rev. Lett. 104, 144801.
Löhl, F., Schreiber, S., Castellano, M., Di Pirro, G., Catani, L., Cianchi, A., Honkavaara, K., 2006. Phys. Rev. ST Accel. Beams 9, 092802.
Loreau, J., Lecointre, J., Urbain, X., Vaeck, N., 2011. Phys. Rev. A 84, 053412.
MacFarlane, J., Golovkin, I.E., Woodruff, P.R., 2006. J. Quant. Spectrosc. Radiat. Transfer 99, 381.
Madey, J.M.J., 1971. J. Appl. Phys. 42, 1906.
Makhotkin, I.A.Q., Sobierajski, R., Chalupský, J., Tiedtke, K., de Vries, G., Störmer, M., Scholze, F., Siewert, F., van de Kruijs, R.W.E., Milov, I., et al., 2018. J. Synchrotron Rad. 25, 77.
Makris, M.G., Lambropoulos, P., Mihelic, A., 2009. Phys. Rev. Lett. 102, 033002.
Maltezopoulos, T., Azima, M.A., Bödewadt, J., Dachraoui, H., Rehders, M., Lechner, C., Schulz, M., Wieland, M., Laarmann, T., et al., 2014. Appl. Phys. B 115, 45.
Maltezopoulos, T., Cunovic, S., Wieland, M., Beye, M., Azima, A., Redlin, H., Krikunova, M., Kalms, R., Frühling, U., Budzyn, F., et al., 2008. New J. Phys. 10, 03302.
Maquet, A., Taïeb, R., 2007. J. Modern Opt. 54, 1847.
Marchesini, S., He, H., Chapman, H.N., Hau-Riege, S.P., Noy, A., Howells, M.R., Weierstall, U., Spence, J.C.H., 2003. Phys. Rev. B 68, 140101.
Martins, M., Wellhöfer, M., Hoeft, J.T., Wurth, W., Follath, R., Feldhaus, J., 2006. Rev. Sci. Instrum. 77, 115108.
Mazza, T., Karamatskou, A., Ilchen, M., Bakhtiarzadeh, S., Rafipoor, A.J., O'Keeffe, P., Kelly, T.J., Walsh, N., Costello, J.T., Meyer, M., Santra, R., 2015. Nature Commun. 6, 6799.
Mazza, T., Papamihail, K.G., Radcliffe, P., Li, W.B., Kelly, T.J., Costello, J.T., Düsterer, S., Lambropoulos, P., Meyer, M., 2012. J. Phys. B: At. Mol. Opt. Phys. 45, 141001.
McNeil, B.W.J., Robb, G.R.M., Poole, M.W., Thompson, N.R., 2006. Phys. Rev. Lett. 96, 084801.
Medvedev, N., Zastrau, U., Förster, E., Gericke, D.O., Rethfeld, B., 2011. Phys. Rev. Lett. 107, 165003.
Medvedev, N., Ziaja, B., Cammarata, M., Harmand, M., Toleikis, S., 2013. Contrib. Plasma Phys. 53, 347.
Meyer, M., Costello, J.T., Düsterer, S., Li, W.B., Radcliffe, P., 2010a. J. Phys. B: At. Mol. Opt. Phys. 43, 194006.

Meyer, M., Cubaynes, D., Glijer, D., Dardis, J., Hayden, P., Hough, P., Richardson, V., Kennedy, E.T., Costello, J.T., Radcliffe, P., et al., 2008. Phys. Rev. Lett. 101, 193002.
Meyer, M., Cubaynes, D., O'Keeffe, P., Luna, H., Yeates, P., Kennedy, E.T., Costello, J.T., Orr, P., Taïeb, R., Maquet, A., et al., 2006. Phys. Rev. A 74, 11401(R).
Meyer, M., Cubaynes, D., Richardson, V., Costello, J.T., Radcliffe, P., Li, W.B., Düsterer, S., Fritzsche, S., Mihelic, A., Papamihail, K.G., Lambropoulos, P., 2010b. Phys. Rev. Lett. 104, 213001.
Milne, C.J., Schietinger, T., Aiba, M., Alarcon, A., Alex, J., Anghel, A., Arsov, V., Beard, C., Beaud, P., Bettoni, S., et al., 2017. Appl. Sci. 7, 720.
Milton, S.V., Gluskin, E., Arnold, N.D., Benson, C., Berg, W., Biedron, S.G., Borland, M., Chae, Y.-C., Dejus, R.J., Den Hartog, P.K., et al., 2001. Science 292, 2037.
Mitzner, R., Sorokin, A.A., Siemer, B., Roling, S., Rutkowski, M., Zacharias, H., Neeb, M., Noll, T., Siewert, F., Eberhardt, W., et al., 2009. Phys. Rev. A 80, 025402.
More, R.M., Warren, K.H., Young, D.A., Zimmerman, G.B., 1988. Phys. Fluids 31, 3059.
Moshammer, R., Jiang, Y.H., Foucar, L., Rudenko, A., Ergler, Th., Schröter, C.D., Lüdemann, S., Zrost, K., Fischer, D., Titze, J., et al., 2007. Phys. Rev. Lett. 98, 203001.
Moshammer, R., Rudenko, A., Ullrich, J., 2013. Phys. Unserer Zeit 1 (44), 20.
Müller, M., Schroedter, L., Oelze, T., Nösel, L., Przystawik, A., Kickermann, A., Adolph, M., Gorkhover, T., Flückiger, L., Krikunova, M., et al., 2015. J. Phys. B: At. Mol. Opt. Phys. 48, 174002.
Nagler, B., Zastrau, U., Fäustlin, R.R., Vinko, S.M., Whitcher, T., Nelson, A.J., Sobierajski, R., Krzywinski, J., Chalupsky, J., Abreu, E., et al., 2009. Nat. Phys. 5, 693.
Nelson, A.J., Toleikis, S., Chapman, H., Bajt, S., Krzywinski, J., Chalupsky, J., Juha, L., Cihelka, J., Hajkova, V., Vysin, L., et al., 2009. Opt. Express 17, 18271.
Neutze, R., Wouts, R., van der Spoel, D., Weckert, E., Hajdu, J., 2000. Nature 406, 752.
Nicolosi, P., Poletto, L., Pelizzo, M.-G., Epulandi, L., Zambolin, P., Feldhaus, J., Jastrow, U., Hahn, U., Ploenjes, E., Tiedtke, K., 2005. J. Electron Spectrosc. Relat. Phenom. 144–147.
Oloff, L.P., Oura, M., Chainani, A., Rossnagel, K., 2016. Femtosecond time-resolved HAXPES. In: Woicik, J. (Ed.), Hard X-Ray Photoelectron Spectroscopy (HAXPES). In: Springer Series in Surface Sciences, vol. 59, Springer, Cham.
Orzechowski, T.J., Anderson, B., Fawley, W.M., Prosnitz, D., Scharlemann, E.T., Yarema, S., Hopkins, D., Paul, A.C., Sessler, A.M., Wurtele, J., 1985. Phys. Rev. Lett. 54, 889.
Palutke, S., Gerken, N.C., Mertens, K., Klumpp, S., Mozzanica, A., Schmitt, B., Wunderer, C., Graafsma, H., Meiwes-Broer, K.-H., Wurth, W., Martins, M., 2015. Rev. Sci. Instrum. 86, 113107.
Pande, K., Hutchison, C.D.M., Groenhof, G., Aquila, A., Robinson, J.S., Tenboer, J., Basu, S., Boutet, S., DePonte, D.P., Liang, M., et al., 2016. Science 352, 72.
Pedersen, H.B., Altevogt, S., Jordon-Thaden, B., Heber, O., Lammich, L., Rappaport, M.L., Schwalm, D., Ullrich, J., Zajfman, D., Treusch, R., 2009. Phys. Rev. A 80, 012707.
Pedersen, H.B., Altevogt, S., Jordon-Thaden, B., Heber, O., Rappaport, M.L., Schwalm, D., Ullrich, J., Zajfman, D., Treusch, R., Guerassimova, N., 2007. Phys. Rev. Lett. 98, 223202.
Pedersen, H.B., Lammich, L., Domesle, C., Jordon-Thaden, B., Heber, O., Ullrich, J., Treusch, R., Guerassimova, N., Wolf, A., 2010. Phys. Rev. A 82, 023415.
Pellegrini, C., 1990. In: Gallardo, J.C. (Ed.), Proc. Workshop on Prospects for a 1 ÅFree-Electron Laser. B.N.L. Rep. 52273, pp. 3–12.
Pellegrini, C., 1992. In: Cornacchia, M., Winick, H. (Eds.), Proc. Workshop on Fourth Generation Light Sources. SSRL Report 92/02.
Pellegrini, C., Marinelli, A., Reiche, S., 2016. Rev. Modern Phys. 88, 015006.
Peltz, C., Varin, C., Brabec, T., Fennel, T., 2014. Phys. Rev. Lett. 113, 133401.
Pfau, B., Schaffert, S., Müller, L., Gutt, C., Al-Shemmary, A., Büttner, F., Delaunay, R., Düsterer, S., Flewett, S., Frömter, R., et al., 2012. Nature Commun. 3, 1100, 1.
Pfeiffer, S., 2014. Symmetric Grey Box Identification and Distributed Beam-Based Controller Design for Free-Electron Lasers, DESY-THESIS-2014-030.
Pflüger, J., 2000. Nucl. Instrum. Methods A 445, 366.
Pietzsch, A., Föhlisch, A., Beye, M., Deppe, M., Hennies, F., Nagasono, M., Suljoti, E., Wurth, W., Gahl, C., Döbrich, K., Melnikov, A., 2008. New J. Phys. 10, 033004.
Plath, T., Amstutz, P., Bödewadt, J., Brenner, G., Ekanayake, N., Faatz, B., Hacker, K., Honkavaara, K., Lazzarino, L.L., Lechner, C., et al., 2016. J. Synchrotron Rad. 23, 1070.
Plönjes, E., Faatz, B., Kuhlmann, M., Treusch, R., 2016. FLASH2: Operation, beamlines, and photon diagnostics. In: AIP Conference Proceedings 1741, p. 020008.
Pontius, N., Kachel, T., Schüßler-Langeheine, C., Schlotter, W.F., Beye, M., Sorgenfrei, F., Chang, C.F., Föhlisch, A., Wurth, W., Metcalf, P., 2011. Appl. Phys. Lett. 98, 182504.
Popruzhenko, S.V., Mur, V.D., Bauer, D., 2008. Phys. Rev. Lett. 101, 193003.
Prince, K.E., Allaria, Callegari, C., Cucini, R., De Ninno, G., Di Mitri, S., Diviacco, B., Ferrari, E., Finetti, P., Gauthier, D., et al., 2016. Nature Photon. 10, 176.
Radcliffe, P., Arbeiter, M., Li, W.B., Düsterer, S., Redlin, H., Hayden, P., Hough, P., Richardson, V., Costello, J.T., Fennel, T., Meyer, M., 2012. New J. Phys. 14, 043008.
Radcliffe, P., Düsterer, S., Azima, A., Redlin, H., Feldhaus, J., Dardis, J., Kavanagh, K., Luna, H., Pedregosa Gutierrez, J., Yeates, P., 2007. Appl. Phys. Lett. 90, 131108.
Raines, K.S., Salha, S., Sandberg, R.L., Jiang, H., Rodríguez, J.A., Fahimian, B.P., Kapteyn, H.C., Du, J., Miao, J., 2010. Nature 463, 214.
Raubenheimer, T.O., for the NLC Design group, 1996. The Zeroth Order Design Report for the Next Linear Collider. Report SLAC 474.
Redlin, A., Al-Shemmary, Azima, A., Stojanovic, N., Tavella, F., Will, I., Düsterer, S., 2011. Nucl. Instrum. Methods A 635, 88.
Reiche, S., 1999. Nucl. Instrum. Methods A 429, 243.
Richardson, V., Costello, J.T., Cubaynes, D., Düsterer, S., Feldhaus, J., van der Hart, H.W., Juranić, P., Li, W.B., Meyer, M., Richter, M., et al., 2010. Phys. Rev. Lett. 105, 013001.
Richardson, V., Li, W.B., Kelly, T.J., Costello, J.T., Nikolopoulos, L.A.A., Düsterer, S., Cubaynes, D., Meyer, M., 2012. J. Phys. B: At. Mol. Opt. Phys. 45, 085601.
Richter, M., 2011. J. Phys. B: At. Mol. Opt. Phys. 44, 075601.
Richter, M., Gottwald, A., Kroth, U., Sorokin, A.A., Bobashev, S.V., Shmaenok, L.A., Feldhaus, J., Gerth, Ch., Steeg, B., Tiedtke, K., Treusch, R., 2003. Appl. Phys. Lett. 83, 2970.
Richter, M., Ya. Amusia, M., Bobashev, S.V., Feigl, T., Juranic, P.N., Martins, M., Sorokin, A.A., Tiedtke, K., 2009. Phys. Rev. Lett. 102, 163002.
Riedel, R., Al-Shemmary, A., Gensch, M., Golz, T., Harmand, M., Medvedev, N., Prandolini, M.J., Sokolowski-Tinten, K., Toleikis, S., et al., 2013. Nature Commun. 4, 1731.

Roling, S., Siemer, B., Wöstmann, M., Zacharias, H., Mitzner, R., Singer, A., Tiedtke, K., Vartanyants, I.A., 2011. Phys. Rev. ST Accel. Beams 14, 080701.
Rönsch-Schulenburg, J., Hass, E., Lockmann, N.M., Plath, T., Rehders, M., Roßbach, J., Brenner, G., Dziarzhytski, S., Golz, T., Schlarb, H., et al., 2014. Operation of FLASH with short SASE-FEL radiation pulses. In: Proc. Intern. FEL Conf. 2014, Basel, Switzerland, pp. 342–345.
Rosenzweig, J.B., Alesini, D., Andonian, G., Boscolo, M., Dunning, M., Faillace, L., Ferrario, M., Fukusawa, A., Giannessi, L., Hemsing, E., et al., 2008. Nucl. Instrum. Methods A 593, 39.
Rossbach, J., 1996. A VUV free electron laser at the TESLA test facility at DESY. Nucl. Instrum. Methods A 375, 269.
Rossbach, J., 2008. First lasing below 7 nm wavelength at FLASH/DESY, Hamburg. In: Proc. of the 30th Intl. FEL Conf. Gyeongju, Korea.
Rossbach, J., 2016. In: Jaeschke, E.J., Khan, S., Schneider, J.R., Hastings, J.B. (Eds.), Synchrotron Light Sources and Free-Electron Lasers. Springer International, pp. 303–328.
Rudenko, R., Foucar, L., Kurka, M., Ergler, K.U., Jiang, Y.H., Voitkiv, A., Najjari, B., Kheifets, A., et al., 2008. Phys. Rev. Lett. 101, 073003.
Rupp, D., Adolph, M., Flückiger, L., Gorkhover, T., Müller, J.P., Müller, M., Sauppe, M., Wolter, D., Schorb, S., Treusch, R., et al., 2014. J. Chem. Phys. 141, 044306.
Rupp, D., Adolph, M., Gorkhover, T., Schorb, S., Wolter, D., Hartmann, R., Kimmel, N., Reich, C., Feigl, T., de Castro, A.R.B., et al., 2012. New J. Phys. 14, 055016.
Rupp, D., Flückiger, L., Adolph, M., Gorkhover, T., Krikunova, M., Müller, J.P., Müller, M., Oelze, T., Ovcharenko, Y., Röben, B., et al., 2016. Phys. Rev. Lett. 117, 153401.
Rusydi, A., Goos, A., Binder, S., Eich, A., Botril, K., Abbamonte, P., Yu, X., Breese, M.B.H., Eisaki, H., Fujimaki, Y., et al., 2014. Phys. Rev. Lett. 113, 067001.
Saalmann, U., 2010. J. Phys. B: At. Mol. Opt. Phys. 43, 194012.
Saldin, E.L., Schneidmiller, E.A., Yurkov, M.V., 2000. The Physics of Free Electron Lasers. Springer-Verlag, Berlin Heidelberg New York, ISBN: 3-540-66266-9.
Schäfer, B., Flöter, B., Mey, T., Juranic, P., Kapitzki, S., Keitel, B., Plönjes, E., Mann, K., Tiedtke, K., 2011. Nucl. Instrum. Methods A 654, 502.
Scheins, J., 2004. Tomographic Reconstruction of Transverse and Longitudinal Phase Space Distributions using the Maximum Entropy Algorithm. DESY-Report TESLA 2004-08.
Schlotter, W.F., Sorgenfrei, F., Beeck, T., Beye, M., Gieschen, S., Meyer, H., Nagasono, M., Föhlisch, A., Wurth, W., 2010. Opt. Lett. 35, 372.
Schmüser, P., Dohlus, M., Rossbach, J., Behrens, C., 2014. Free-Electron Lasers in the Ultraviolet and X-Ray Regime: Physical Principles, Experimental Results, Technical Realization. In: Springer Tracts in Modern Physics, Springer International Publishing, http://dx.doi.org/10.1007/978-3-540-79572-8.
Schneidmiller, E.A., Faatz, B., Kuhlmann, M., Roensch-Schulenburg, J., Schreiber, S., Tischer, M., Yurkov, M.V., 2017. Phys. Rev. ST Accel. Beams 20, 020705.
Schneidmiller, E.A., Yurkov, M.V., 2012. Phys. Rev. ST Accel. Beams 15, 080702.
Schneidmiller, E.A., Yurkov, M.V., 2013. Phys. Rev. ST Accel. Beams 16, 110702.
Schnorr, K., Senftleben, A., Kurka, M., Rudenko, A., Foucar, L., Schmid, G., Broska, A., Pfeifer, T., et al., 2013. Phys. Rev. Lett. 111, 093402.
Schnorr, K., Senftleben, K.A., Kurka, M., Rudenko, A., Schmid, G., Pfeifer, T., Meyer, K., Kübel, M., Kling, M.F., Jiang, Y.H., et al., 2014. Phys. Rev. Lett. 113, 073001.
Schnorr, K., Senftleben, A., Schmid, G., Augustin, S., Kurka, M., Rudenko, A., Foucar, L., Broska, A., Meyer, K., Anielski, D., Boll, R. et al., 2015. J. Electron Spectroscopy and Related Phenomena 204, 245.
Schreiber, S., Faatz, B., 2015. High Power Laser Sci. Eng. 3, e20. http://dx.doi.org/10.1017/hpl.2015.16.
Schroedter, L., Müller, M., Kickermann, A., Przystawik, A., Toleikis, S., Adolph, M., Flückiger, L., Gorkhover, T., Nösel, L., Krikunova, M., et al., 2014. Phys. Rev. Lett. 112, 183401.
Schulz, S., Grguras, I., Behrens, C., Bromberger, H., Costello, J.T., Czwalinna, M.K., Felber, M., Hoffmann, M.C., Ilchen, M., Liu, H.Y., et al., 2015. Nature Commun. 6, 5938.
Singer, A., Lorenz, U., Sorgenfrei, F., Gerasimova, N., Gulden, J., Yefanov, O.M., Kurta, R.P., Shabalin, A., Dronyak, R., Treusch, R., et al., 2013. Phys. Rev. Lett. 111, 034802.
Singer, A., Sorgenfrei, F., Mancuso, A.P., Gerasimova, N., Yefanov, O.M., Gulden, J., Gorniak, T., Senkbeil, T., Sakdinawat, A., Liu, Y., et al., 2012. Opt. Express 20, 17480.
Singer, A., Vartanyants, I.A., Kuhlmann, M., Duesterer, S., Treusch, R., Feldhaus, J., 2008. Phys. Rev. Lett. 101, 254801.
Sobierajski, R., Bruijn, S., Khorsand, A.R., Louis, E., van de Kruijs, R.W.E., Burian, T., Chalupsky, J., Cihelka, J., Gleeson, A., Grzonka, J., et al., 2011. Opt. Express 19, 193.
Sobierajski, R., Jacyna, I., Dluzewski, P., Klepka, M.T., Klinger, D., Pelka, J.B., Burian, T., Hajkova, V., Juha, L., Saksl, K., et al., 2016. Opt. Express 24, 15468.
Sobierajski, R., Jurek, M., Chalupsky, J., Krzywinski, J., Burian, T., Dastjani Farahani, S., Hajkov, V., Harmand, M., Juha, L., Klinger, D., et al., 2013. J. Instrum. 8, P02010.
Sobierajski, R., Krzywinski, J., Andrejczuk, A., Hahn, U., Treusch, R., Jurek, M., Klinger, D., Nietubyć, R., Pełka, J.B., Reniewicz, H., et al., 2005. Rev. Sci. Instrum. 76, 013909.
Solem, J.C., Baldwin, G.C., 1982. Science 218, 229.
Sorgenfrei, F., Schlotter, W.F., Beeck, T., Nagasono, M., Gieschen, S., Meyer, H., Föhlisch, A., Beye, M., Wurth, W., 2010. Rev. Sci. Instrum. 81, 043107.
Sorokin, A.A., Bobashev, S.V., Feigl, T., Tiedtke, K., Wabnitz, H., Richter, M., 2007. Phys. Rev. Lett. 99, 213002.
Stanciu, C.D., Hansteen, F., Kimel, A.V., Kirilyuk, A., Tsukamoto, A., Itoh, A., Th. Rasing, 2007. Phys. Rev. Lett. 99, 047601.
Steeg, B., Juha, L., Feldhaus, J., Jacobi, S., Sobierajski, R., Michaelsen, C., Andrejczuk, A., Krzywinski, J., 2004. Appl. Phys. Lett. 84, 657.
Steffen, B., Casalbuoni, S., Knabbe, E.-A., Schlarb, H., Schmidt, B., Schmüser, P., Winter, A., 2005. Electro optic bunch length measurements at the VUV-FEL at DESY. In: Proc. PAC 2005 Conf. Knoxville, Tennesee, pp. 3111–3113.
Strüder, L., Epp, S., Rolles, D., Hartmann, R., Holl, P., Lutz, G., Soltau, H., Eckart, R., Reich, C., Heinzinger, K., et al., 2010. Nucl. Instrum. Methods A 614, 483.
TESLA collaboration, 1993. A Proposal to Construct and Test Prototype Superconducting RF Structures for Linear Colliders. DESY-Report TESLA 93-01.
TESLA collaboration, 2001. The Superconducting Electron-Positron Linear Collider with an Integrated X-Ray Laser Laboratory. DESY-Report 2001-011, ISBN: 3-935702-00-0.
Thiele, R., Sperling, P., Chen, M., Bornath, Th., Fäustlin, R.R., Fortmann, C., Glenzer, S.H., Kraeft, W.-D., Pukhov, A., Toleikis, S., et al., 2010. Phys. Rev. E 82, 056404.
Tiedtke, K., Azima, A., von Bargen, N., Bittner, L., Bonfigt, S., Düsterer, S., Faatz, B., Frühling, U., Gensch, M., Gerth, Ch., et al., 2009. New J. Phys. 11, 023029.
Tiedtke, K., Feldhaus, J., Hahn, U., Jastrow, U., Nunez, T., Tschentscher, T., Bobashev, S.V., Sorokin, A.A., Hastings, J.B., Möller, S., et al., 2008. J. Appl. Phys. 103, 094511.
Tigner, T.M., 1993. In: Edwards, H. (Ed.), TTF Linac Conceptional Design Report in TESLA Collaboration Meeting. DESY-Report TESLA 1993-35.

Toleikis, S., Bornath, T., Döppner, T., Düsterer, S., Fäustlin, R.R., Förster, E., Fortmann, C., Glenzer, S.H., Göde, S., Gregori, G. et al., 2010b. J. Phys. B: At. Mol. Opt. Phys. 43, 194017.
Toleikis, S., Fäustlin, R.R., Cao, L., Döppner, T., Düsterer, S., Förster, E., Fortmann, C., Glenzer, S.H., Göde, S., Gregori, G., et al., 2010a. High Energy Density Phys. 6, 15.
Tschentscher, T., Bressler, C., Grünert, J., Madsen, A., Mancuso, A.P., Meyer, M., Scherz, A., Sinn, H., Zastrau, U., 2017. Appl. Sci. 7, 592.
Ullrich, J., Moshammer, R., Dorn, A., Dörner, R., Schmidt, L.Ph.H., Schmidt-Böcking, H., 2003. Rep. Progr. Phys. 66, 1463.
Usenko, S., Przystawik, A., Jakob, M.A., Lazzarino, L.L., Brenner, G., Toleikis, S., Haunhorst, C., Kip, D., Laarmann, T., 2017. Nature Comm. 8, 15626.
Varin, C., Peltz, C., Brabec, T., Fennel, T., 2012. Phys. Rev. Lett. 108, 175007.
Vinko, S.M., Zastrau, U., Mazevet, S., Andreasson, J., Bajt, S., Burian, T., Chalupsky, J., Chapman, H.N., Cihelka, J., Doria, D., et al., 2010. Phys. Rev. Lett. 104, 225001.
von Korff Schmising, C., Weder, D., Noll, T., Pfau, B., Hennecke, M., Ch. Strüber, Radu, I., Schneider, M., Staeck, S., Günther, Ch.M.and others, 2017. Rev. Sci. Instrum. 88, 053903.
Wabnitz, H., Bittner, L., de Castro, A.R.B., Döhrmann, R., Gürtler, P., Laarmann, T., Laasch, W., Schulz, J., Swiderski, A., von Haeften, K., et al., 2002. Nature 420, 482.
Wabnitz, H., de Castro, A.R.B., Gürtler, P., Laarmann, T., Laasch, W., Schulz, J., Möller, T., 2005. Phys. Rev. Lett. 94, 023001.
Wang, G.L., 2017. Proceedings of IPAC2017, Copenhagen, Denmark, p. 2709.
Wellhöfer, M., Hoeft, J.T., Martins, M., Wurth, W., Braune, M., Viefhaus, J., Tiedtke, K., Richter, M., 2008. J. Instrum. 3, P02003.
Wellhöfer, M., Martins, M., Wurth, W., Sorokin, A.A., Richter, M., 2007. J. Opt. A: Pure Appl. Opt. 9, 749.
Wenthaus, L., 2018. Laser-Assisted Photoemission from Solids with Free-Electron Lasers (Ph.D Thesis). Universität Hamburg.
Wesch, S., Schmidt, B., Behrens, C., Delsim-Hashemia, H., Schmüser, P., 2011. Nucl. Instrum. Methods A 665, 40.
Wiedorn, M.O., Oberthür, D., Bean, R., Schubert, R., Werner, N., Abbey, B., Aepfelbacher, M., Adriano, L., Allahgholi, A., Al-Qudami, N., et al., 2018. Nature Commun. 9, 4025.
Willner, A., 2012. A High Repetition Rate XUV Seeding Source for FLASH2, DESY-THESIS-2012-015.
Wöstmann, M., Mitzner, R., Noll, T., Roling, S., Siemer, B., Siewert, F., Eppenhoff, S., Wahlert, F., Zacharias, H., 2013. Phys. Rev. B 46, 164005.
Yu, L.H., 1991. Phys. Rev. A 44, 5178.
Zagorodnov, I., Dohlus, M., 2011. Phys. Rev. ST Accel. Beams 14, 014403.
Zapolnova, E., Golz, T., Pan, R., Klose, K., Schreiber, S., Stojanovic, N., 2018. J. Synchrotron Rad. 25, 39.
Zastrau, U., Burian, T., Chalupsky, J., Döppner, T., Dzelzainis, T.W.J., Fäustlin, R.R., Fortmann, C., Galtier, E., Glenzer, S.H., Gregori, G., et al., 2012. Laser Part. Beams 30, 45.
Zastrau, U., Fortmann, C., Fäustlin, R.R., Cao, L.F., Döppner, T., Düsterer, S., Glenzer, S.H., Gregori, G., Laarmann, T., Lee, H.J., et al., 2008. Phys. Rev. E 78, 066406.
Zastrau, U., Sperling, P., Becker, A., Bornath, T., Bredow, R., Döppner, T., Dziarzhytski, S., Fennel, T., Fletcher, L.B., Förster, E., et al., 2014a. Phys. Re. E 90, 013104.
Zastrau, U., Sperling, P., Fortmann-Grote, C., Becker, A., Bornath, T., Bredow, R., Döppner, T., Fennel, T., Fletcher, L.B., Förster, E., et al., 2015. J. Phys. B : At. Mol. Opt. Phys. 48, 224004.
Zastrau, U., Sperling, P., Harmand, M., Becker, A., Bornath, T., Bredow, R., Dziarzhytski, S., Fennel, T., Fletcher, L.B., Förster, E., et al., 2014b. Phys. Rev. Lett. 112, 105002.
Zhao, Z.T., Wang, D., Chen, J.H., Chen, Z.H., Deng, H.X., Ding, J.G., Feng, C., Gu, Q., Huang, M.M., Lan, T.H., et al., 2012. Nature Photon. 6, 360.
Ziaja, B., Weckert, E., Möller, T., 2007. Laser Part. Beams 25, 407.